



NTNU – Trondheim
Norwegian University of
Science and Technology

Accidental Impact Resistance of non-disconnectable bouy type FPSO

Martin Slagstad

Marine Technology

Submission date: June 2014

Supervisor: Jørgen Amdahl, IMT

Co-supervisor: Martin Storheim, IMT

Norwegian University of Science and Technology
Department of Marine Technology

Scope of work

With large prospects of oil and gas field development in the Arctic and sub-Arctic areas, there is a current market demand for robust field development solutions. The Arctic areas are characterized by long distances, severe weather conditions and the possibility for ice encounters, both from level ice and icebergs. This leads to severe accidental impact scenarios with return period of 10 000 years, which in turn leads to conservative and costly field development solutions. Possible reductions in the field development cost is of great interest in order to provide for an efficient and economical extraction of oil and gas in these areas, and is critical in order to ensure that the fields are actually developed.

With the threat of iceberg impact as an accidental load, either very heavy gravity based structures or disconnectable floating solutions have been opted for in the past. With the Arctic basin water depth of around 3-400 m, gravity based structures with sufficient iceberg impact resistance is far too costly, and floating solutions are thus preferred. However, the cost increase due to the disconnectable system can be in the range of 10-25 % of the project cost depending on the floater and disconnection preferences.

Projects with disconnectable solutions have shown that the mooring system can be designed to withstand a large impact, but with a too large offset for safety of the riser system. A non-disconnectable system should thus have the possibility to shut down the risers, and in a worst case situation disconnect them. In addition, a conventional fairlead and chain stopper system will have the possibility to disconnect the mooring system in an emergency. Consequently, a non-disconnectable system is not non-disconnectable, but lacks the possibility of a quick emergency disconnection and a hopefully quick reconnection. Thus, the consequences of an extreme impact event is limited in terms of environmental damage and human risk, but the economic losses due to a shutdown and possible long time before reconnection could be significant. This is balanced by the savings of the initial investment, and thus the lower break even production price requirement.

From e.g. the NORSOK code, the requirement to the accidental impact resistance is normally that no progressive collapse of the structure should occur, and safe evacuation of the personnel should be possible. In the Accidental Limit State the resistance may be assessed by non-linear methods of analysis; the structure may undergo yielding, buckling and large permanent deformations on member and sub-structure level. This can only be assessed accurately if both interacting bodies are modeled, and the interaction between the two bodies is accounted for in a realistic manner.

Additional limit state requirements might be enforced by the platform operators, relating to minimizing the production loss due to downtime after an accidental event. The question boils down to a risk assessment, in which the risk of losing money due to downtime is balanced by the increased cost of the initial investment.

Due to the long distances from the discovered fields to shore, pipeline transport

of the produced hydrocarbons could be technically and economically challenging. Thus, offshore offloading from the platform could be a preferred solution. With offshore offloading, large tankers will operate in close proximity to the platform, and accidental impacts will be probable. If a Suezmax tanker with a ballast displacement of 50 000 ton impacts the platform in 5 knots, the available kinetic energy is 170 MJ.

An iceberg impact can be of varying magnitude based on the field location. The size can be massive, but with increasing size comes decreasing drift velocity. If an impact energy corresponding to an accidental tanker impact should be defined, it could for instance represent a 1 million ton iceberg drifting at 0.5 m/s. This is likely in the very high range both for mass and impact velocity for the southwestern parts of the Arctic, e.g. in the area around Bjørnøya. Thus, an iceberg threat is in the same or lower range as an accidental impact from an offloading tanker, and could depending on the field location not provide additional hazards to the platform.

As a case study for the current work, the Moss Maritime's Octopus buoy design is to be used in a field located southeast of Bjørnøya.

The purpose of this project is to study impacts from offloading tankers on the non-disconnectable Octopus buoy. The goal is perform realistic simulations where both the ship, the platform and the surrounding water are modelled and where interaction between them is taken into account. The results from integrated simulations shall be compared with simplified methods based on decoupling of the problem into external and internal mechanics. The work may be carried out in the following steps:

1. Describe the structural configuration of the Octopus platform side structure
2. Describe the structural configuration of a realistic offloading tanker
3. Determine relevant impact scenarios for: among others impact geometry, speed of the two bodies and in case of iceberg, size and shape of iceberg
4. Establish a detailed finite element model of the Octopus side structure connected to a coarse global model of the entire platform. The finite element model for the platform shall be sufficiently fine to capture the governing deformation mechanisms in way of the impact zone, but still meet requirements with respect to acceptable CPU consumption. The mass of the global platform model should be representative of the actual platform in terms of magnitude, center of gravity and radii of gyration.
5. Establish a model of a large tanker for use in the integrated collision simulations. An existing detailed bow model should be extended. The mass of the global vessel model should be representative of a reference vessel in terms of magnitude, center of gravity and radii of gyration.
6. By means of external impact mechanics, estimate the amount of impact energy that must be dissipated as strain energy for the selected impact scenarios.

7. Conduct simulations with LS DYNA using ALE FSI coupling on a simple vessel geometry (barge). Validate the behavior against hand calculations or other hydrodynamic software.
8. Conduct impact simulations of the global tanker model with the global Octopus model with FSI for the selected scenarios.
9. Compare results of the global impact analysis with simplified methods. Assess and explore the validity limits for:
 - The accuracy of the ALE approach for FSI in collision analysis
 - Treatment of added mass
 - Integrated FSI analysis compared with the decoupling between external and internal mechanics w.r.t. the dissipated strain energy and damage extent.
 - Explore the effect of including ballast water on the collision response by using integrated FSI analysis.
 - Conclusions and recommendations for further work

Literature studies of specific topics relevant to the thesis work may be included.

The work scope may prove to be larger than initially anticipated. Subject to approval from the supervisors, topics may be deleted from the list above or reduced in extent.

In the thesis the candidate shall present his personal contribution to the resolution of problems within the scope of the thesis work.

Theories and conclusions should be based on mathematical derivations and/or logic reasoning identifying the various steps in the deduction.

The candidate should utilise the existing possibilities for obtaining relevant literature.

Thesis format

The thesis should be organised in a rational manner to give a clear exposition of results, assessments, and conclusions. The text should be brief and to the point, with a clear language. Telegraphic language should be avoided.

The thesis shall contain the following elements: A text defining the scope, preface, list of contents, summary, main body of thesis, conclusions with recommendations for further work, list of symbols and acronyms, references and (optional) appendices. All figures, tables and equations shall be numerated.

The supervisors may require that the candidate, in an early stage of the work, presents a written plan for the completion of the work. The plan should include a budget for the use of computer and laboratory resources which will be charged to the department. Overruns shall be reported to the supervisors.

The original contribution of the candidate and material taken from other sources shall be clearly defined. Work from other sources shall be properly referenced using an acknowledged referencing system.

The report shall be submitted in two copies:

- Signed by the candidate
- The text defining the scope included
- In bound volume(s)
- Drawings and/or computer prints which cannot be bound should be organised in a separate folder.
- The report shall also be submitted in pdf format along with essential input files for computer analysis, spreadsheets, Matlab files etc in digital format.

Ownership

NTNU has according to the present rules the ownership of the thesis. Any use of the thesis has to be approved by NTNU (or external partner when this applies). The department has the right to use the thesis as if the work was carried out by a NTNU employee, if nothing else has been agreed in advance.

Moss Maritime designs will be utilized in the thesis work. With the intention of allowing the results of the thesis work publicly available, Moss Maritime reserves the right to ensure that commercially sensitive information is not included in the public part of the thesis. If such issues should arise, confidential information is suggested to be included as an appendix which is omitted from the openly available thesis.

Thesis supervisors

Prof. Jørgen Amdahl

Ph.d student Martin Storheim

Deadline

June 10, 2014

Jørgen Amdahl


Preface

This Master thesis is the result of work performed by Stud. Tech. Martin Slagstad during the tenth semester at The Norwegian University of Science and Technology. The Master thesis corresponds to the full work load during the semester. The work presented here is a continuation of the project thesis performed during the fall semester of 2013. Basic theories for collision problems were reviewed in the project thesis and are therefore not included here in this Master thesis.

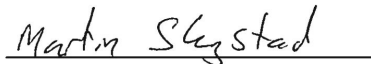
The main focus and most time consuming subjects in this thesis has been to model the fluid environment correctly, and to give a correct coupling between the fluid and the Lagrangian parts. The latter proved to be much more difficult than anticipated. Work regarding these subjects was especially demanding since there is little literature, and none of the supervisors have any modeling experience in the subject.

I would in particular like to thank the following for being available to discuss problems with the thesis work:

- Prof. Jørgen Amdahl for guidance and motivation.
- Ph.d student Martin Storheim for constructive conversations and for sharing his knowledge about FEA.
- Marilena Greco for help understanding fluid dynamics.

A thanks is also given to Moss Maritime for providing structural drawings and general information for the Octopus.

Trondheim, June 9, 2014


Martin Slagstad

Summary

The surroundings of offshore structures consist of many components controlled by nature, but also some that are managed by people; ships. Due to these factors, ship collisions are a constant threat to offshore installations because human error can occur.

This report consists of two main problems: the effect of ballast water in collisions, and the effects of decoupling the collision problem into internal and external mechanics. Both of the problems are analyzed using LS-DYNA. The finite element models for the analyses are created using MSC Patran.

Ideally, the effects from fluids were to be included in both problems. How to model fluids and fluid structure interaction was therefore learned. A simple analysis where a platform floated with an almost constant draft, was successfully performed. The vertical motion was only 8 cm.

To verify the fluid modeling in LS-DYNA, analyses were performed to calculate added mass coefficients. The coefficients were compared to added mass coefficients calculated in Wadam with the same geometry. When comparing the added mass coefficients, it was found that they did not match at all for periods over 10 seconds.

The first collision problem investigated, is the effects of internal fluids in collisions. The case used in the analyses, is a rigid sphere impacting a stiffened tank. Analyses are performed for different filling levels and impact velocities. The energy dissipations and contact forces are compared to that of the empty tank.

The results show that the presence of ballast water has a clear effect on both the contact force and energy dissipation. The contact force, for a given deformation, increases when water is present in the tank. The increase is however small when the impact speed is 2 m/s before the water reaches the ceiling of the tank. For larger impact velocities, the presence of water strengthens the ballast tank for all deformations.

When there is water in the tank, the energy dissipation is larger and the maximum contact force is in the same range as for the empty tank. It is concluded that since the ballast water strengthens the tank, it is conservative to neglect the internal fluid for the tank, and non-conservative to neglect the internal fluid in the tank for the impacting structure.

The second problem considered, was to study the effect of decoupling the collision problem into internal mechanics and external dynamics. Unlike the first problem, analyses including the effects from water without simplification are not successfully performed. A collision between Moss Maritimes Octopus and a shuttle tanker is used as a case. Four different realistic collision scenarios are chosen to be analyzed. The scenarios are analyzed using integrated analyses, and by decoupling the problem into external and internal mechanics.

The results for the decoupled analyses were quite similar to the integrated analyses.

The energy dissipation was successfully calculated within 10 % for all the analyses with an impact angle of 30 degrees and less using simplified methods. It was seen from the analyses that the deformation of the ship estimated decoupling the problem was typically too small, and the deformation of the platform, typically too large. The decoupled analyses were therefore conservative from the platforms point of view, and non-conservative from the ships point of view.

Samandrag

Omgivnadane til offshore-konstruksjonar består av mange faktorar kontrollert av naturen, men også nokre som er styrt av menneske - skip. På grunn av dette er det ein konstant fare for skipskollisjonar då menneskelig feil kan oppstå.

Denne rapporten presenterar i hovudsak to problem: effekten av ballastvatn i kollisjonar, og effekten av å dele kollisjonsproblemet inn i ekstern og intern mekanikk. Begge problema er analysert ved bruk av LS-DYNA. Elementmodellane for analysane er laga i MSC Patran.

Ideelt sett, skulle av effekten av vatn bli inkludert i begge problema. Korleis å modellere væske og væskestruktur-interaksjon vart difor lært. Ei enkel analyse vart gjennomført der ein plattform flaut ved konstant djupgang. Den vertikale rørsla var kun 8 cm.

For å verifisere modellen vart det gjennomført analysar for å berekne tilleggs massekoeffisientar til plattformen. Koeffisientane blei samanlikna med tilleggs massekoeffisientar kalkulert i Wadam, med den samme geometrien. Ved samanlikning av koeffisientane, var det sett at dei ikkje var like i heile tatt for periodar over 10 sekund.

Det fyrste kollisjonsproblemet som blei undersøkt var effekten av internvæske i kollisjonar. Eksempelet brukt i analysa er ein kollisjon mellom ei rigid kule og ein avstiva tank. Analysane vart gjennomført for ulike fyllingsgrader og kollisjonsfart. Energiabsorbasjonen og kontaktkrafta er sett i forhold til den tomme tanken.

Resultata viser at vatn i tanken har ein klar effekt på både kontaktkrafta og energiabsorbasjonen. Kontaktkrafta, for ein gitt deformasjon, er større når vatn er i tanken. Aukinga er forøvrig liten for den minste kollisjonsfarten før vatnet når taket av tanken. For større kollisionsfartar gir vatnet ein tydelig styrkande effekt for alle deformasjonar.

Når det er vatn i tanken vil energiabsorbasjonen vere større og den maksimale kontaktkrafta er i samme område som for den tomme tanken. Det er konkludert med at sidan vatnet styrkar tanken, er det konservativt å sjå vekk frå vatn for tanken, og ukonservativt for det som treffer tanken.

Det andre problemet var å studere effekten av å dele kollisjonsproblemet inn i ekstern og intern mekanikk. I motsetnad til det fyrste problemet, vart ikkje analysar gjennomført utan å bruke forenklingar for å ta med effekten av vatn. Ein kollisjon mellom Moss Maritime sin Octopus og ein tanker er brukt som eksempel. Fire ulike, realistiske kollisjonsscenarioar vart valgt for analyse. Dei tilfella som vart valgt, blei analysert med integrerte analysar og ved å dele problemet inn i intern og ekstern mekanikk.

Resultata frå dei forenkla analysane var ganske like som for den integrerte analysa. Energiabsorbasjonen var beregna innanfor 10 % for alle tilfella unntatt eitt, ved å bruke enkle metodar. Resultata viste at deformasjonen av skipet var typisk for

lite, og deformasjonen av platformen for stor når problemet er delt opp. Analysane der problemet er delt opp, var difor konservativt for platformen, og ukonservativt for skipet.

Contents

Introduction	1
1 General methods	3
1.1 General principles	3
1.1.1 Design principles	4
1.2 External dynamics	5
1.2.1 One degree of freedom	5
1.2.2 de Jonge and Laukeland, two degrees of freedom	6
1.2.3 Lui and Amdahl, six degrees of freedom	7
1.3 Internal mechanics	8
2 Literature study of fluid modelling in collisions	9
2.1 Previous work	9
2.1.1 Internal fluids	9
2.1.2 External fluids	11
2.1.3 Verification of fluid modeling	12
2.2 Chosen fluid modeling method	13
2.2.1 Limitations	14
3 Finite element analysis in LS-DYNA	15
3.1 Time integration	15
3.2 Time step size	16
3.3 Lagrangian modeling	17
3.3.1 Element type	17
3.3.2 Material models	17
3.3.3 Contact	20
3.4 Eulerian	20
3.4.1 Mesh and element type	20
3.4.2 Material models	21
3.5 Fluid structure interaction	21
4 Fluid and FSI modeling in practice	23
4.1 Environment	23
4.2 Fluid structure interaction	24
4.2.1 Procedure	24

4.2.2	Final parameters	29
4.2.3	Validating model	30
5	Collision analyses with internal FSI	35
5.1	Analysis set- up	35
5.2	Finite element modelling	36
5.2.1	Software	36
5.2.2	Ballast tank and sphere	37
5.2.3	Water environment	38
5.2.4	Fluid structure interaction	40
5.3	Results	41
5.3.1	Force displacement curves	41
5.3.2	Dissipated energy- displacemnt curves	43
5.4	Discussion	44
5.4.1	Contact force	45
5.4.2	Energy absorption	52
5.4.3	Fluid response	53
5.4.4	Numerical errors	55
5.5	Conclusion	55
6	Ship-platform collisions	57
6.1	Collision scenarios	57
6.1.1	Structures	58
6.1.2	Impact scenarios	60
6.1.3	Mass properties	61
6.1.4	Dissipated energy	65
6.1.5	Collision scenarios to be analyzed	67
6.2	Finite element modeling	68
6.2.1	Software	68
6.2.2	Reference ship	68
6.2.3	Moss Maritime's Octopus	70
6.2.4	Material	74
6.3	Attempt at a collision analysis with external FSI	75
6.4	Analysis set- up	77
6.4.1	Integrated analysis	77
6.4.2	Decoupled analysis	78
6.4.3	Contact	78
6.5	Results	79
6.5.1	Head on collision, ship in ballast	80
6.5.2	Head on collision, ship in full load	85
6.5.3	Glancing impact, 30 degrees, ship in ballast	90
6.5.4	Glancing impact, 45 degrees, ship in ballast	93
6.5.5	Bulb impact	98
6.5.6	Effect of hull angle	99
6.6	Discussion	101
6.6.1	Added mass	101

6.6.2	Energy dissipation estimates	102
6.6.3	Damage	105
6.6.4	Numerical errors	106
6.6.5	Octopus' boundary conditions	108
6.7	Conclusion	110
7	Conclusion	111
8	Further work	113
A	Deformations for glancing impact. 45 deg, ship in ballast	i
B	Deformation area for head on impact, ship in full load	iii
C	Dissipated Energy, Matlab code	v

List of Figures

1.1	Force displacement curve for a ship-platform collision.	4
1.2	Energy dissipation for strength, ductile and shared energy design, Norsok N-004.	4
1.3	Definition of hull angles.	7
2.1	Deformation energy- time curve for ship collision with a liquid filled cargo tank.	10
2.2	View of collision environment.	11
2.3	Lateral velocities for 80 degree collision.	12
2.4	Comparison of actual and simulated Iceberg sway motion.	13
3.1	Time integration loop, LS-DYNA Theory manual [2006].	16
3.2	Element necking model	19
3.3	Sketch of penalty Eulerian-Lagrangian penalty coupling, Aquelet et al. [2006].	22
4.1	Water environment with stable pressure.	24
4.2	Two dimensional box impacting water.	25
4.3	Three dimensional box impacting water.	26
4.4	Improvement of Octopus mesh.	27
4.5	Motions of the Octopus floating in water with a mesh size of two meters.	28
4.6	Motions of the Octopus floating in water with a mesh size of one meter.	29
4.7	Leakage in the Octopus.	31
4.8	Force displacement curve with different hull angles.	31
4.9	Comparison of added mass coefficients from LS-DYNA and Wadam.	32
5.1	Stiffened ballast tank used for collision analyses.	36
5.2	Boundary conditions for the ballast tank.	38
5.3	Collision set-up for a collision between a solid sphere and a ballast tank.	38
5.4	Air and water environment for the collision analyses with the un- stiffened ballast tank.	39

5.5	Effect using a reduced bulk modulus.	39
5.6	Effect increasing of number of coupling points.	40
5.7	Static pressure in the ballast tank before the collision.	41
5.8	Force- displacement curves for a ballast tank with different filling levels. Impact speed 2 m/s.	41
5.9	Force- displacement curves for a ballast tank with different filling levels. Impact speed 5 m/s.	42
5.10	Force- displacement curves for a ballast tank with different filling levels. Impact speed 8 m/s.	42
5.11	Force- displacement curves for an empty ballast tank with different impact velocities.	43
5.12	Dissipated energy- displacement curves for a ballast tank with different filling levels. Impact speed 2 m/s.	44
5.13	Dissipated energy- displacement curves for a ballast tank with different filling levels. Impact speed 5 m/s.	44
5.14	Dissipated energy- displacement curves for a ballast tank with different filling levels. Impact speed 8 m/s.	45
5.15	Additional force- displacement curves for the ballast tank with different filling levels compared to Tank0. Impact speed 2 m/s.	46
5.16	Additional force- displacement curves for the ballast tank with different filling levels compared to Tank0. Impact speed 5 m/s.	46
5.17	Additional force- displacement curves for the ballast tank with different filling levels compared to Tank0. Impact speed 8 m/s.	47
5.18	Buckling modes for the side of the ballast tank. Impact speed 8 m/s.	48
5.19	Sketch of the problem for the added mass estimate from Greco [2001].	49
5.20	Additional force- displacement curves for the ballast tank with different filling levels. No FSI for the top plate. Impact speed 2 m/s.	51
5.21	Additional force- displacement curves for the ballast tank with different filling levels. No FSI for the top plate. Impact speed 5 m/s.	51
5.22	Additional force- displacement curves for the ballast tank with different filling levels. No FSI for the top plate. Impact speed 8 m/s.	52
5.23	Deformation of the ballast tank with a 90 % filling level. Red part - Shell, Blue part - Water.	53
5.24	Water motion during impact for Tank07. Impact velocity 5 m/s.	54
6.1	Profile of reference ship.	58
6.2	Bow, center line reference ship.	59
6.3	Octopus stinger decks between.	60
6.4	Vertical impact positions.	61
6.5	Octopus tank arrangement seen from above.	62
6.6	Impact angles.	62
6.7	Added mass for the ship in surge, sway and heave.	63
6.8	Added mass for the ship in roll, pitch and yaw.	63
6.9	Added mass for the Octopus in surge and heave	64
6.10	Added mass for the Octopus in roll and yaw	64
6.11	Energy dissipation ratio for head on collision without added mass.	66

6.12	Bow model used in the collision analyses.	68
6.13	Tanker model used in collision analyses.	69
6.14	Simplification of girder/stiffener connection.	71
6.15	Stiffening arrangement of outer shell and stinger decks.	72
6.16	Structural model of the Octopus.	72
6.17	Environment used in the collision analyses.	75
6.18	Set-up for the collision analyses with constant velocity.	79
6.19	Energy absorption for a head on impact in ballast.	81
6.20	Force- displacement curves for a head on impact in ballast.	82
6.21	Failure shape for the deck for a head on collision in ballast.	83
6.22	Energy absorption- displacement curves for a head on impact in ballast.	83
6.23	Deformations for a head on collision. Ship in ballast.	84
6.24	Energy absorption for a head on impact in full load.	85
6.25	Comparison of force deformation curves for collision with fully loaded ship.	86
6.26	Effect of vertical motion on the deformation of the bow for FullOR and FullOS.	87
6.27	Contact area at a 5 m deformation for the ship.	87
6.28	Comparison of energy absorption deformation curves for collision with fully loaded ship.	88
6.29	Deformations for a head on collision. Ship in full load.	89
6.30	Plastic strains in outer shell. Ship in full load.	89
6.31	Energy absorption for a glancing on impact in ballast. Impact angle 30 deg.	91
6.32	Comparison of force deformation curves for 30 deg impact. Ship in Ballast.	91
6.33	Comparison of energy absorption- deformation curves for 30 deg impact. Ship in Ballast.	92
6.34	Deformations for glancing impact.30 deg, ship in Ballast.	93
6.35	Plastic strains for glancing impact.30 deg, ship in Ballast.	93
6.36	Energy absorption for a glancing on impact in ballast. Impact angle 45 deg.	94
6.37	Comparison of force deformation curves for 45 deg impact. Ship in Ballast.	95
6.38	Comparison of energy absorption- deformation curves for 45 deg impact. Ship in Ballast.	96
6.39	Deformations for glancing impact.45 deg, ship in Ballast.	97
6.40	Plastic strains for glancing impact.45 deg, ship in Ballast.	98
6.41	Analysis set-up for bulb impact	99
6.42	Force displacement curve for bulb impact.	99
6.43	Force displacement curve with different hull angles.	100
6.44	Vertical motions at the tip of the bow for Full0 and FullOR.	103
6.45	Comparison of energy dissipation with single and double precision.	107
6.46	Comparison force displacement with single and double precision.	108
6.47	Fixed edges for Boundary 1 and Boundary 2.	109

6.48 Comparison of force displacement curves for Boundary 1 and Boundary 2. 109

A.1 Deformations for glancing impact.45 deg, ship in Ballast. i

A.2 Plastic strains for glancing impact.45 deg, ship in Ballast. ii

B.1 Plastic strains in bow for head on collision in full load. iii

List of Tables

4.1	Important parameters for the <code>CONSTRAINED_LAGRANGE_IN_SOLID</code> card.	30
5.1	Filling levels for ballast tank.	36
5.2	Mass of sphere and impact velocities.	36
5.3	Material parameters for the ballast tank.	37
6.1	General dimensions, reference ship.	58
6.2	Added mass coefficients for the Octopus and ship.	65
6.3	Estimates for the energy dissipation for selected collision scenarios.	67
6.4	Mass properties for the ship, full load.	69
6.5	Mass properties for the ship, ballast.	69
6.6	Mass properties, Octopus.	73
6.7	Material parameters for the shuttle tanker.	74
6.8	Material parameters for the Octopus.	74
6.9	Air and water properties.	75
6.10	Overview for head on collision analyses in ballast.	80
6.11	Ship and platform deformations. Ship in ballast.	84
6.12	Overview for head on collision in full load.	85
6.13	Ship and platform deformations. Ship in full load.	88
6.14	Overview for central impact with a 30 degree angle. Ship in ballast.	90
6.15	Ship and platform deformations. 30 deg, ship in ballast.	92
6.16	Overview for central impact with a 45 degree angle. Ship in ballast	94
6.17	Ship and platform deformations. 30 deg, ship in ballast.	96
6.18	Energy dissipation for head on collision with added mass.	101

Nomenclature

A_s	Surface area of the element
A_{ii}	Added mass in i direction
B_{ii}	Damping in i direction
C_{ii}	Restoring coefficient in i direction
D	Damage
E_k	Kinetic energy
E_s	Strain energy
F	Force
F_s	Static force
H	Height of the water
I_b	Moment of inertia of spar around horizontal axis including added mass
K	Strength coefficient
L_c	Characteristic element length
L_n	Length of element sides
M	Mass
R	Distance from spar c.o.g. to point of impact
R_i	Contact force installation
R_r	Reduction factor
R_s	Contact force ship
T	Stress triaxiality
V	Volume
V_n	Volume, local neck

V_r	Volume, outside necking region
\bar{m}	Equivalent mass
\ddot{s}	Relative acceleration
\dot{D}	Rate of damage
\dot{v}	Change of velocity
b	Width
c	Speed of the stress wave
d	Depth
g	Gravitational acceleration
l_e	Length of undeformed element
m_a	Mass of the ship including added mass
m_b	Mass of the installation including added mass
n	Material parameter
r	Radius of sphere
t	Time
v	Velocity
v_{a0}	Initial velocity of the ship
v_{a1}	Final velocity of the ship
v_{b0}	Initial velocity of the installation
x	Deformation
F	Stress divergence vector
H	Hour glass resistance
M	Diagonal mass matrix
P	External and body forces
a	Nodal acceleration
u	Nodal displacement
v	Nodal velocity
Δt_c	Critical time step
Δv_i^2	Change of velocity squared
α	Water line angle

β	Frame angle
β'	Normal frame angle
$\dot{\varepsilon}_{eq}$	Rate of equivalent strain
η_i	Motion in i direction
γ	Shear angle
ω_b	Final angular velocity of spar
ρ	Density of water
σ_Y	Initial yield stress
σ_m	Hydrostatic stress
σ_{eq}	Equivalent stress
ε_{cr}	Critical equivalent strain
ε_{eq}	Equivalent strain
ε_{plat}	Equivalent strain at plateau exit
FSI	Fluid structure interaction
NLFEA	Non-linear finite element analysis

Introduction

Ship collisions are a constant threat to offshore structures since there often are a number of vessels in their immediate surroundings. To minimize the risks and consequences of collisions, rules have been developed for both the design of offshore structures and operation in the vicinity of them. However, it is seen that even with regulations, ship collisions still occur and with higher energies than predicted. In 2004, a supply vessel collided with a semi-submersible drilling platform in the North Sea. The energy involved was three times higher than the design recommendations for classification companies.

Since collisions always will be a risk, structures must be designed to withstand them. To ensure safe designs, damage must be calculated accurately. Non-linear finite element analysis (NLFEA) can give accurate results if done properly. However, due to the time consuming nature of such analyses, simplified methods with less accuracy are often used for design.

Two main problems are investigated in this thesis. The first is the effect ballast water has in collisions. A simple problem is studied, and different impact velocities and filling levels are used in the analyses. The second problem is to investigate the effects of decoupling the collision problem into external dynamics and internal mechanics. A collision between Moss Maritimes Octopus and a shuttle tanker is used as a case for these analyses.

It was intended to use ALE modeling with fluid structure interaction for both problems. ALE and FSI modeling is a new topic for the candidate and the supervisors, so a vast amount of time was spent learning the modeling technique. Modeling the fluid and especially the FSI proved to be much more difficult than expected and a ship platform collision analysis with external FSI was not successfully performed.

Trying to learn how to model the FSI correctly proved to be much more time consuming than predicted. The results for the ship platform collisions are therefore not discussed as detailed as wished. In agreement with the supervisor, relevant collision scenarios for iceberg collisions was dropped.

The report consists of four parts. First some general theory is presented. This includes a literature study of collisions with FSI and a short summary of important modeling parameters in LS-DYNA. Then there is a short chapter about ALE mod-

eling in LS-DYNA before the effects of internal FSI interaction are investigated. Finally ship platform collisions are analyzed in Chapter 6.

Chapter 1

General methods

Collisions between offshore structures and ships are very complex. Determining the damage in a ship and/or platform can be done by using non-linear finite element analyses or by using simplified methods along with energy considerations, [NORSOK N-004, 2004]. The latter is often favored since finite element modelling and running numerical analyses is very time consuming.

1.1 General principles

According to NORSOK N-004 [2004], the ship collision action is characterized by kinetic energy. The kinetic energy in a ship collision is determined by the mass of the colliding vessels, including added mass, as well as the speed at impact. The majority of the kinetic energy will after the collision either be dissipated as strain energy or remain as kinetic energy.

For ship collisions, it is customary to distinguish between external dynamics and internal mechanics. External dynamics deal with the rigid body motions of the structures and specifies the amount of energy to be dissipated in the collision. Internal mechanics specifies the structural response and damage due to energy absorption in the structures.

In collisions, the strain energy must be absorbed by one or both of the vessels. This will generally give large plastic strains and deformations. Figure 1.1 shows a force deformation curve for a ship-platform collision. The energy dissipated in the collision is represented by the area below the curves, i.e.

$$E_s = \int R_s dw_s + \int R_i dw_i \quad (1.1)$$

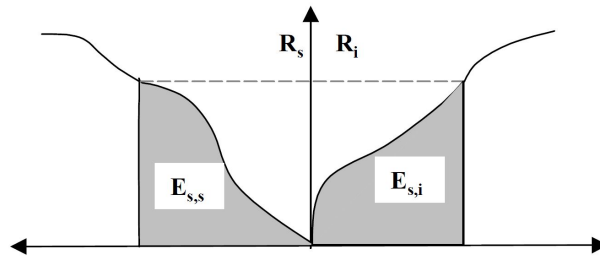


Figure 1.1: Force displacement curve for a ship-platform collision.

1.1.1 Design principles

Taking into account how the strain energy is absorbed, NORSOK N-004 [2004] has defined three design principles shown in Figure 1.2.

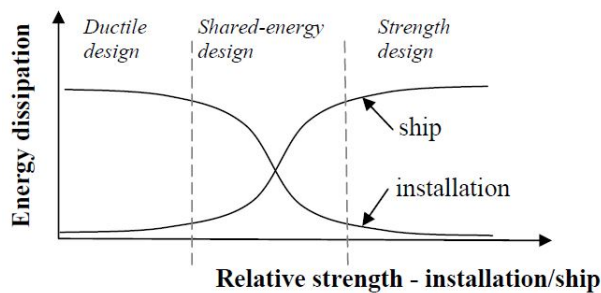


Figure 1.2: Energy dissipation for strength, ductile and shared energy design, Norsok N-004.

Strength design

The structural strength of the installation is larger than the structural strength of the ship. Structural deformation will mainly take place in the ship.

Ductile design

The structural strength of the ship is larger than the structural strength of the installation. Structural deformation will mainly take place on the installation.

Shared energy design

The ship and installation have similar structural strength. Both the ship and the installation will undergo large deformations.

Calculations are often simplified by either assuming strength design or ductile design. When applying these methods, either the ship or the installation is assumed to be rigid. All of the strain energy must then be absorbed by the non-rigid structure. Deformation of the non-rigid structure can be found by using a simplified geometry of the rigid structure along with simple plastic methods.

In cases where neither strength nor ductile design can be assumed, the more complicated shared energy design must be utilized. Both of the structures will deform; changing the impact geometry as well as the relative strength. Such an analysis should be done incrementally since the relative strength of the structures may change.

Determining which design principle to use for a given structure can be very difficult. Small differences in relative strength can cause large differences in deformations.

1.2 External dynamics

There have been developed many simplified methods for determining the energy dissipation, some more complex than others. Due to the complex nature of ship-platform collisions, some simplifications are often assumed:

- The duration of the collision is short.
- The collision force is large and is the only force taken into account.
- The added mass is constant.

The methods applied in this thesis for calculating the energy dissipation in collisions are presented in the following.

1.2.1 One degree of freedom

By assuming one degree of freedom, an equation for the strain energy can be derived by using conservation of energy and momentum, [NORSOK N-004, 2004].

$$E_s = \frac{1}{2} m_a v_{a0}^2 \frac{\left(1 - \frac{v_{b0}}{v_{a0}}\right)^2}{1 + \frac{m_a}{m_b}} \quad (1.2)$$

Assuming the installation has no initial velocity

$$E_s = \frac{\frac{1}{2} m_a v_{0a}^2}{1 + \frac{m_a}{m_b}} \quad (1.3)$$

m_a = Mass of the ship including added mass.

m_b = Mass of the installation including added mass.

v_{a0} = Initial velocity of the ship.

v_{b0} = Initial velocity installation.

E_s = Strain energy.

This method will give reasonable results when the collision force acts through, or close to, the center of gravity for both structures. When significant rotational motions (yaw or roll) are exited, the one degree of freedom assumption will not be valid. Strain energies that are calculated using this method for off center collisions will typically be too high, since all the kinetic energy must remain in the same degree of freedom. The one degree of freedom method (DOF) is in this thesis referred to as the 1 DOF method.

1.2.2 de Jonge and Laukeland, two degrees of freedom

Using a head on collision between a ship and a spar as an example, de Jonge and Laukeland [2013] derived an equation for the dissipated energy for a two degree of freedom system. The two degrees of freedom taken into account are translation in the x-direction and rotation around the y-axis. It is assumed that the collision is completely inelastic. For the two degree of freedom system, the equations for conservation of momentum and angular momentum can be written as

$$m_a v_{a0} = m_a v_{a1} + m_b v_{b1} \quad (1.4)$$

$$m_a v_{a0} R = m_a v_{a1} R + I_b \omega_b \quad (1.5)$$

where the notation is the same as for the one degree of freedom problem. In addition the following variables are defined as

v_{a1} = Final velocity of the ship.

v_{b1} = Final velocity spar.

ω_b = Final angular velocity of spar.

I_b = Moment of inertia of spar around horizontal axis including added mass.

R = Distance from spar c.o.g to point of impact.

The two structures will lose contact when the velocities at the contact point are equal, i.e.

$$v_{a1} = v_{b1} + R\omega_b \quad (1.6)$$

Solving the equations above for v_{a1} , v_{b1} and ω_b , the kinetic energy before and after the collision can be found. The dissipated energy is the difference between these two quantities resulting in

$$E_s = \frac{1}{2} \left[\frac{m_a v_{a0}^2}{1 + \frac{m_a}{m_b} + \frac{m_a R^2}{I_b}} \right] \quad (1.7)$$

Comparing Eq. (1.7) to Eq. (1.3) we see that the dissipated energy is reduced when the collision force does not act through the center of gravity. The two DOF method is in this thesis referred to as the 2 DOF method.

1.2.3 Lui and Amdahl, six degrees of freedom

A new method for off center collisions is presented in Liu and Amdahl [2010]. This method is an application of Stronge's impact mechanics model and takes all six degrees of freedom into account. It is assumed that deformations are limited to a small area within the contact surface. In this thesis, this method is referred to as the 6 DOF method.

Each of the colliding structures have as usual its own coordinate system, through the center of gravity. A local coordinate system, consisting of orthogonal vectors $\bar{n}_1\bar{n}_2\bar{n}_3$, is defined at the point of impact. Using a transformation matrix, Eq. (1.8) along with the hull angles for the struck structure, Figure 1.3, parameters such as mass and velocity can be transformed from the global coordinate systems to the local coordinate system.

$$T = \begin{bmatrix} \cos(\alpha) & -\sin(\alpha) & 0 \\ -\sin(\alpha)\cos(\beta') & -\cos(\alpha)\sin(\beta') & -\cos(\beta') \\ \sin(\alpha)\cos(\beta') & \cos(\alpha)\cos(\beta') & -\sin(\beta') \end{bmatrix} \quad (1.8)$$

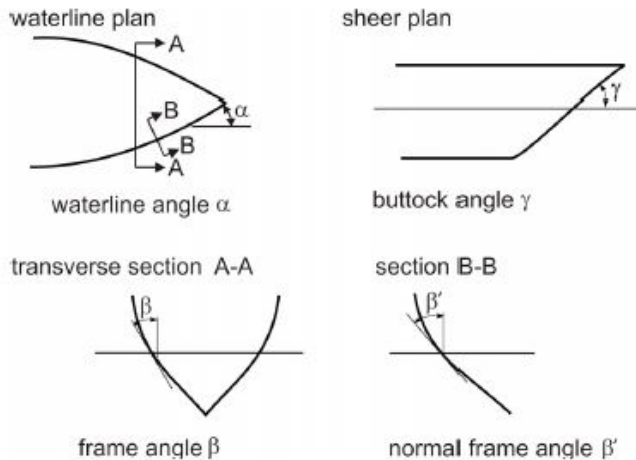


Figure 1.3: Definition of hull angles.

Using the local coordinate system, two analytical solutions for Eq. (1.9) can be found. Equating them to each other, the complicated six degree of freedom problem

can be reduced to a one degree of freedom problem for each direction. The strain energy for each direction \bar{n}_i can be calculated from Eq. (1.10).

$$\int_0^t \ddot{s} ds_i \quad (1.9)$$

$$E_i = \frac{1}{2} abs(\bar{m}_i \Delta v_i^2) \quad (1.10)$$

Here \ddot{s} is the relative acceleration, t the impact duration, Δv_i^2 the change of the squared relative velocities and \bar{m} is the equivalent mass.

In order to use Eq. (1.10) the equivalent mass, \bar{m}_i , and the change of the relative velocity squared, must be found. In order to determine these quantities proper boundary conditions such as the friction definition and relative velocities must be introduced. Detailed solutions are found in Liu and Amdahl [2010].

This method gives excellent agreement with the two dimensional model created by Pedersen and Zhang when the vertical eccentricity is not taken into account. However, when the vertical eccentricity is taken into account there is a significant influence on the dissipated energy when the roll motion is excited.

1.3 Internal mechanics

Internal mechanics determine the deformation and how the energy is absorbed in collisions. There are in general two methods used for calculating the internal mechanics. The first is by using simplified methods. The simplified methods vary greatly from Minorsky's empirical formula to Amdahl's formula which is based on theoretical considerations. The second method is by using non-linear finite element analysis (NLFEA). NLFEA is more accurate than the simplified methods if performed properly, but is much more time consuming both with regard to modelling and computation time. Due to its superior accuracy the non-linear finite element method is used to calculate the internal mechanics in this thesis. The NLFE program used to perform the calculations is LS-DYNA.

Chapter 2

Literature study of fluid modelling in collisions

In ship collisions, the effects of fluids are often neglected or greatly simplified. The most common simplification is to assume constant added mass during the collision. Although simple assumptions are often used, the effects of using them are not studied in depth due to the high cost of experiments and numerical simulations.

2.1 Previous work

For ship collisions, numerical simulations accounting for FSI have been performed for ship-ship, and ship- ice collisions. Both external and internal fluids have been modeled to investigate their effects. The ALE formulation is consequently used to model the fluids in all of the previous work. Although ALE formulation clearly is the most widely used method for FSI in ship collisions, little has been done to verify the FSI with regard to ship collisions.

2.1.1 Internal fluids

Normally when assessing the structural damage in ship collisions it is customary to assume that the tanks in the structures are empty or filled with a solid mass. However, this does not represent reality; there will in most cases be fluids in several tanks.

During a collision, a ship will have large accelerations which will give sloshing in liquid filled tanks. The sloshing movement of the liquids inside the ship will effect both the collision force and the deformation energy. A numerical study of a collision with a liquid filled cargo tank is presented in Zhang and Suzuki [2006].

The case studied by Zhang and Suzuki [2006] is a collision between a container ship and a VLCC with a double hull. The container ship impacts the side of the VLCC at a right angle. In the numerical simulation the cargo tank has a filling rate of 95 %, while the ballast tanks are empty. The fluid is modelled using the ALE finite element formulation. To isolate the effect of the fluid-structure interaction in the cargo tank, the water surrounding the ship is replaced with an added mass constant. Both the striking and struck ship are modeled using finite elements. The numerical simulation are performed using LS-DYNA.

The results from the analysis (ALE FE) are compared to results from an analysis where the mass of the fluid is assumed to be completely rigid. Important parameters such as deformation energy, impact force and kinetic energy are compared. Here, only the deformation energy is presented. It is seen that both models give similar results in the early stage of the collision. However, as seen in Figure 2.1, the results deviate after about 0.25 seconds. After that point, the deformation energy is higher for the rigid model.

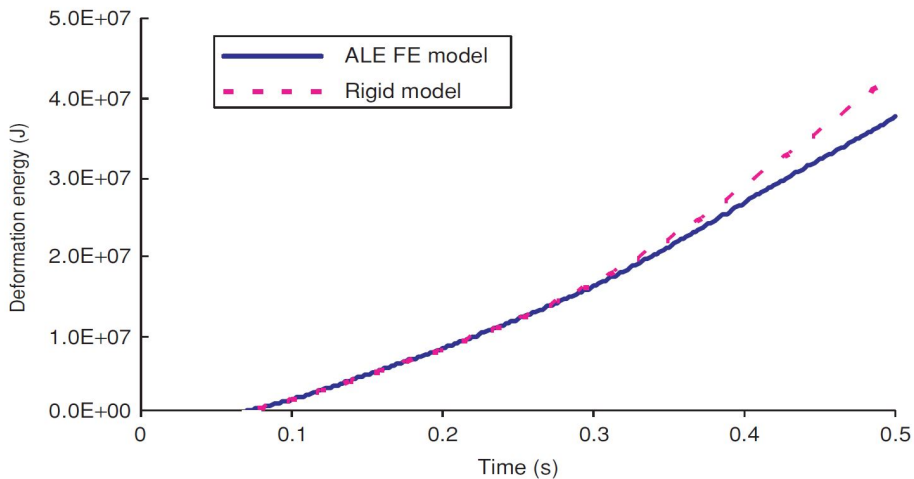


Figure 2.1: Deformation energy- time curve for ship collision with a liquid filled cargo tank.

Since the initial energy for both collisions were equal to begin with, more energy has remained as kinetic energy for the case where the fluid in the cargo tank is modeled using ALE. Less energy must therefore be absorbed by the colliding structures. This is due to the fact that the fluid in the cargo tank can have larger motions than the ship. It is seen that it is slightly conservative to neglect the effects of the motions of the fluid during the collision.

2.1.2 External fluids

Robert E. Gagnon and Sang-Gab Lee have published most of the articles presenting results from ship collision where external FSI interaction is taken into account. Gagnon has published articles focusing on ship- ice collisions while Lee has published results from both ship- ship and ship- ice collisions. Since the collision scenario studied in this thesis is a ship- platform collision, the work presented by Lee is the most relevant. An excerpt of Lee's work is presented below.

Lee et al. [2013] presents results from numerical analyses for ship- ship collisions. In all the collision analyses, a specialized ship with DWT of 2600 ton is the struck ship. The DWT of the striking ships vary from 500 to 35 000 ton. A number of different collision scenarios were analyzed with different impact angles. The environment used for the collision analyses is shown in Figure 2.2.

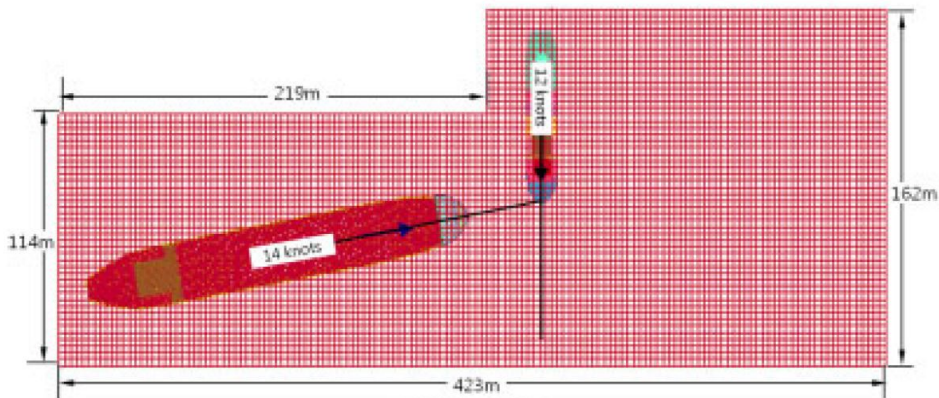


Figure 2.2: View of collision environment.

It was found that the most severe collision angle was not 90 degrees as commonly assumed, but 80 degrees. In both cases the inner hull was ruptured, but the ruptured area for the 80 degree collision was larger, almost twice as large. The reason may be that both ships have a forward velocity. Since the ships have an angle to each other, as shown in Figure 2.2, there is a velocity component from both of the ships that acts against each other.

Another interesting finding is the lateral movement of the struck ship during the collision. For the collision at 80 degrees where both ships have a forward velocity, it was seen that the struck ship starts moving laterally before contact. The struck ship reaches a lateral velocity of about two knots due to interference effects between the two ships, Figure 2.3. Contact initiates at 4.8 seconds.

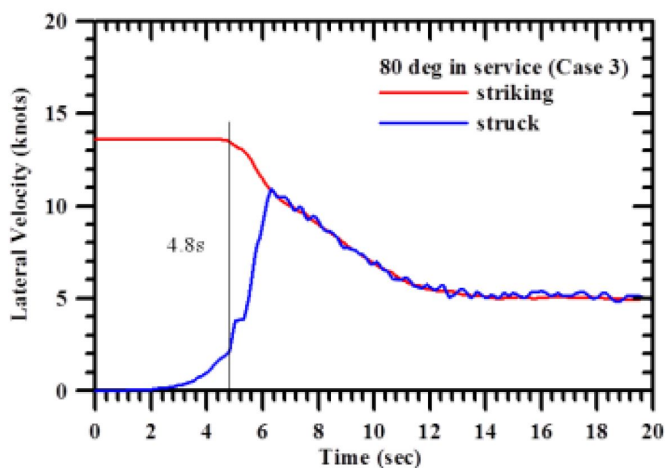


Figure 2.3: Lateral velocities for 80 degree collision.

2.1.3 Verification of fluid modeling

Sway motion of iceberg

To validate the ALE modelling technique, Gagnon and Derradji-Aouat [2006] replicates iceberg- ship collision experiments in LS-DYNA. The parameter used to verify that the ALE method models the fluid correctly, is the sway motion of the iceberg. The length- width- depth dimensions of the numerical water and air environment were 124m x 69m x 26m. The top 5 meters of the environment were modelled as air.

Results for the sway motion of the iceberg were calculated for three different mesh densities; 250 000, 1 000 000 and 2 000 000 elements. It was seen that the results converged when at least 1 000 000 elements were used to model the environment. The results from the comparison are shown in Figure 2.4. It is seen that the simulation gives a good compliance to the measurements obtained in the experiments.

Drop test of liquid filled tanks

Anghileri et al. [2005] compared different fluid modeling methods with experiments. The case used in the comparison is a drop test of a stiffened liquid filled tank (helicopter fuel tank). The tank was dropped from a height of 7.5 m giving an impact velocity of about 12 m/s. The fluid inside the tank was modeled using four different methods; Lagrangian, Eulerian, ALE and smoothed particle hydrodynamics (SPH). The tank itself was modeled using finite elements (Lagrangian).

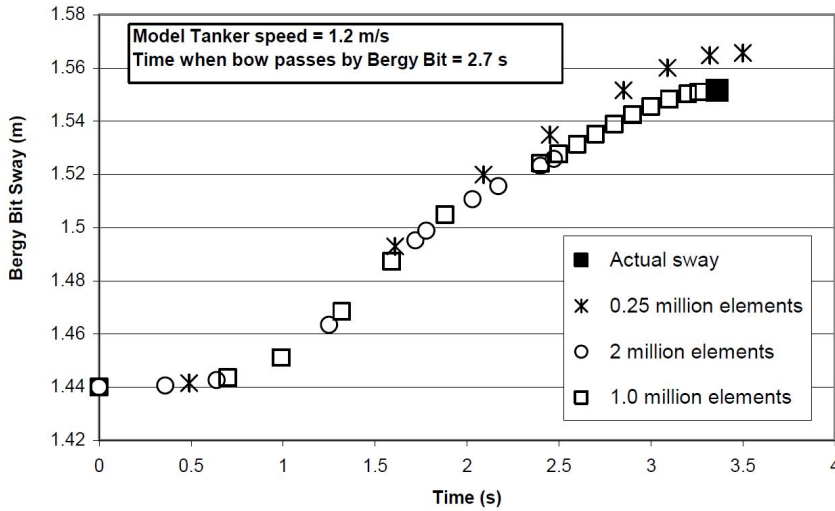


Figure 2.4: Comparison of actual and simulated Iceberg sway motion.

Both the Eulerian and ALE models gave a relatively accurate description of the sloshing of the water. However, the numerical results of the deformation of the tank obtained using the Eulerian or ALE method differ the most from the experiments. The Eulerian and the ALE models seem to suffer from typical problems arising from coupling between different solvers.

The Lagrangian FE model gave numerical results close to the experimental data with a relatively low computation time. However, due to the severe distortion of the mesh, this approach is only feasible in the early stages of the event. The method giving the best results is the SPH model. Analyses using this model gives a good agreement with the experimental results, in addition it reproduces the sloshing motion in the tank according to intuition and common experience. The drawback of the SPH model is the large computation time needed.

Based on the findings, Anghileri et al. [2005] concluded that the Lagrangian FE model seems to be a reliable numerical tool for structural design while the SPH model is found to be appropriate for design verification.

2.2 Chosen fluid modeling method

Studying published work, it is seen that the fluids in ship-ship collisions and ship-ice collisions is often modelled using ALE formulation. There are other methods to model the fluid, but the ALE formulation is computationally effective compared to other methods and can produce good results. Since it is widely used, it is the chosen method for this thesis.

To simplify the ALE modeling technique a fixed mesh will be used in this thesis. This is commonly known as an Eulerian approach which is a special case of the ALE method where the mesh has no motion. In the general ALE method the mesh can be directed to move in a prescribed manner as the solution progresses. To use the Eulerian method in LS-DYNA one must use LS-DYNA's ALE solver with a fixed mesh.

2.2.1 Limitations

The ALE solver in LS-DYNA is not perfect. Through the literature study some limitations have been discovered.

The ALE solver in LS-DYNA is developed to handle short duration problems with high pressure and velocity gradients, [Day, 2010]. Due to this fact, the solver is not well suited for problems lasting more than a few seconds or for problems with low pressure gradients.

There are often problems in the coupling between the Lagrangian and ALE/ Eulerian solvers as mentioned in Anghileri et al. [2005]. Tuning the coupling stiffness is often necessary to achieve a correct fluid structure interaction. With a too soft coupling there will be excessive leakage, and with a too stiff coupling the coupling may become too stiff. A large coupling stiffness will also reduce the time step driving up the computation time.

The ALE solver in LS-DYNA is based on conservation laws with the material behavior uncoupled from the system of governing equations. In traditional CFD-type Navier-Stokes solvers, the material behavior variables can be explicitly integrated into the equations. The solver does not account for boundary layer effects such as drag, and cannot handle turbulent dominated processes. Effects of fluid viscosity are only included through material model as dynamic viscosity, [Day, 2010].

Chapter 3

Finite element analysis in LS-DYNA

LS_DYNA is used to run the numerical simulations in this thesis. A brief presentation of relevant features is given below. Unless stated otherwise, the information is found in LS-DYNA Theory manual [2006].

3.1 Time integration

The central difference method is used to solve the equations of motion. Eq. 3.1 shows the semi- discrete equations of motion at time n .

$$\mathbf{M}\mathbf{a}^n = \mathbf{P}^n - \mathbf{F}^n + \mathbf{H}^n \quad (3.1)$$

here \mathbf{M} is a diagonal mass matrix, \mathbf{a} the nodal acceleration, \mathbf{P} external and body forces, \mathbf{F} the stress divergence vector and \mathbf{H} the hourglass resistance. The central difference method is used to solve the equation for t^{n+1}

$$\mathbf{a}^n = \mathbf{M}^{-1} (\mathbf{P}^n - \mathbf{F}^n + \mathbf{H}^n) \quad (3.2)$$

$$\mathbf{v}^{n+1/2} = \mathbf{v}^{n-1/2} + \mathbf{a}^n \Delta t^n \quad (3.3)$$

$$\mathbf{u}^{n+1} = \mathbf{u}^n + \mathbf{v}^{n+1/2} \Delta t^{n+1/2} \quad (3.4)$$

$\Delta t^{n+1/2}$ is defined as

$$\Delta t^{n+1/2} = \frac{\Delta t^n + \Delta t^{n+1}}{2} \quad (3.5)$$

here \mathbf{u} is the nodal displacement and \mathbf{v} the nodal velocity. The geometry is updated by adding the displacement increments to the initial geometry

$$\mathbf{x}^{n+1} = \mathbf{x}^0 + \mathbf{u}^{n+1} \quad (3.6)$$

Figure 3.1 shows an example of a time integration loop.

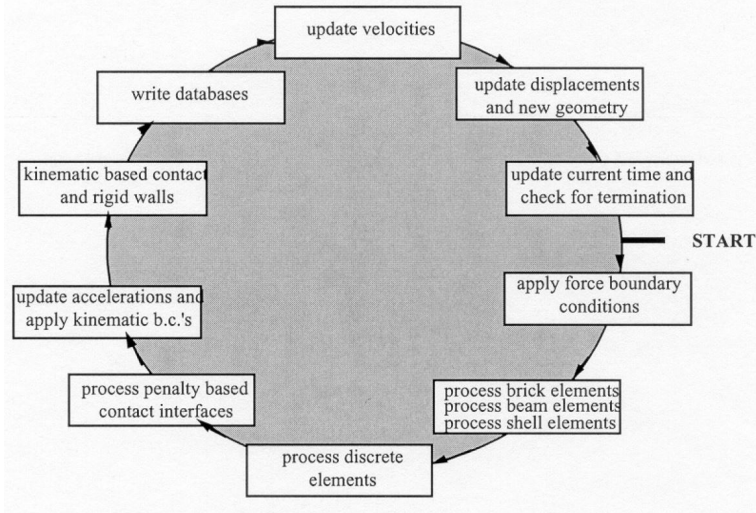


Figure 3.1: Time integration loop, LS-DYNA Theory manual [2006].

3.2 Time step size

To ensure the stability of the explicit solver, the time step in the analyses must be smaller than the critical time step. Two factors controlling the size of the time step are the time it takes a pressure wave to pass through an element and contact between two bodies. For shell elements the critical time step is given by [Time step size, 2014]

$$\Delta t_c = \frac{L_c}{c} \quad (3.7)$$

here L_c is the characteristic element length and c is the speed of the stress wave (sound) in the material. The default option is used for calculating L_c :

$$L_c = \frac{A_s}{\max(L_1, L_2, L_3, L_4)} \quad (3.8)$$

A_s is the surface area of the element and L_n is the length of the element sides. A safety factor of 0.9 is used in the analyses to ensure that the critical time step is not violated.

3.3 Lagrangian modeling

3.3.1 Element type

Belytshco-Lin-Tsay shell element

The shell element type used for all the shell elements in in this thesis is the Belytshco-Lin-Tsay shell element. Five through thickness integration points are used in all the analyses. The reason for using this element type is due to its computationally efficiency. For a shell element with five integration points, the Belytshco-Lin-Tsay element needs 725 mathematical operations. Another element type implemented in LS-DYNA, the Hughes-Liu element, needs 4050 mathematical operations. The efficiency of the Belytshco-Lin-Tsay shell element is due to the fact that it is based on a combined co-rotational and velocity-strain formulation. The co-rotational portion of the formulation helps the element avoid some of the complexities of non- linear mechanics by letting the coordinate system follow the element.

Solid elements

Solid hex elements are used to model solid rigid parts in this thesis. Element formulation 1 is used giving the elements constant stress.

3.3.2 Material models

Two material models are used in this thesis for the Lagrangian parts. A user defined material model with a fracture criterion is used for the deformable parts. The rigid parts are modelled with a rigid material.

Rigid material

The rigid material is very cost efficient since no storage is allocated to history variables for elements with rigid material properties. Correct values for the Young's

modulus, density and Poisson ratio should be used to get the correct sliding effect in contact simulation.

To allow different rigid parts to be connected to each other, a card called `CONSTRAINED_RIGID_BODIES` is used. This card merges the rigid bodies while maintaining the correct mass distribution.

User defined material with fracture criterion

Information about the user defined material model is found in Alsos et al. [2009]. A summary is given below.

Predicting fracture initiation and propagation is especially important for structural members which resist accidental forces, such as ship collisions, by membrane action. To predict fracture accurately, a material model with a suitable fracture criterion must be used. The deformable material model used in the analyses, is a user defined material model that uses a modified power law hardening as a basis. The stress strain relationship is shown in Eq. 3.9. The material model includes an element size dependent fracture criterion.

$$\sigma_{eq} = \begin{cases} \sigma_Y & \text{if } \varepsilon_{eq} \leq \varepsilon_{plat} \\ K (\varepsilon_{eq} + \varepsilon_0)^n & \text{otherwise} \end{cases} \quad (3.9)$$

$$\varepsilon_0 = \left(\frac{\sigma_Y}{K} \right)^{\frac{1}{n}} - \varepsilon_{plat} \quad (3.10)$$

where

σ_{eq} - equivalent stress.

σ_Y - initial yield stress.

K - strength coefficient.

n - material parameter.

ε_{eq} - equivalent strain.

ε_{plat} - equivalent plastic strain at plateau exit.

The fracture criterion used in the material model is the RTCL damage criterion which is composed of the modified Cockcroft- Latham- Oh damage criterion and the Rice- Tracey damage criterion. Both models are functions of the hydrostatic stress state. The expression for the RTCL damage criterion is shown below.

$$D = \frac{1}{\varepsilon_{cr}} \int \dot{D} dt \quad (3.11)$$

where

$$\dot{D} = \begin{cases} 0 & \text{if } T < -1/3 \\ \frac{\sigma_1}{\sigma_{eq}} \dot{\varepsilon}_{eq} & \text{if } -1/3 \leq T < 1/3 \\ \exp\left(\frac{3T-1}{2}\right) \dot{\varepsilon}_{eq} & \text{otherwise} \end{cases} \quad (3.12)$$

and

$$T = \frac{\sigma_m}{\sigma_{eq}}$$

σ_m - hydrostatic stress.

\dot{D} - rate of damage.

σ_1 - major principle stress.

$\dot{\varepsilon}_{eq}$ - rate of equivalent strain.

ε_{cr} - critical equivalent strain.

In ship collisions, the structures undergoing severe deformation are generally modelled with elements with a characteristic length of 5- 15 times the plate thickness. It is of course impossible to detect local instabilities with such large elements since failure mechanisms such as necking, typically take place in narrow bands as wide as the plate thickness. However, reducing the elements size will force the time step to drop, driving up the computation time significantly. A remedy is to make the failure criterion element size dependent by scaling the failure strain.

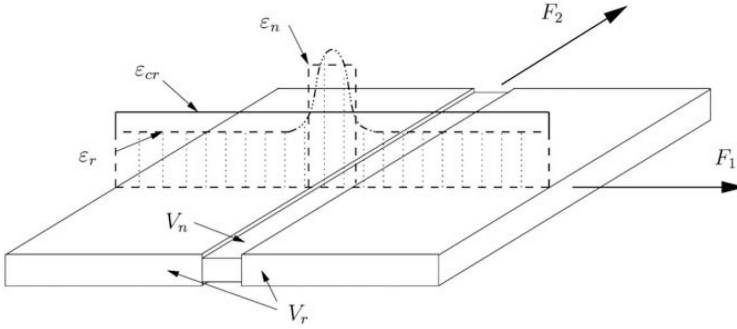


Figure 3.2: Element necking model

Considering an element at failure, Figure 3.2, the average critical strain can be expressed as

$$\varepsilon_{cr} = \frac{\varepsilon_r V_r + \varepsilon_n V_n}{V_{el}} \quad (3.13)$$

V_{el} is the volume of the element, while V_n is the volume of the neck and V_r is the difference between the two. ε_n and ε_r are the average strains for V_n and V_r .

Assuming that the neck forms parallel to one of the element sides and has a width equal to the element thickness t , the volume of the neck can be expressed as Eq. 3.14. The volume of the remainder of the element can then be written as Eq. 3.15.

$$V_n = t^2 l_e \quad (3.14)$$

$$V_r = t l_e^2 - t^2 l_e \quad (3.15)$$

l_e is the length of the undeformed element and t is the thickness.

Inserting Eqs. 3.14 and 3.15 into Eq. 3.13 gives an element size dependent critical strain.

$$\varepsilon_{cr}(l_e) = \varepsilon_r + (\varepsilon_n - \varepsilon_r) \frac{t}{l_e} \quad (3.16)$$

It should be noted that correcting the failure level as a function of the element size can give poor results. Fracture can occur without the creation of local deformation mechanisms. Element size scaled fracture criterions should therefore be applied with caution.

3.3.3 Contact

For contact between the Lagrangian parts, LS-DYNAs standard penalty based formulation is used. At each time step LS-DYNA checks if a slave node penetrates through a master segment. If penetration is discovered, a contact force is applied to remove the penetration. The force is applied between the slave node and its contact point and is proportional to the penetration.

3.4 Eulerian

3.4.1 Mesh and element type

The ALE mesh should consist of hexahedral elements with reasonable aspect ratios. Element shapes such as tetrahedrons and pentahedrons should be avoided. Degenerate element shapes may lead to reduced accuracy and perhaps numerical instability during the advection. The ALE elements should have approximately the same size as the Lagrangian elements where coupling is to take place.

Solid hex elements are used to model the water and air in the collision environment. The element type used is element formulation 11. This element type has one integration point and is capable of modeling multiple materials. The element formulation is the most versatile and widely used element formulation for ALE analyses in LS-DYNA.

When element formulation 11 is used, multiple materials can exist inside the ALE mesh. To track a specific material, the material must be assigned to a unique ALE multi-material group (AMMG). Only parts sharing identical material properties may be included in the same AMMG.

Since two or more materials can be in the same element simultaneously, the material boundaries do not generally coincide with the mesh lines. The material interfaces are internally reconstructed at each time step based on the volume fractions of the materials within a specific element. [Day, 2010].

3.4.2 Material models

To model the fluid and air, the NULL material is used. Equations of state can be called through this model to avoid deviatoric stress calculations. A viscous stress and a pressure cut off may also be specified.

3.5 Fluid structure interaction

The interaction between ALE parts and Lagrangian parts is in LS-DYNA defined in the *CONSTRAINED_LAGRANGE_IN_SOLID card. Here, parameters such as the coupling algorithm, coupling stiffness, number of coupling points and where the coupling is to take place, defined. The specific Lagrangian parts and ALE materials that are to interact are also defined.

The FSI works in the following matter. The program searches for Lagrangian parts inside the area where coupling is to take place. The area where coupling is to take place is defined by an ALE mesh. "If a coupled Lagrangian surfaces is detected inside an ALE element, LS-DYNA marks the Lagrangian- Eulerian coupling points (NQUAD) at t^- ", [Do and Day, 2014]. The coupling points are distributed over the Lagrangian elements. The independent motions of the two materials are then tracked over a time step to calculate the penetration distance. Finally coupling forces are calculated and redistributed to the materials based on the penetration.

Coupling forces are normally computed based on a penalty method which is similar to the penalty method used for standard Lagrangian contact. Penalty based coupling is generally favored since it conserves energy and is robust. The drawback with the penalty based coupling method is that it is subject to leakage. Figure 3.3 shows a sketch of the penalty coupling algorithm.

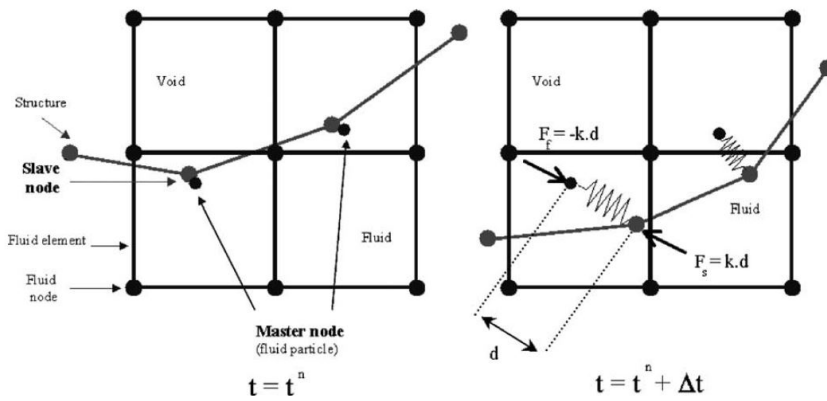


Figure 3.3: Sketch of penalty Eulerian-Lagrangian penalty coupling, Aquelet et al. [2006].

Chapter 4

Fluid and FSI modeling in practice

Although there is some literature presenting results from collision analyses with internal fluid structure interaction (FSI), none of the articles present the modeling technique in detail. Learning how to model fluids has been done by following recommendations in Day [2010] and Do and Day [2014], and also by using examples these refer to. Keyword Manual [2007] has also been used actively.

4.1 Environment

Modeling of a fluid environment is performed by following small examples presented in Day [2010], and through trial and error. Using the examples actively, an environment with a stable pressure was successfully modeled, Figure 4.1. The environment has the correct theoretical value for the static pressure at the bottom of the environment. Elements along the free surface allow for inflow and outflow while keeping the correct pressure along the boundaries. Some important commands used to model the initial environment conditions are listed below. The water is given a density of 1025 kg/m^3 and the air 1.185 kg/m^3 .

- ***LOAD_BODY:** Gives a constant acceleration to all parts in the model. Necessary to create pressure in the water.
- ***INITIAL_HYDROSTATIC_ALE:** Reduces the time it takes to initialize the hydrostatic pressure.
- ***DAMPING_PART_MASS:** Is used to minimize pressure oscillations in the pressure initialization phase. Damping is turned off once the pressure is stabilized.

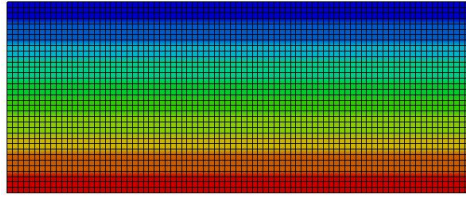


Figure 4.1: Water environment with stable pressure.

- ***EOS_LINEAR_POLYNOMIAL:** Is used to determine the hydrostatic, or bulk, behavior of a material. This card is used to describe both water and air.
- ***ALE_AMBIENT_HYDROSTATIC (AAH):** Can be used to create a boundary with a correct pressure allowing for inflow and outflow. Surrounding the sides and bottom of the regular ALE domain with layer of elements defined as ambient parts (parts with AET=4 under *SECTION_SOLID), AAH can be applied to give the correct hydrostatic pressure along the boundaries.
- ***BOUNDARY_SPC_SET:** Is used to fix the four lateral sides and the bottom of the environment. The sides are fixed in the normal direction and are free in-plane.
- ***INITIAL_VOLUME_FRACTION_GEOMETRY:** Can be used to replace the water inside a structure with air or vice-versa before the analysis begins.
- ***CONTROL_ALE:** A control for the ALE formulation is needed. Among other things, the motion of the mesh and which solver to use is defined here.

4.2 Fluid structure interaction

4.2.1 Procedure

Learning how to model the FSI proved to be a time consuming and difficult task. Due a lack of literature, modelling of the FSI has been mostly self-taught through trial and error and by using Keyword Manual [2007].

Two dimensional box impact

The first step in the modelling procedure was to get a correct fluid structure interaction for a simple geometry. A fluid structure interaction example was found, ref. DYNA Examples [2014]. Using the example file actively, the fluid structure

interaction of a two dimensional box impacting a pool of water was successfully modeled. Figure 4.2 shows the box impacting the water. The height and width of the box are 1 and 2 m respectively. The standard element size used both to model the box and the water is 0.05 m. Solid elements are used for both the box and the water. The FSI seems to be reasonable when comparing the response of the water to experience. It is also seen that the static displacement is correct. At 50 seconds the box is floating with a correct draft of 0.5 m.

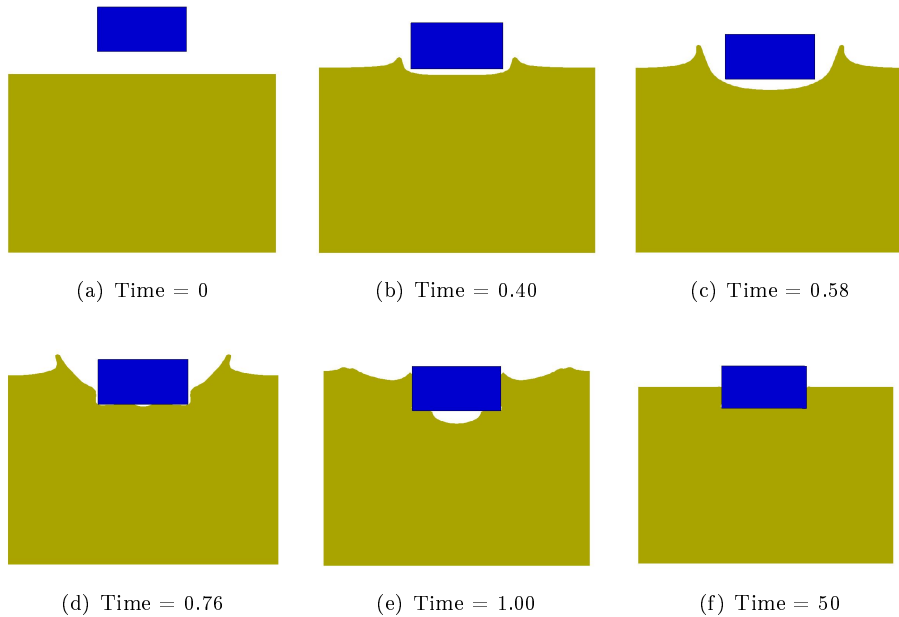


Figure 4.2: Two dimensional box impacting water.

Three dimensional box impact

With good results for a two dimensional case, a three dimensional case was modeled. Here the environment is modelled according to 4.1. Since the platform used later will have shell elements, shell elements were used to model a box. The dimensions of the box are (HxWxD) 2x2x1 m. The mesh size used for box and water are 0.15 m and 0.1 m, respectively.

Using parameters similar to the ones used for the two dimensional case for the FSI gave poor results. The initial phase where the box impacted the water seemed reasonable, Figure 4.3, but there was excessive leakage and the box could not find a reasonable equilibrium after impact.

Following recommendations in Keyword Manual [2007] to control leakage, IKLEAK was changed to two. This resulted in less leakage. However, changing the leakage

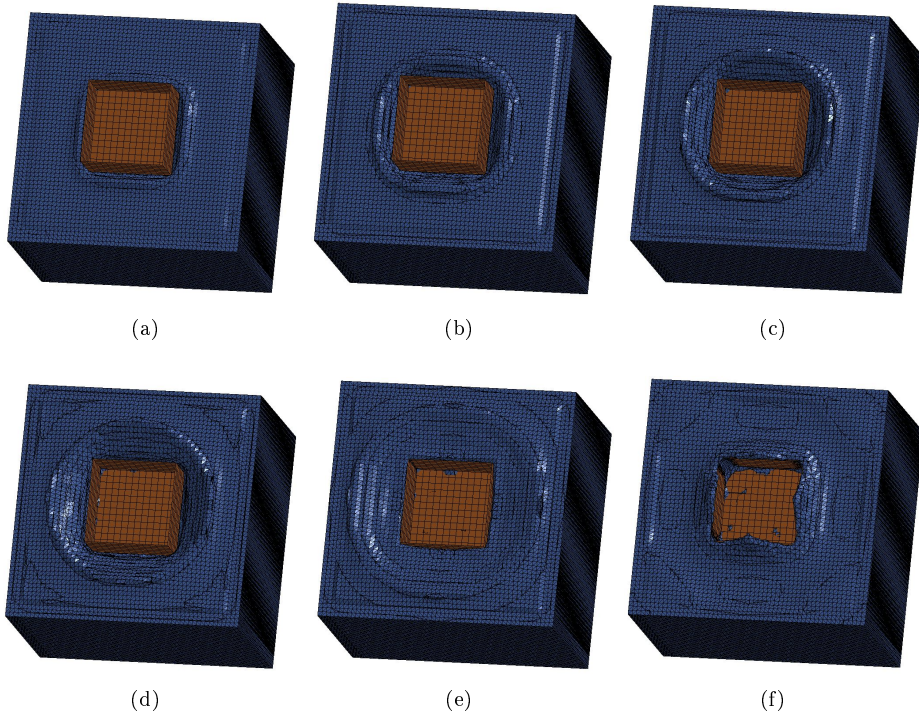


Figure 4.3: Three dimensional box impacting water.

parameter to two gave the box unrealistic movements in all directions. The box could not find an equilibrium. Attempts were made to control leakage while reducing the spurious motions, but the attempts were not successful. It was noticed that the box was able to find equilibrium when a large damping in the `DAMPING_PART_MASS` card was present. The large damping was however very unrealistic.

The results for the three dimensional box are not very good. More work could have been done tuning the FSI. A smaller mesh could have also been used. The reason for moving away from the box is due to the fact that sharp corners are difficult for the program to handle and may be part of the reason for the poor results.

FSI with Octopus

An analysis with a shell model of Moss Maritimes Octopus was created. The shell model is created using rigid shell elements. The goal for the analysis was to achieve a static equilibrium, where the platform floats at a constant draft, and hopefully retrieve added mass constants. Due to the size of the model, the platform will start in equilibrium in the analyses. The environment used in the analyses is modeled according to 4.1.

The element size used in the analysis is 2 m for the structure, water and air. Elements for the different parts have an equal size since Day [2010] stated that elements should roughly have the same size where coupling takes place. The element size is chosen on the basis of element sizes used in Gagnon and Wang [2012] and Lee and Nguyen [2011], where element sizes of 2 and 3 m were used to model the fluid, respectively.

Initially the parameters used to model the platform were similar to the parameters used for the case with the three dimensional box. The use of these parameters gave poor results. When ILEAK was equal to two the platform had spurious motions, and when ILEAK was equal to zero leakage was a problem. Following recommendations in Keyword Manual [2007] the PFAC parameter was changed from a constant to a curve. A lot of time was used to tune the curve and other parameters to produce better results.

After many attempts of tuning the parameters without an acceptable result, the model was sent to LS-DYNA support in Sweden. One of the first comments they had was that the mesh at the center of the bottom of the platform was poor and would like to re-mesh it. The before and after meshes are presented in Figure 4.4. It was not certain that the mesh would affect the results, but it is good modelling practice to use the best possible mesh in analyses.

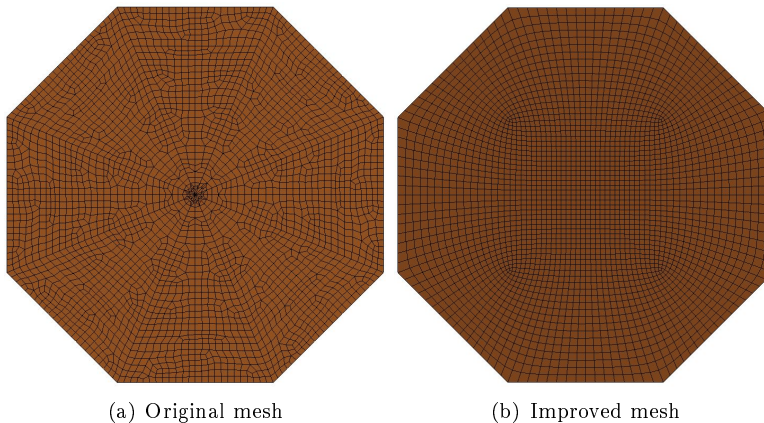


Figure 4.4: Improvement of Octopus mesh.

Many of the changes LS-DYNA support did had a large effect on the computation time. The computation time went from 12 hours on 160 cores to 22 min on 32 cores. Among other things, the bulk modulus was reduced by a factor of approximately 20 to $1e8$ Pa. The results were however not impressive. Figure 4.5 shows the motions of the platform for a 20 second analysis. The platform is supposed to be in equilibrium at the start of the simulation.

As the results from the analysis with a mesh size of two meters did not give a

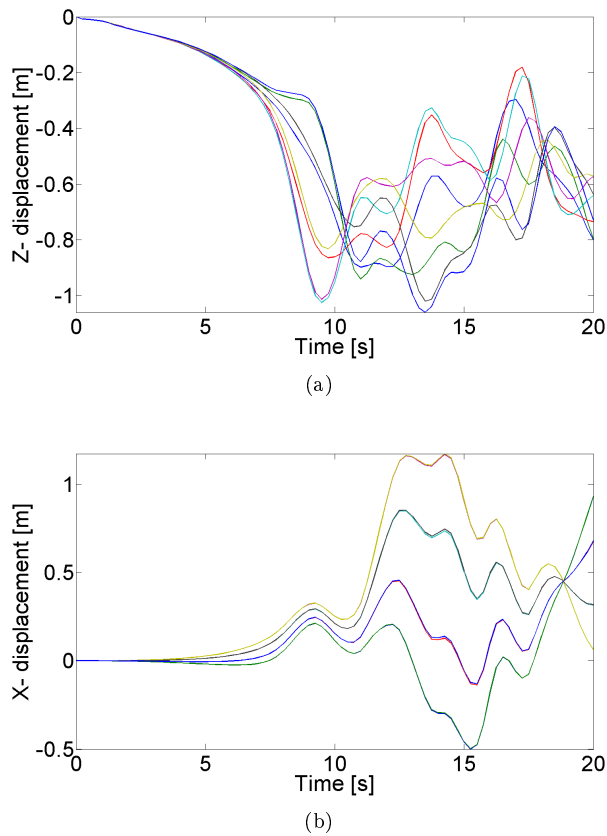


Figure 4.5: Motions of the Octopus floating in water with a mesh size of two meters.

satisfactory results, LS-DYNA support was contacted again to help improve the model. It became clear that in order to achieve better results, a finer mesh must be used. It was pointed out that it may also help to remove sharp corners from the model.

The Octopus and the environment were re-meshed with one meter elements and the bilge keels sharp corners were replaced with rounder edges. Figure 4.6 shows the results from the analysis with one meter elements. It is seen that the platform is not in complete equilibrium, but the motions are quite small. Considering the fact that the ALE solver is developed to handle short duration problems with high pressure gradients, the results are satisfactory.

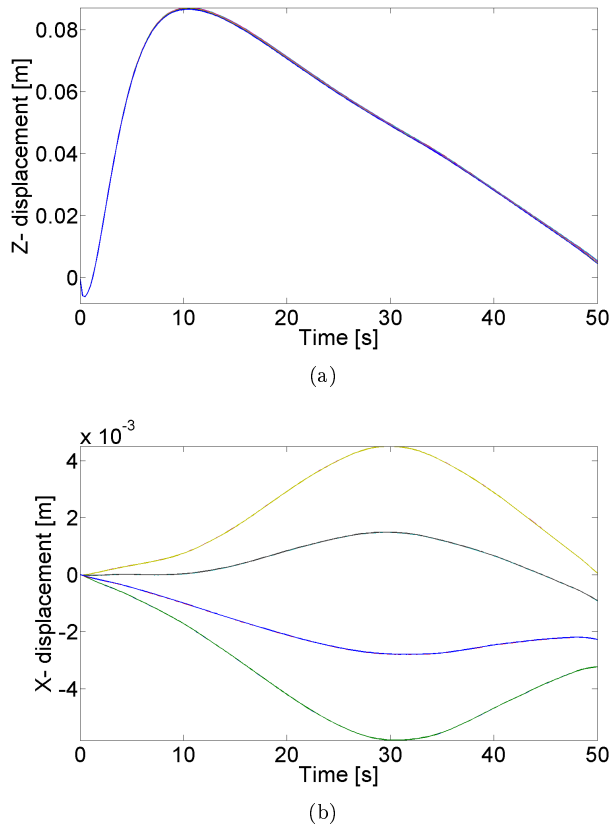


Figure 4.6: Motions of the Octopus floating in water with a mesh size of one meter.

4.2.2 Final parameters

The final parameters defining interaction between the Lagrangian parts the Eulerian parts are shown in Table 4.1. The `CONSTRAINED_LAGRANGE_IN_SOLID` card is used to define the interaction. The parameters presented here are the parameters that gave the platform the most realistic buoyancy. The effects of the parameters on added mass is not taken into account when determining their value.

The most physically correct parameter is not used for DIREC, the coupling direction. Coupling only in compression (`DIREC =2`) gives the best representation of reality. However, under recommendation from LS-DYNA support in Sweden, `DIREC` equal to 1, coupling in tension and compression, is used although Keyword Manual [2007] states that `DIREC` equal to 2 should give the best results.

A negative value for `MCOUP` specifies that the interaction is to take place between

Table 4.1: Important parameters for the `CONSTRAINED_LAGRANGE_IN_SOLID` card.

Variable	Function	Value
NQUAD	Number of coupling points	3
CTYPE	Coupling type	4 (penalty based)
DIREC	Coupling direction	1 (compression and tension)
MCOUP	Material to couple to	Negative
PFAC	Penalty factor	Curve
FRCMIN	Volume fraction to activate coupling	0.3
NORMTYP	Penalty spring direction	1
DAMP	Damping factor	0.1
ILEAK	Leakage control	0 (None)

the defined Lagrangian part and a specific ALE material. Which ALE material is to participate in the interaction is determined by the value negative number used.

To improve the interaction, the volume fraction to activate coupling is reduced from the default value to 0.3. The reduction gave an increase in computation time. A small value for the damping gave also better results, so a value of 0.1 was used.

When a negative value for PFAC is used, the stiffness in the interaction is defined using a user defined curve. The curve used in the analyses consists of two points. The first point is 0,1 and the second point is $5e-2$, $1e6$. Further increasing the stiffness gave similar results and drove up the computation time.

Leakage control gives generally less leakage. The results with and without leakage control were for this case very similar. Leakage control was therefore not used since spurious motions occurred when leakage control was used earlier.

4.2.3 Validating model

The interaction has been checked using three methods. The first is visual inspection, i.e. seeing that the FSI interaction behavior of the Octopus seems realistic. The second method used to verify the FSI is by checking the Octopus' mass compared to the draft at "equilibrium". The last is by checking the platforms added mass.

Visual inspection

Studying the air inside of the Octopus, which should have the same shape as the Octopus hull, it is possible to see the amount of leakage there is in the analysis. Figure 4.7 shows the air inside of the Octopus at the start and end of the analysis.

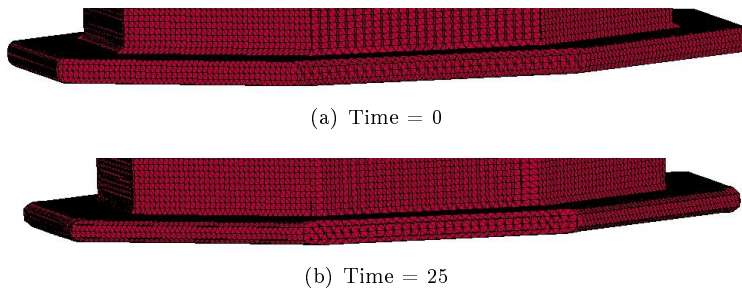


Figure 4.7: Leakage in the Octopus.

It is seen that the shape of the Octopus is very similar at the start and end of the simulation. However, if Figure 4.7 is studied closely it is seen that there is some leakage on Octopus' bilge keel. The corners are not as sharp at the end of the analysis as they are at the beginning. This is due to leakage and will reduce the Octopus' buoyancy.

An analysis is performed to see if the water reacts in a realistic manner. To get a visual result, the Octopus is given a rather large motion in surge. Figure 4.8 shows the wave that is created in front of the Octopus due to the motion. The wave looks realistic, and is not reflected by the boundary conditions. It is also seen that the water is sucked down behind the Octopus which is also correct according to experience.

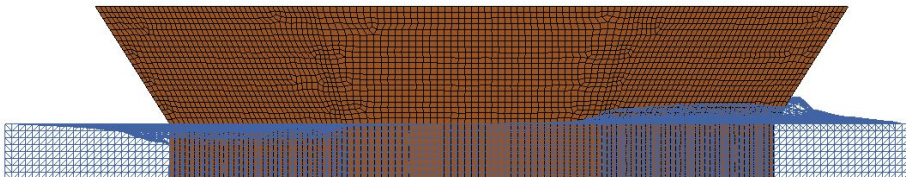


Figure 4.8: Force displacement curve with different hull angles.

Mass at equilibrium

In the Wadam analysis performed to calculate added mass values for the Octopus, ref. 6.1.3, the volume of the Octopus was accurately calculated. The displaced mass at a given draft is therefore given. Using a correct mass for the Octopus to float statically at the operation draft, it is seen that the platform sinks in LS-DYNA. The platform does however float with a motion similar of that in Figure 4.6 when the mass of the platform is reduced by 1 %. The buoyancy volume is less than it should be in LS-DYNA due to leakage, as seen in the visual inspection. The difference between the actual buoyancy and the buoyancy in LS-DYNA is small.

Added mass

Added mass estimates are calculated in LS-DYNA by forcing the Octopus to oscillate by applying a harmonic force history in the x- direction (surge). The platform is fixed in the y- and z- direction to isolate the x- motion. Using the time history for the platforms accelerations and displacement, added mass coefficients for the Octopus in surge were calculated for seven different frequencies. The added mass coefficients are found using the following procedure.

The time instant for maximum displacement is found. At this time the velocity of the Octopus will be zero. When the velocity is zero, the only contribution from the Octopus will be inertia forces, Eq. 4.1

$$(M + A_{11})\ddot{x} + B_{11}\dot{x} = F(t) \quad (4.1)$$

Here M is the mass of the platform, A_{11} is the added mass in surge, B_{11} is the damping constant in surge and $F(t)$ is the harmonic force. \dot{x} and \ddot{x} is the velocity and acceleration of the platform, respectively.

The added mass coefficient is found by solving Eq. 4.1 with respect to A_{11} and using the value for the acceleration and force at the time instant where the velocity is zero. The values are made dimensionless by dividing the added mass with the real mass of the platform at the given draft. The results are plotted against the added mass values from the Wadam analysis, ref. 6.1.3, in Figure 4.9.

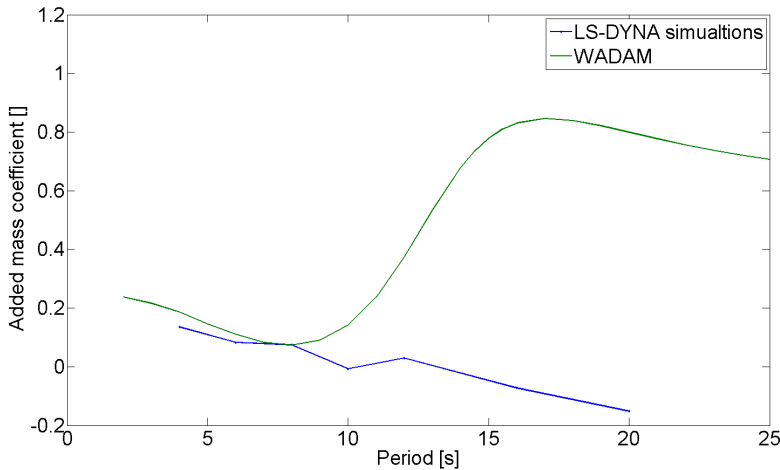


Figure 4.9: Comparison of added mass coefficients from LS-DYNA and Wadam.

It is seen that the added mass values calculated in LS-DYNA are very close to the values calculated in Wadam for periods of 4, 6 and 8 seconds. The added mass

values calculated from the LS-DYNA simulation for larger periods, 10, 12, 16 and 20 seconds, do not coincide with the values calculated in Wadam at all. For 10 and 12 s the added mass coefficients are around zero and for 16 and 20 s the added mass coefficients are negative. Having zero as an added mass coefficient means that the water does not add inertia effects to the equation of motion. Having negative values however, mean that the water reduces the inertia effects. This is strange, and may be due to a modelling error. To verify that the platform had the correct mass in the analyses an analysis was performed without FSI. The analysis confirmed the mass of the platform.

One of the limitations presented in 2.2.1 states that the ALE solver is developed to handle problems with large pressure gradients that last over a short period of time. The problem at hand does not satisfy any of these demands. This may however be a clue to why the results are better for small periods. For small periods the duration of the problem will be shorter and the pressure gradient larger. Although the results for small periods are close to each other, more analyses should be performed before conclusions can be made.

Conclusion

Through visual inspection and by checking the displaced volume of the structure, the FSI seemed to be fine. The error in buoyancy is acceptable for a collision analysis. However, when checking the added mass it is seen that the added mass contribution is not properly taken care of in LS-DYNA. The added mass coefficients were reasonable for small values, but completely wrong for periods above 10. The collision between a tanker and a platform will typically last between 5 and 10 seconds making the added mass values for double these periods important. With the parameters used in this thesis it is unlikely that a collision analysis with FSI will give realistic results. More work should be performed to find more adequate parameters for the ALE modeling.

Chapter 5

Collision analyses with internal FSI

The effects of ballast water in the ballast tank during a collision is investigated in this chapter. Previously some research has been done investigating the effects of liquids in cargo tanks in collisions, Zhang and Suzuki [2006]. However, no literature has been found studying the effects of liquids in ballast tanks, or ship tanks that deform during a collision.

5.1 Analysis set- up

To clearly and easily see the effects of the ballast water, a simple ballast tank construction is used for the collision analyses. The ballast tank is shaped as a rectangular prism with dimensions 5x5x2 m (breadth x height x depth). Figure 5.1(a) shows a finite element model of the shell of the ballast tank. There is a hole at the top of the ballast tank for ventilation. The ventilation hole is shaped as a square with 400 mm long edges.

The ballast tank is stiffened with horizontal stiffeners with a stiffener spacing of approximately 700 mm. The stiffeners on the long sides have a height of 300 mm while the stiffeners on the short sides have a height of 200 mm. Figure 5.1(b) shows the stiffening arrangement in the ballast tank. The shell of the ballast tank has a constant plate thickness of 15 mm.

Twelve different cases are analysed using the stiffened ballast tank. In all the cases a solid sphere with a radius of 3.625 m is used as the indenter while the ballast tank is fixed. Impact speed and filling levels are varied. Tables 5.1 and 5.2 show the different impact velocities and filling levels analysed. The mass of the sphere

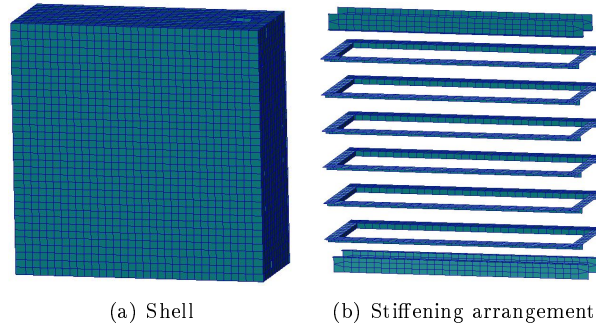


Figure 5.1: Stiffened ballast tank used for collision analyses.

is scaled so the kinetic energy of the sphere remains constant for all analyses. All filling levels are analysed for each velocity.

Table 5.1: Filling levels for ballast tank.

Name	Filling level [%]
Tank0	0
Tank07	0.7
Tank09	0.9
Tank095	0.95

Table 5.2: Mass of sphere and impact velocities.

Impact velocity [m/s]	Mass [kg]
2	97895441
5	1566327
8	611846

5.2 Finite element modelling

5.2.1 Software

The software used for the finite element modeling and numerical simulations are: MSC Patran, LS-PrePost and LS-DYNA. MSC Patran is used for establishing a finite element model of the ballast tank, and LS-PrePost for setting up the collision analysis. The very efficient non-linear finite element solver LS-DYNA is used for solving the numerical simulations. Post processing of the results is done in LS-PrePost and MATLAB.

5.2.2 Ballast tank and sphere

The ballast tank is modelled with Belyshco-Lin-Tsay elements with five integration points. Reasons for using this element type are mentioned in 3.3.1. The standard element size is 150 mm. Care is taken to ensure that there are at least three elements over the stiffeners height to achieve a proper bending stiffness during deformation. To simplify the modelling, the stiffener flanges are not connected to intersection geometry. They are only joint to the web of the stiffener. This simplification is often used when modeling stiffeners, and gives a good representation of reality.

The material model used for the ballast tank is an in house material model created for LS-DYNA with an RTCL fracture criterion. The material parameters used for the unstiffened ballast tank are shown in Table 5.3.

Table 5.3: Material parameters for the ballast tank.

Density [kg/m^3]	7850
Young's modulus [Pa]	2.07E+11
Poisson ratio	0.3
Shear modulus [Pa]	7.96E+10
Bulk modulus [Pa]	1.73E+11
Yield stress [Pa]	2.75E+08
Strength coefficient, K [Pa]	7.40E+08
Powerlaw exponent, n	0.24
Equivalent plastic strain at plateau exit	1.00E-02
Critical strain	0.71

The boundary conditions for the ballast tank are chosen as if the ballast tank was part of a ship. All the vertical edges of the ballast tank marked in Figure 5.2(a) are fixed in x- and z- directions. The fixed nodes are marked with a black cross. Figure 5.3 shows the collision set-up with a coordinate system. The vertical edges on the back of the ballast tank (not the impacting side) are in addition fixed in the y- direction. The longitudinal stiffeners (stiffeners in the x- direction) are fixed in the x- direction, Figure 5.2(b). The fixed nodes are also here marked with a black cross.

The sphere is modelled with rigid solid elements and is given a density to give the sphere a correct mass. To easily calculate how much kinetic energy is absorbed in the collision the sphere is only given an initial velocity in the y- direction and is fixed in the x- and z- directions. The energy dissipated in the collisions can then be calculated using the velocity-history of the sphere. Figure 5.3 shows the collision set- up.

A penalty based contact is used for both the contact between sphere and the shell of the ballast tank and for the contact within the ballast tank. A static friction coefficient of 0.3 is used in the analyses.

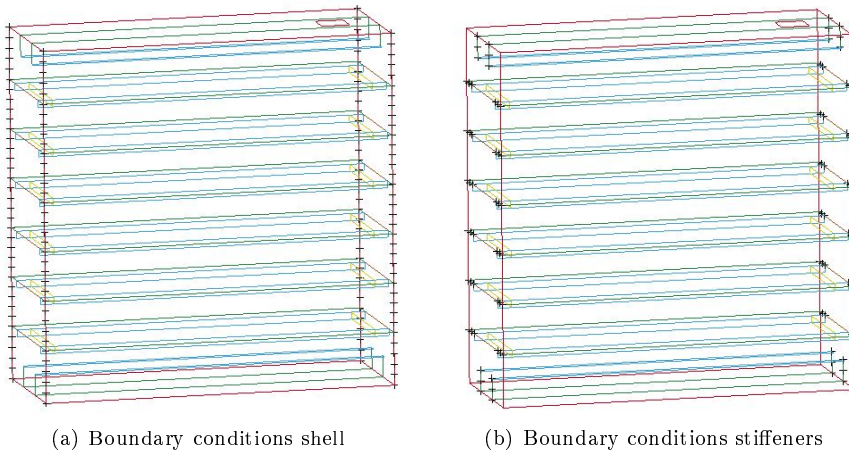


Figure 5.2: Boundary conditions for the ballast tank.

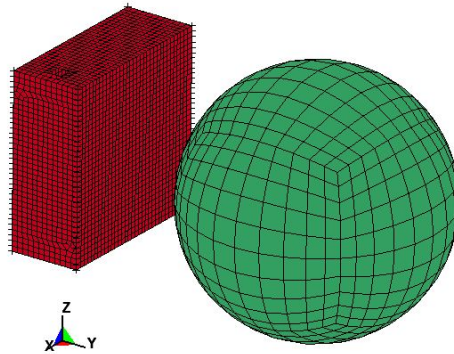


Figure 5.3: Collision set-up for a collision between a solid sphere and a ballast tank.

5.2.3 Water environment

The water environment consists of two parts, ref. Figure 5.4. The blue part represents the water, while the red part represents the air. The water part has a width of 5 m and a depth of 2 meters filling the ballast tank completely up to the desired water level. To avoid fluid structure interaction on element boundaries, a layer of three elements is modelled outside of the ballast tank. These elements are filled with air. The elements inside the ballast tank above the desired water level are also given air properties.

The air and water environment are modelled using solid hex elements with a typical element dimension of 0.15 m. Interacting elements (Lagrangian and Eulerian)

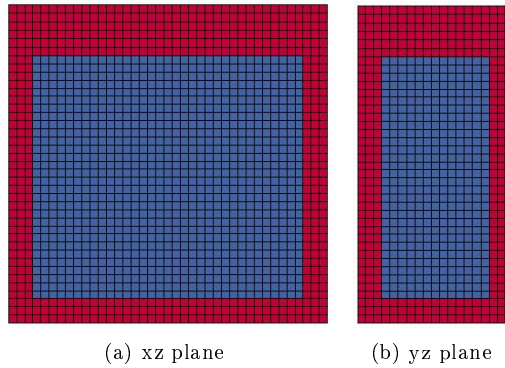


Figure 5.4: Air and water environment for the collision analyses with the unstiffened ballast tank.

should have approximately the same dimensions according to Day [2010]. The outer sides of the air environment are fixed in a pool like condition to keep the air from flowing out of the mesh during the analysis.

The water is given a density of 1025 kg/m^3 while the air is given a density of 1.185 kg/m^3 . To reduce the computation time, the waters' bulk modulus is reduced by a factor of 20. This reduces the computation time by a factor of almost 2. The bulk modulus used in the analyses is $1\text{e}8 \text{ Pa}$. To confirm that reducing the bulk modulus does not change the results sufficiently, an analysis with a real bulk modulus is compared to an analysis with a reduced bulk modulus, Figure 5.5. The differences between the two analyses are small, supporting the reduction of the bulk modulus.

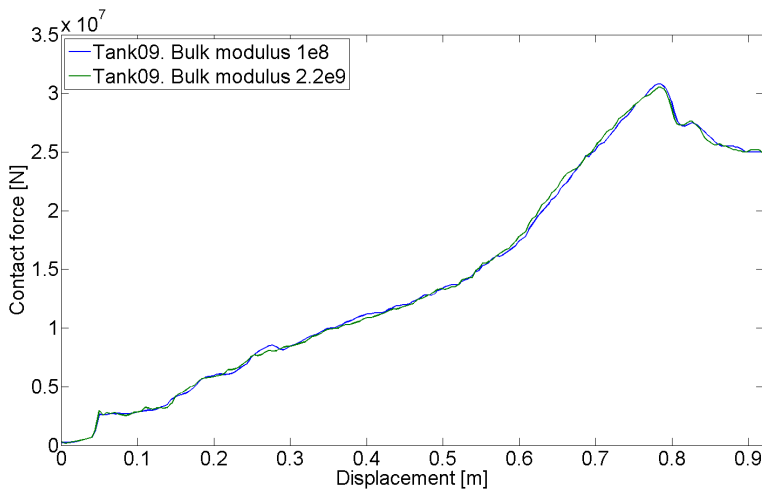


Figure 5.5: Effect using a reduced bulk modulus.

5.2.4 Fluid structure interaction

The interaction between the water and the ballast tank is defined using the *CONSTRAINED_LAGRANGE_IN_SOLID card. Since the ballast tank has sharp corners, a rectangular grid of 3x3 coupling points are used in addition to the element nodes, (NQUAD = -3). To simplify the analysis, FSI is only defined between the shell of the ballast tank and the water inside the ballast tank. The air and the stiffeners do not participate in the interaction.

Three cases were run to see the effect of increasing the number of coupling points, Figure 5.6. The cases were run with both NQUAD = -3 and NQUAD = -6 (3x3 grid and 6x6 grid in addition to the nodes). It is seen that the number of coupling points has some effect on the result. The difference is however not of practical importance. The reason for using NQUAD = -3 and not = -6 for the analysis has to do with the computation time. Increasing NQUAD to -6 resulted in more than a doubling of the computation time.

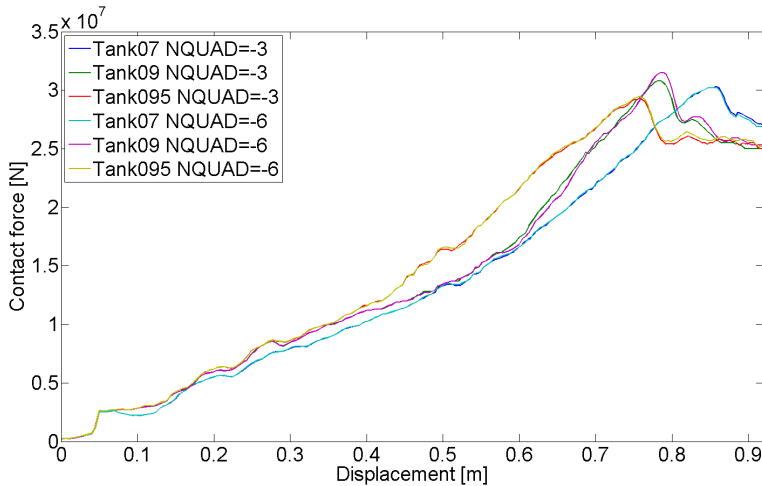


Figure 5.6: Effect increasing of number of coupling points.

The penalty factor for the interaction between the water and the shell of the ballast tank is defined with a user defined curve. Since large pressures may arise during the collision, a very stiff loading curve is used. The loading curve is defined using two points; 0,1 and 1e-2, 5e7.

Figure 5.7 shows the pressure in the ballast tank before the collision. It is seen that the pressure distribution is not perfect. The Eulerian and Lagrangian materials are constantly coupling to prevent the fluid for leaking out of the tank. The coupling forces give small changes to the pressure distribution.

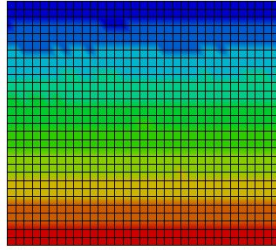


Figure 5.7: Static pressure in the ballast tank before the collision.

5.3 Results

The results from the analyses are presented in this chapter. Only the most important results are presented here, i.e. the force- displacement curves and energy dissipation- displacement curves. The analyses are all stopped when the displacement reaches 0.92 m.

5.3.1 Force displacement curves

The force displacement curves are created by plotting the contact force between the sphere and the ballast tank against the largest indentation on the impacted side of the ballast tank. The force displacement curves are presented in Figures 5.8 to 5.10.

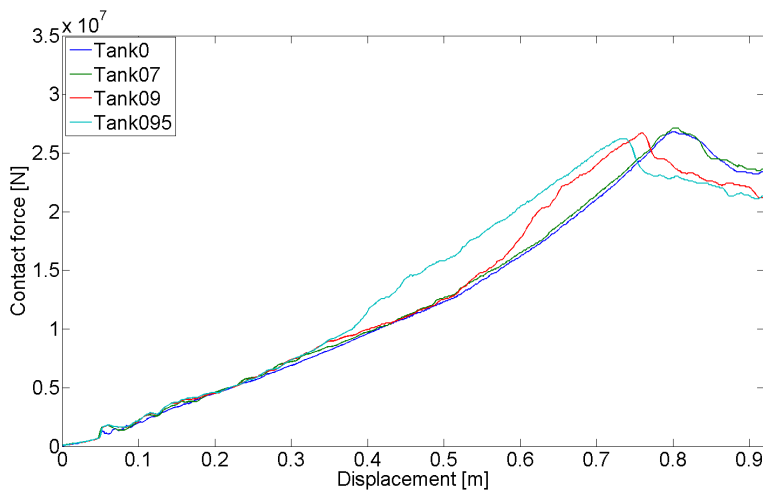


Figure 5.8: Force-displacement curves for a ballast tank with different filling levels. Impact speed 2 m/s.

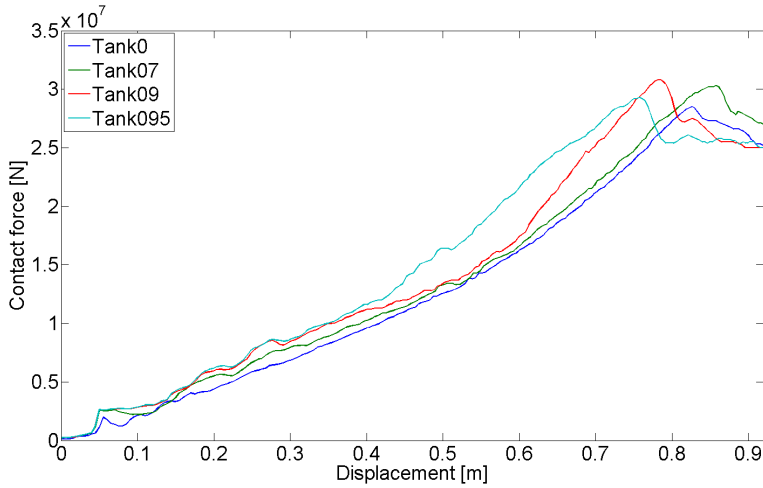


Figure 5.9: Force- displacement curves for a ballast tank with different filling levels. Impact speed 5 m/s.

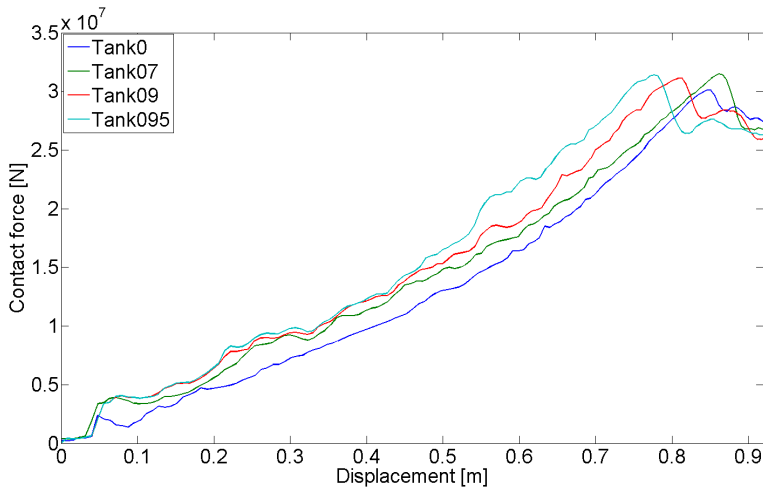


Figure 5.10: Force- displacement curves for a ballast tank with different filling levels. Impact speed 8 m/s.

It is seen that the contact force is larger for a given displacement for higher filling levels. It is also seen that the increase in contact force is larger for increased impact velocities.

The force displacement curves for the different velocities are unfortunately not directly comparable. The maximum load is larger for higher velocities due to

dynamic effects, Figure 5.11.

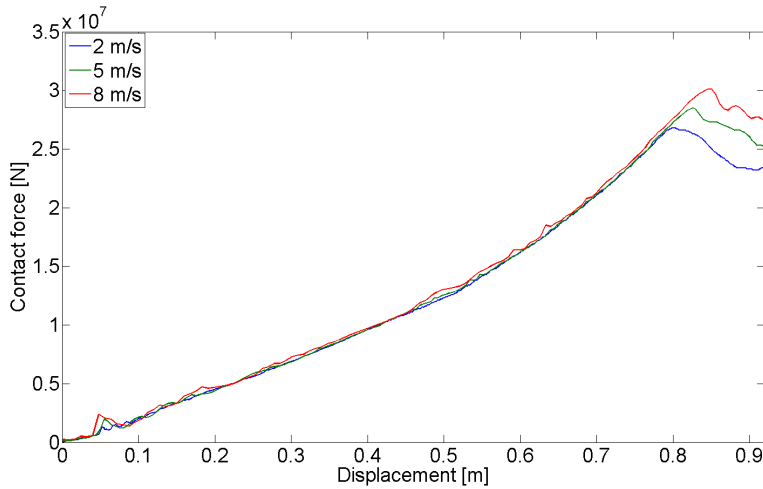


Figure 5.11: Force- displacement curves for an empty ballast tank with different impact velocities.

5.3.2 Dissipated energy- displacement curves

The energy dissipation- displacement curves are created similarly to the force displacement curves. The energy absorbed in the collision is plotted against the largest indentation on the impacted side of the ballast tank. The energy absorption is calculated using the change of the spheres kinetic energy. Since energy cannot disappear, the energy must be absorbed by the ballast tank and the water inside.

The energy dissipation- displacement curves are presented in Figures 5.12 to 5.14. It is seen that the tanks with the highest filling levels absorbed the most energy. The difference between empty and water filled tanks is the largest for the highest impact velocity.

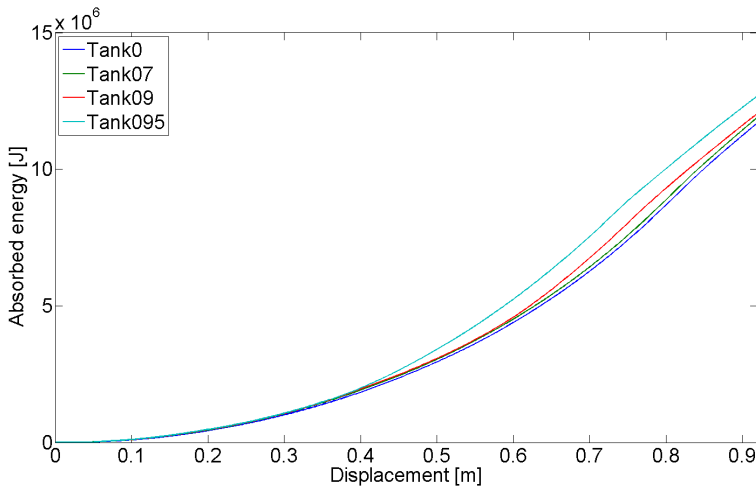


Figure 5.12: Dissipated energy- displacement curves for a ballast tank with different filling levels. Impact speed 2 m/s.

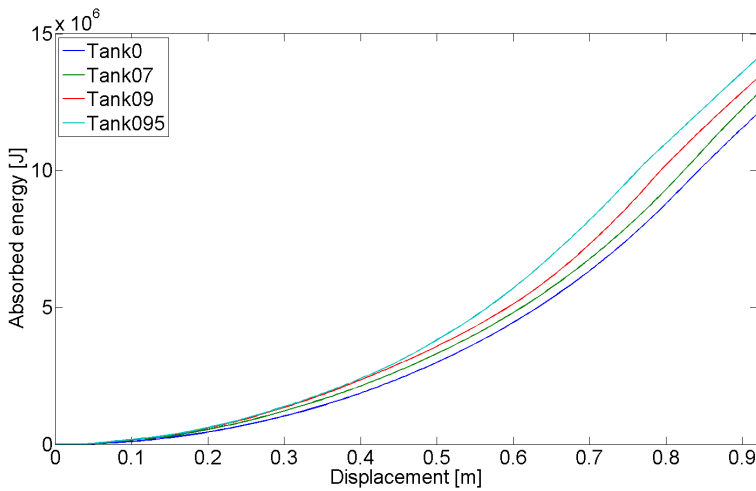


Figure 5.13: Dissipated energy- displacement curves for a ballast tank with different filling levels. Impact speed 5 m/s.

5.4 Discussion

The results are discussed in this section. It is seen that the effect of ballast water is the largest for the highest impact velocity. For the smallest impact velocity, the effect of ballast water is small before there is a sudden change in the slope for

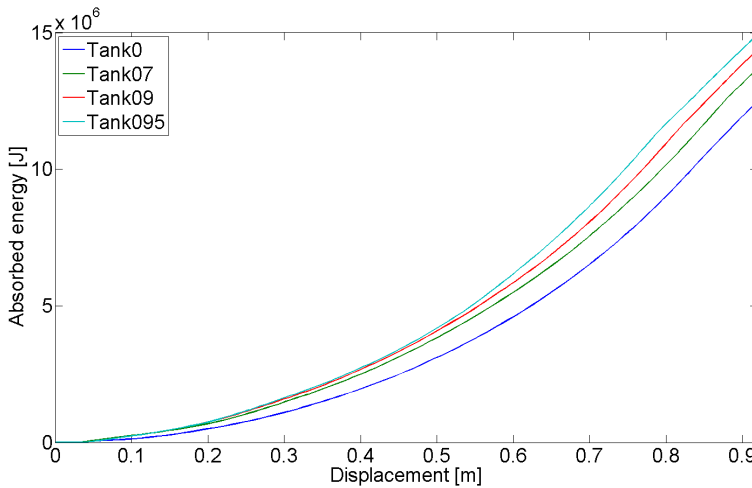


Figure 5.14: Dissipated energy- displacement curves for a ballast tank with different filling levels. Impact speed 8 m/s.

Tank09 and Tank095.

5.4.1 Contact force

It is seen from Figure 5.8 to 5.10 that the presence of fluid gives an increased force throughout the collision. The increase is however very small for the smallest impact velocity. This is also seen in Figures 5.15 to 5.17 which show the contact force of water filled tanks minus the contact force of the empty tank. This force is referred to as the additional contact force.

It is seen that the additional contact force is approximately constant with an exception of displacements larger than 0.4 m for Tank095 and 0.6 m for Tank09. For large displacements there is a sudden drop in the additional contact force. This is due to the fact that the ballast tank fails at different displacements.

Although the additional contact force is small compared to the maximum contact force, it is seen that the contact force is fairly large compared to the total contact force for small displacements. This is especially seen for the largest impact velocity where the additional contact force is approximately 2 MN for a 0.1 m displacement. This can lead to a change in relative strength. The deformation may be forced to take place in the impacting structure although the impacting structure is stronger than the impacted structure when the effects of ballast water is not included. Not including the ballast water in the analysis will therefore be slightly conservative for the impacted structure and slightly non-conservative for the impacting structure.

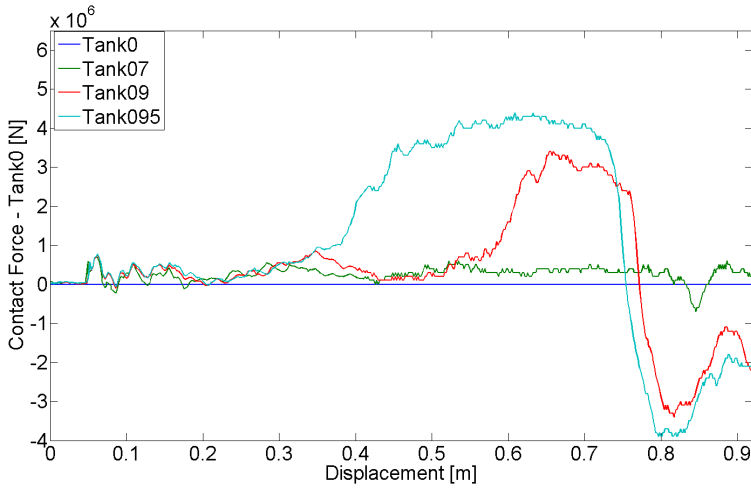


Figure 5.15: Additional force- displacement curves for the ballast tank with different filling levels compared to Tank0. Impact speed 2 m/s.

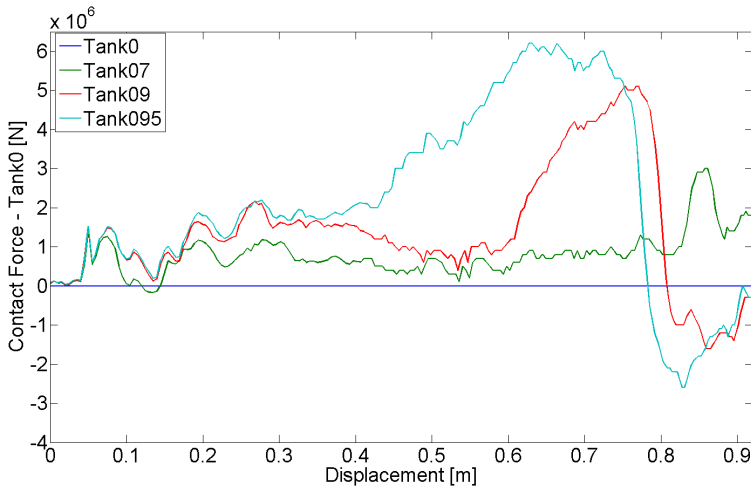


Figure 5.16: Additional force- displacement curves for the ballast tank with different filling levels compared to Tank0. Impact speed 5 m/s.

Maximum contact force

Studying Figures 5.8 to 5.10 it is seen that all of the force displacement curves have a distinct maxima. However, the maximum force occurs at a different displacement for all of the cases. The maximum load for each case occurs just before the short

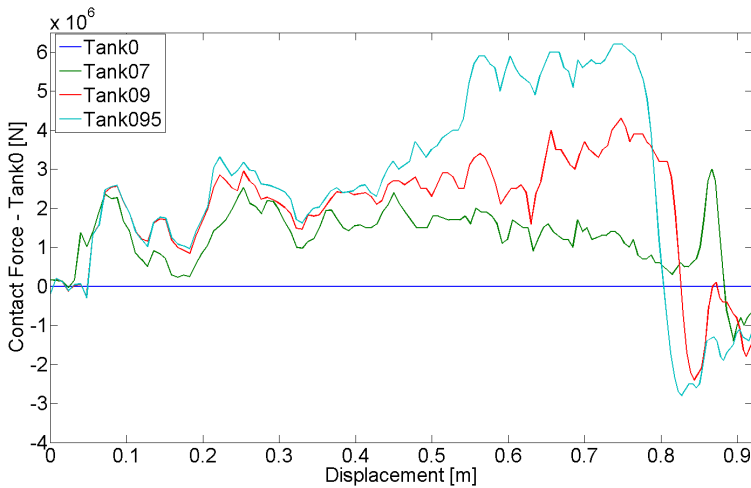


Figure 5.17: Additional force- displacement curves for the ballast tank with different filling levels compared to Tank0. Impact speed 8 m/s.

sides of the ballast tank buckle.

Tank09 and Tank095 reach their maximum load at a smaller displacement than Tank0 for all velocities. Tank095 reaches its maximum contact force at the smallest displacement. The reason is that when the sphere deforms the tank, the water level will rise. At a certain displacement, the water level will reach the top of the ballast tank. When this happens pressure will build up inside the ballast tank. The increase in pressure will force the sides of the tank outward. The deformation of the sides reduces the tanks buckling capacity and forces the sides to buckle at a smaller displacement. The reduction in force is due to a change in the stiffeners buckling mode for Tank09 and Tank095 compared to Tank0. The change in buckling mode should give an increased resistance, but due to the deformation, the total capacity is reduced.

Contrary to Tank09 and Tank095, the maximum load for Tank07 occurs at a larger displacement than Tank0. Although not certain, the increase in contact force might be due to a change in buckling mode. With an 8 m/s impact velocity, it is clear that the some of the stiffeners change their buckling mode, Figure 5.18. With a 5 m/s impact velocity there is some change, but the change is not as apparent.

It is seen that the maximum contact force for the water filled tanks is in all cases larger than Tank0, except for Tank095 with a 2 m/s impact speed. The reduction in maximum contact force is however not of practical importance.

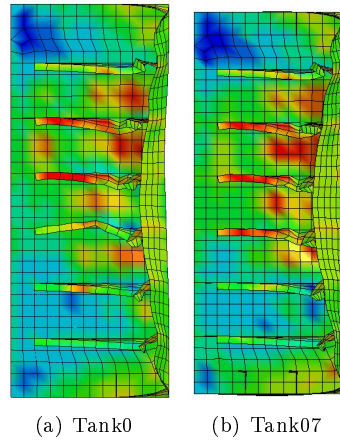


Figure 5.18: Buckling modes for the side of the ballast tank. Impact speed 8 m/s.

Change in slope

Studying the figures for the additional contact force, Figures 5.15 to 5.17, it is seen that the slope of the force displacement curves change at a certain displacement for Tank09 and Tank095. The change is very clear for all cases except for Tank09 with an impact velocity of 8 m/s. The increase in slope occurs when the water inside the tank reaches the top of the tank and is forced through the ventilation hole. The effect of the water reaching the top of the tank is clearly seen comparing Figures 5.15 to 5.17 with Figures 5.20 to 5.22.

The ventilation hole at the top of the tank is most likely larger than it should be. Ship classification rules were not checked before creating the model of the tank. Reducing the size of the hole will most likely lead to an ever larger pressure build up in the tank when the water reaches the top of the tank. The effect of reducing the size of the ventilation hole is however not clear. On one side the pressure acting on the plate undergoing deformation will be higher, which can lead to a larger additional impact force. However, the increase in pressure will cause even larger deformations in the tank sides reducing their buckling strength.

Simple estimate for the additional contact force

An attempt has been made to understand the additional contact force by using simple theoretical considerations. The part of the additional impact force where the water impacts the top of the ballast tank is not taken into consideration.

A possibility is that part of the additional contact force can be described by Eq. 5.1. The first term is associated with the change of wetted surface and the second the added mass force.

$$F_m = \dot{A}_{11}v + A_{11}\dot{v} \quad (5.1)$$

here F_m is a force, A_{11} is the added mass of the water, v the velocity of the side of the tank and \dot{A}_{11} and \dot{v} their derivatives. v and \dot{v} are taken directly from the numerical simulations. The velocity and acceleration of the sphere are used since the plate has very large accelerations during the collision. The plate has in principle the same acceleration and velocity as the sphere after impact, but the initial acceleration of the plate will not be included in the acceleration history.

The estimate for added mass per unit length is taken from Greco [2001] Appendix F. The problem at hand in this thesis is not the same, but similar. The main difference is that there is motion along the whole beam and that the length of the water pool is infinite in Grecos added mass estimate, Figure 5.19.

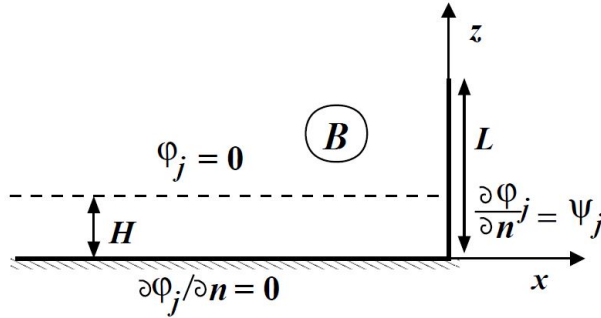


Figure 5.19: Sketch of the problem for the added mass estimate from Greco [2001].

Using the expressions from Greco [2001] an estimate for the added mass is found, Eq. 5.2. The expression is derived using only the first mode.

$$A_{11} = 16 \frac{\rho H^2}{\pi^3} \quad (5.2)$$

Here ρ is the density of water, and H is the height of the water. The derivative of A_{11} is found using

$$\dot{A}_{11} = \frac{dA_{11}}{dH} \frac{dH}{dt} \quad (5.3)$$

Assuming that the tank deforms perfectly with the sphere, a lower estimate of the volume displaced by the sphere, V , can be found, Eq. 5.4. Although not true, it is assumed that the water level remains above the sphere cap for the whole analysis. x is the indentation into the tank.

$$V = \frac{\pi x^2}{3} (3r - x) \quad (5.4)$$

Assuming that the water is incompressible, the height of the water in the tank can be calculated as a function of time, Eq. 5.5.

$$H = H_0 + \frac{V}{bd} \quad (5.5)$$

here H_0 is the height of the water before impact, b is the width of the ballast tank and d the depth. $\frac{dH}{dt}$ can be found by differentiating Eq. 5.5 with respect to time.

The estimate used for the added mass assumes a constant velocity along the whole beam. In the present case, the motion of the plate is fairly concentrated to the area where the sphere is in contact with the plate. To account for this the velocity and acceleration of the plate are averaged using a reduction factor, R_r . The averaging is performed by dividing the projected area of the sphere cap in contact with the tank, with the area of the wetted side in the ballast tank, Eq. 5.6. It is also here assumed that the water remains above the sphere cap for the whole analysis.

$$R_r = \frac{\pi a^2}{b * H} \quad (5.6)$$

where $a = \sqrt{x(2r - x)}$, H is the height of the water, x the height of the sphere cap and r the radius of the sphere. The height of the sphere cap x , is equal to the spheres indentation into the tank.

Another contribution to the additional contact force is the static force, F_s . The static force is found by integrating the pressure over the wetted side of the tank.

$$F_s = \frac{1}{2} \rho g H^2 b \quad (5.7)$$

The total force, F , acting from the water on the tank side is then:

$$F = F_m + F_s \quad (5.8)$$

To better compare with the results from LS-DYNA with the simple theoretical considerations, new analyses were performed where the coupling between the plate at the top of the ballast tank and the water was removed. The simple estimate for the additional contact force is shown together with the results from LS-DYNA in Figures 5.20 to 5.22. T07 refers to the theoretical estimate for Tank07, etc.

The velocity and acceleration history used for the sphere to calculate the simple estimate, is the velocity history for that specific analysis. The velocity and acceleration history from Tank09 is used to calculate the simple estimate for Tank09, T09. However, using the history variables for Tank0 would give similar results since the velocity and acceleration of the sphere are similar.

It is seen that the simple estimations give quite good results when the impact speed is 2 m/s and 5 m/s. For an impact speed of 2 m/s the static force dominates

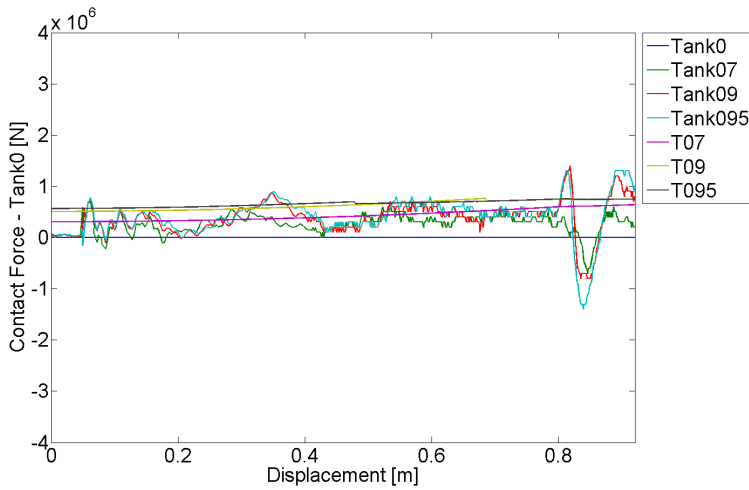


Figure 5.20: Additional force- displacement curves for the ballast tank with different filling levels. No FSI for the top plate. Impact speed 2 m/s.

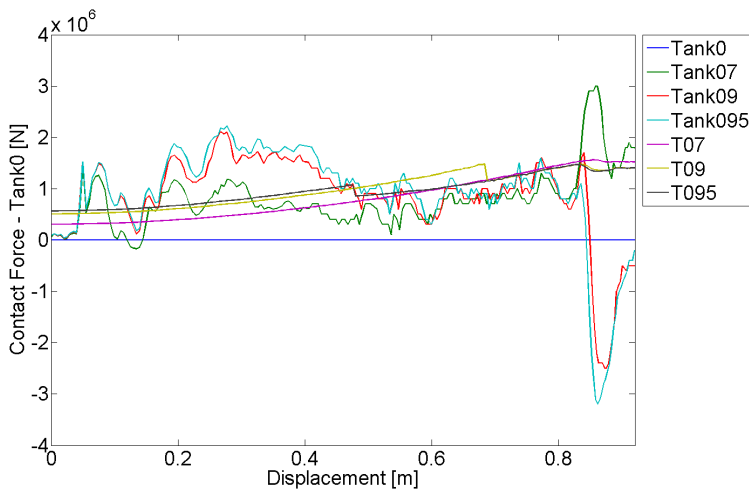


Figure 5.21: Additional force- displacement curves for the ballast tank with different filling levels. No FSI for the top plate. Impact speed 5 m/s.

giving little variation in the additional contact force throughout the collision. For 5 m/s the simple estimate fits well after the displacement reaches approximately 0.45 m. Both the size of the force and the slope are nicely estimated which is very promising. The force is a little high for both impact speeds, but in the right range.

The estimate is not very accurate for the early stages of the collision. It is however

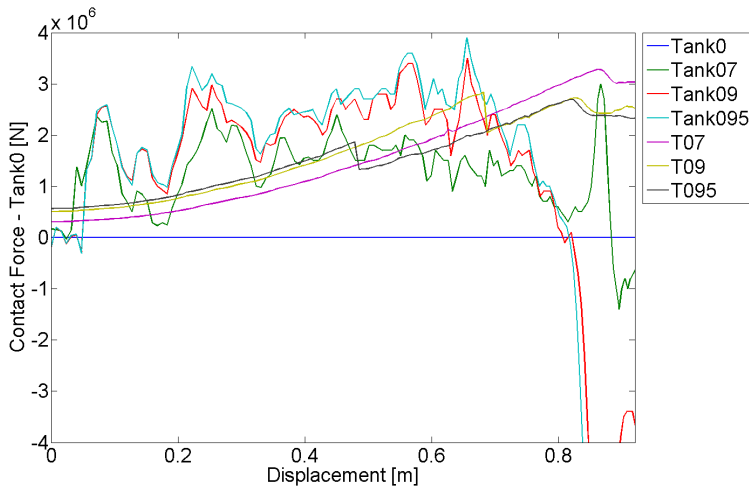


Figure 5.22: Additional force- displacement curves for the ballast tank with different filling levels. No FSI for the top plate. Impact speed 8 m/s.

not expected that this simple consideration captures the effects of the initial impact. The initial acceleration of the plate is in addition not included in the acceleration history since the accelerations of the sphere are used. It is also seen from Figure 5.24 that it takes the water some time to respond to the impact.

The simple estimate does not give a very good estimate for the additional contact force when the initial velocity is 8 m/s. The reason for the deviation is thought to be due to the initial impact of the plate. The whole collision lasts only 0.14 seconds, making the effects of initial impact important for the whole analysis. The size of the force is however quite similar at the end of the simulation, indicating the reason for the deviation may be due to the initial impact.

5.4.2 Energy absorption

In ship collisions, energy absorption is a very important parameter. NORSOK N-004 [2004] defines the collision action in terms of energy. It is seen from Figure 5.13 that all of the cases with ballast water have a larger energy absorption at a given displacement than Tank0. It will therefore be conservative to neglect the effects of the ballast water in a design case for the ballast tank. However, for an impacting structure more energy dissipation might be forced to take place in the impacting structure since the strength of the ballast tank is increased due to the water.

5.4.3 Fluid response

The fluid structure interaction is difficult to model correctly. The most difficult parameter to determine has been the penalty stiffness. It is often difficult to give a correct penalty factor to achieve a visually correct fluid structure interaction. Even more difficult is to give a penalty factor that is correct physically. Since checking if the stiffness is physically correct requires model testing, the results here are only inspected visually.

Figure 5.23 shows the deformation of the ballast tank together with the water inside the tank for Tank09. It is seen that the water penetrates the shell, but this is expected for penalty based coupling. There is more penetration towards the end of the analysis than in the beginning, but the fluid follows the deformed shape of the tank quite nicely. The fluid structure interaction seems therefore to be visually correct.

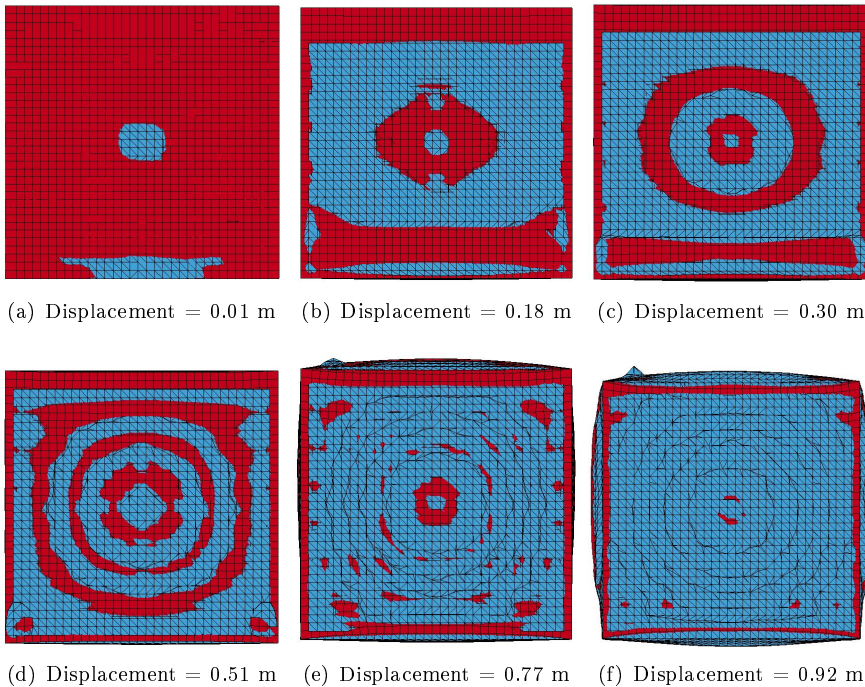


Figure 5.23: Deformation of the ballast tank with a 90 % filling level. Red part - Shell, Blue part - Water.

The motion of the water inside the ballast tank is also checked to see if it seems to be realistic. Figure 5.24 shows the water inside the ballast tank for Tank07 where the sphere has an initial velocity of 5 m/s.

It is seen that the water fills the tank nicely in before impact. The interaction between the tank and the water is however not perfect due to the fact that the top edges do not have a right angle. Just after impact it is seen that all the edges lose their sharp corner. This is due to leakage that occurs because of the increase in pressure.

The shape of the free surface during impact is how one should expect. The surface has the shape of a wave where the highest point is on the side of impact. The size of the wave increases as the displacement increases which is also expected. The fluid structure interaction seems therefore to be visually correct based on Figures 5.23 and 5.24

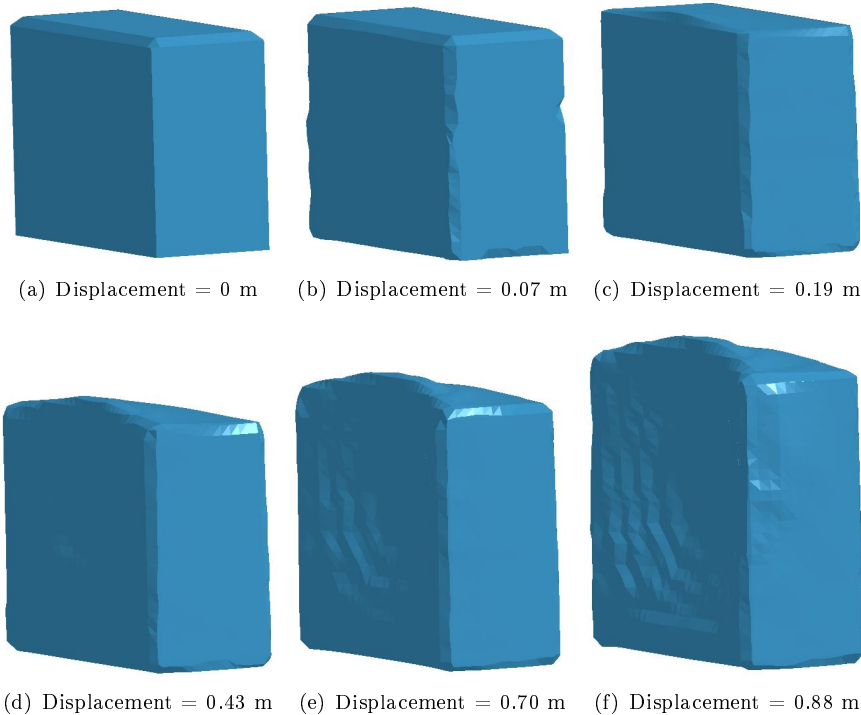


Figure 5.24: Water motion during impact for Tank07. Impact velocity 5 m/s

It is not clear how much the results depend on the penalty stiffness. The penalty stiffness was changed until the fluid structure interaction seemed visually correct. A study should be performed to see the effect of changing the penalty stiffness. This is however time consuming, and may not give any clear answers. The only possibility to check the FSI is to compare with a model test.

5.4.4 Numerical errors

Numerical errors will always be an issue in collision analyses. Care is taken to ensure that the numerical error is small in the analyses. The collision response is checked to see if it seems physical, and the total energy is checked to see if it remains approximately constant throughout the analyses.

No signs indicating numerical errors were found in the analyses with the internal FSI. There were no spurious stresses or motions. It was also seen that the total energy in the analysis was fairly constant. The total energy dropped less than 5 % for all the analyses.

5.5 Conclusion

It is seen that the ballast water has a clear effect on both the contact force and the energy dissipation in the collision analyses. Both the contact force and energy dissipation are increased. The effects are however very small and not of practical importance for the smallest impact velocity before the water in the ballast tank reaches the ceiling. For higher impact velocities the ballast water strengthens the ballast tank throughout the analysis. The error of not including ballast water in collision analyses is therefore larger for higher impact velocities.

Based on the results it is concluded that it is conservative to neglect the effects of ballast in a design case for the ballast tank. The maximum contact forces are all in the same range and the energy dissipation is higher for a given displacement. Neglecting the effects of ballast water will, however, be non-conservative in a design case for the impacting structure since the strength of the ballast tank is increased.

Chapter 6

Ship-platform collisions

Ship collisions are often analysed using simple formulas both for the internal and external mechanics. Alternatively, a more complicated option is to calculate both the internal damage and the energy dissipation using a non-linear finite element program. To use this method, deformable parts and mass distributions for both colliding structures must be created.

In this chapter, realistic collision scenarios between Moss Maritimes Octopus and a shuttle tanker are presented and analysed using non-linear finite element analysis (NLFEA). Both integrated analyses and analyses where the problem is decoupled into external dynamics and internal mechanics are performed. The structures involved in the collision and their finite element models are also presented.

One major point in this thesis was to perform ship-platform collisions with external FSI. This proved to be much more difficult than expected, and was postponed to further work. The attempts are described in 6.3.

The mass models for the structures were created before the collision analyses, with external FSI, were postponed to further work. Added mass is therefore not included in the mass distributions. All the analyses are performed without taking added mass into account.

6.1 Collision scenarios

In this section, realistic collision scenarios between the Octopus, a FPSO design by Moss Maritime, and a shuttle tanker are presented. Only bow collisions will be evaluated in this thesis. A brief description of the structures involved in the collisions is given.

6.1.1 Structures

Reference ship

The reference ship used in the collision analyses is a 147 500 d.w.t. Samsung shuttle tanker shown in Figure 6.1. The Samsung shuttle tanker is chosen as a reference ship since NTNU is in possession of a detailed bow model for the tanker. Table 6.1 shows general data for the reference ship.

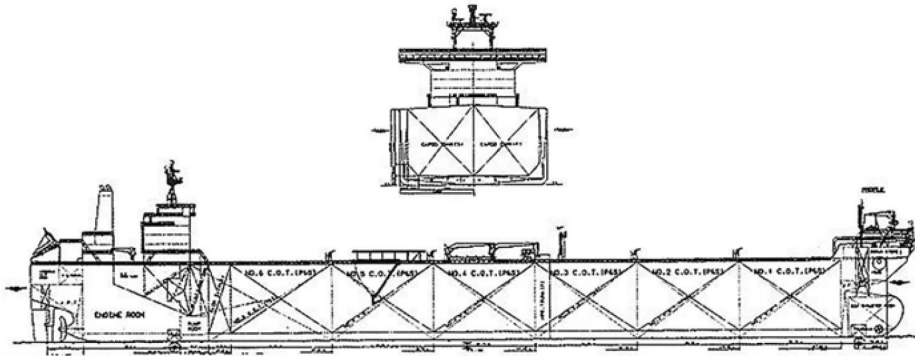


Figure 6.1: Profile of reference ship.

Table 6.1: General dimensions, reference ship.

Length O. A.	[m]	278
Length P.P	[m]	262
Length Scantling	[m]	259
Breadth moulded	[m]	46
Depth moulded	[m]	26.6
Draft design	[m]	15.9
Draft scantling	[m]	17.0

The design of the bow structure will have an effect on the impact position and geometry in a ship- platform collision. However, due to classification rules the dimensions of the structural components (plating, stiffeners, and girders) do not vary much between similar ships. Ships of a similar size will therefore have similar strength. Figure 6.2 shows the geometry of the reference ship in the centerline.

The prow of the shuttle tanker is vertically stiffened with a stiffener spacing of approximately 800 mm. In the centerline there is a longitudinal bulkhead with some longitudinal stiffening below the main deck. Also stiffening the prow in the longitudinal direction are two decks; the upper deck and the forecastle deck. Both of these decks are mainly stiffened in the longitudinal direction with a 800 mm

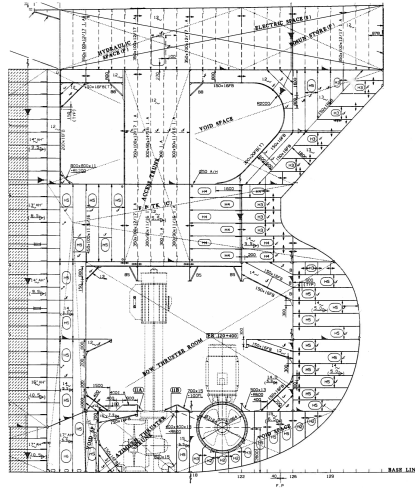


Figure 6.2: Bow, center line reference ship.

stiffener spacing. The plating in the prow varies from 10 to 20 mm. The largest plate dimensions are used in the shell, while the smallest dimensions are used in the bulkhead and decks. Typical stiffener heights vary from 200 to 400 mm.

The bulb is stiffened longitudinally with a stiffener spacing of 750 mm. The bulb has three stringers in addition to a longitudinal bulkhead with longitudinal stiffening. The distance between the stringers is approximately 4500 mm. The middle stinger is stiffened in the longitudinal direction, while the two other stringers are stiffened in the transverse direction at the most forward part. Dimensions of plating used in the bulb vary from 10 to 20 mm. The thickest plating is used in the shell. Typical stiffener heights vary from 250 to 400 mm.

It should be noted that the bow of the reference ship may not have the most critical shape since the forecastle is the most forward part of the ship. The bulb is often stronger than the rest of the bow, and will most likely cause more damage if it makes contact with the platform during the collision.

Octopus

The Octopus is shaped as a cylinder with eight flat sides. Each side is approximately 40 meters wide. While operating, the draft of the Octopus will be held constant

by ballasting.

Structural drawings of Octopus were provided by Moss Maritime. Since the Octopus is still in the design phase, the drawings were not complete. For areas without drawings, assumptions were made. The structural configuration of the critical side, ref 6.1.2, is presented below.

Figure 6.3 show the stinger decks below the water line. Drawings were not available above the waterline, so in this area the structural dimensions are assumed by the candidate. The stringer spacing is 4 meters. Stringers in the ballast tank are stiffened with flat bar stiffeners with 660 mm spacing, while the stringers in the main tank have L-profiles with the same spacing.

Vertically, the structure has girders with a spacing of 2640 mm. Between the girders are vertical stiffeners with a 660 mm spacing. There are two decks at 45 and 50 meters above the keel. The decks have girders in the "radial" direction and stiffeners normal to the girders. The stiffener and girder spacing is as before. Plate thicknesses used in the structure are approximately 20 mm.

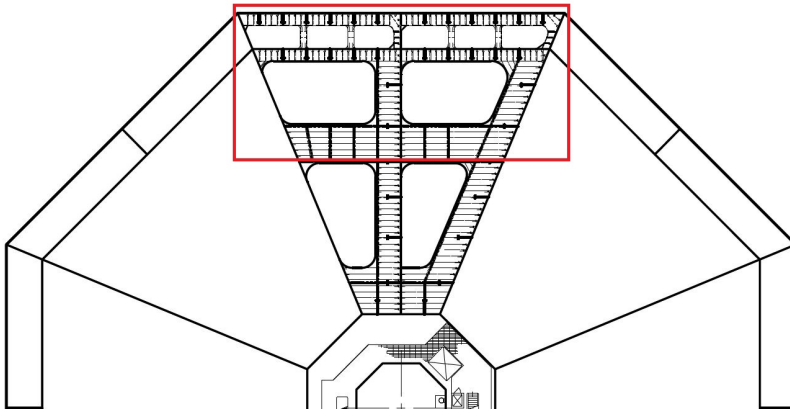


Figure 6.3: Octopus stinger decks between.

6.1.2 Impact scenarios

Impacts are most likely to occur when the shuttle tanker approaches for offloading. In an offloading scenario, the weather should be nice giving only small vertical motions for both the Octopus and the shuttle tanker. Vertical motions are therefore not taken into consideration. The impact position is therefore assumed to be only dependent of the draft of the shuttle tanker since the Octopus' draft is kept constant by ballasting. Two impact elevations are of main interest

- Shuttle tanker in ballast condition, 9 m draft.

- Shuttle tanker in full load condition, 17 m draft.

The scantling draft is used as the maximum draft since a low impact is the most critical for the Octopus. For a low impact, the bulb of the ship may impact the Octopus and puncture the hull. The scantling draft is the absolute maximum draft the ship is designed for.

Vertical impact positions are shown in Figure 6.4

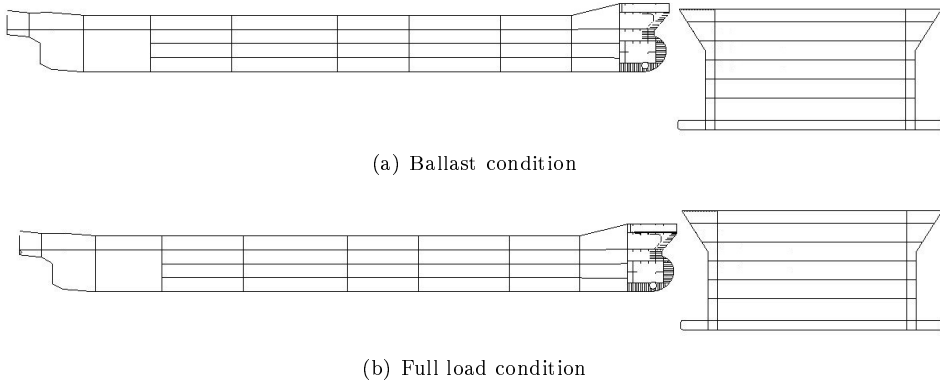


Figure 6.4: Vertical impact positions.

Studying the tank arrangement of the Octopus, Figure 6.5, it is seen that collisions on certain sides are more critical than others. The worst case for both the platform and the environment will be to puncture a cargo tank. This is most likely to happen on a side like the one indicated in Figure 6.5. The collision is therefore assumed to take place here. The impact position is assumed to be in the middle of the flat side.

Head on impacts where the force vector penetrates the center of gravity for both structures is commonly assumed to be the most critical impact direction. However, normal operating procedures dictate that the incoming vessels should approach with an angle to the platform. Thereby making a glancing impact more probable. Impacts with an angle of 30 and 45 degrees are therefore also highly relevant. Figure 6.6 shows the three different impact angles.

Combining the impact position and impact angles gives a total of six different collision scenarios. The specific scenarios analyzed in this thesis are presented in 6.1.5.

6.1.3 Mass properties

Correct mass, mass distribution and added mass must be used for both the ship and the platform, to properly estimate the energy to be dissipated in the collision.

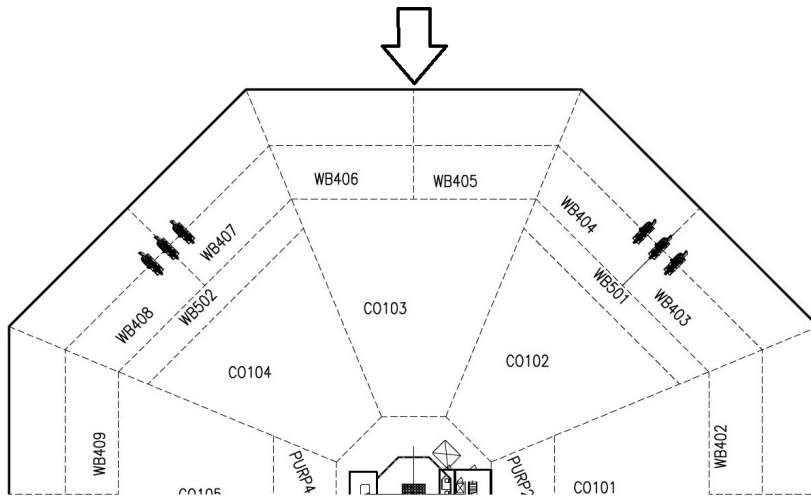


Figure 6.5: Octopus tank arrangement seen from above.

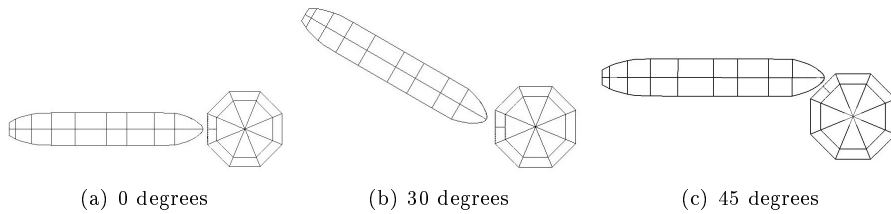


Figure 6.6: Impact angles.

Added mass

The added mass values are calculated by running a Wadam analysis. The Wadam analysis was created using HydroD. The analyses were run at operation draft for the Octopus and with a draft of 9 and 17 meters for the ship.

Figures 6.7 to 6.10 show the results from the analyses. The added mass values are made dimensionless by dividing the added mass with its corresponding mass. Values for A_{22} and A_{55} are not presented for the Octopus since they are identical to A_{11} and A_{44} .

To see if the analyses gave reasonable results, the added mass coefficient for the ship in heave is compared to Figure 3-20 in Pettersen [2007]. The draft- width ratios do not match exactly, but by adapting the curve to the relevant draft- width ratios, it is seen that the added mass coefficients are in the correct range.

Using a collision between the Octopus and the shuttle tanker as a reference, it was found reasonable to use added mass values for periods around 15 seconds. The

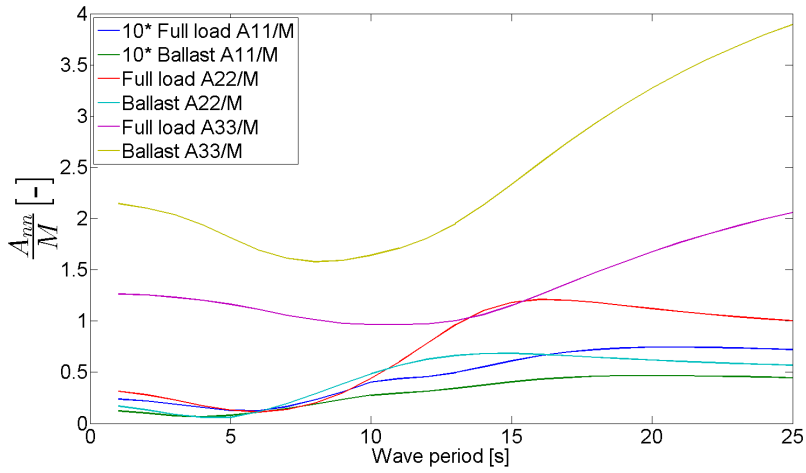


Figure 6.7: Added mass for the ship in surge, sway and heave.

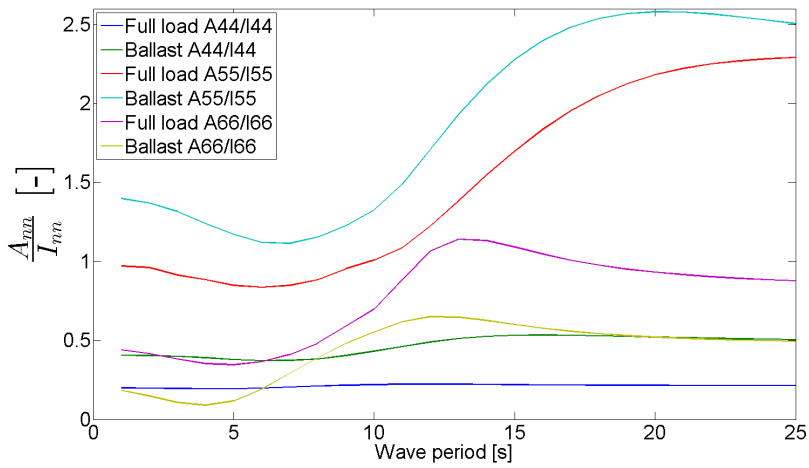


Figure 6.8: Added mass for the ship in roll, pitch and yaw.

collision lasted between 4 and 8 seconds. 15 seconds is chosen under the assumption that the collision is half of a period. The added mass values that are found most suitable to use in the collision are presented in Table 6.2.

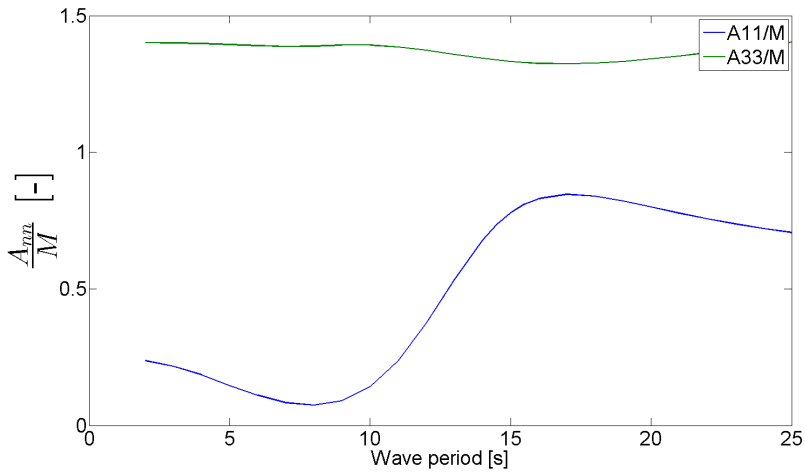


Figure 6.9: Added mass for the Octopus in surge and heave

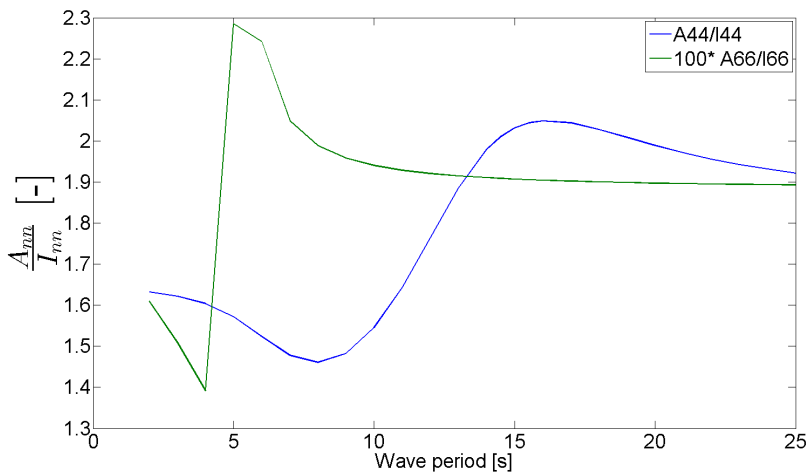


Figure 6.10: Added mass for the Octopus in roll and yaw

Mass and mass distribution

Estimates for the ships radius of gyration are made according to Faltinsen [1998]. The typical values are $0.25 * L_{pp}$ for pitch and yaw, and $0.35 * B$ for roll. The radius of gyration in roll is typically larger for ballast condition than it is for full load conditions. However, to simplify the mass modelling a value of $0.35 * B$ is also assumed for the ballast condition.

Table 6.2: Added mass coefficients for the Octopus and ship.

Added mass coef.	Ship full load	Ship ballast	Octopus
A_{11}	0.066	0.043	0.82
A_{22}	1.2	0.67	0.82
A_{33}	1.2	2.5	1.33
A_{44}	0.22	0.53	2
A_{55}	1.8	2.4	2
A_{66}	1.05	0.6	0.019

The vertical center of gravity for the ship fully loaded is estimated by using the vertical center of gravity in the cargo tanks. For the ballast condition, the weight of the ship will have a larger contribution to the center of gravity than for full load. The vertical center of gravity for the ballast condition is estimated by choosing a position that makes the distance from the center of gravity to metacenter in roll, 10 meters. The distance from the meta center to the center of gravity is typically larger for ships in ballast. For both full load and ballast condition, the longitudinal center of gravity is placed at the center of buoyancy. This is a good estimate for the full load condition, but perhaps not for the ballast condition. Ships in ballast have often a constant pitch angle to keep the stern of the ship submerged.

Values used for the radius of gyration and center of gravity for the Octopus are provided by Moss Maritime. The platform is still in the project phase, so the values are only estimates.

The total mass for the ship and platform is calculated in Wadam using the assumed drafts from 6.1.2. The mass properties for the ship and platform are show in Tables 6.4, 6.5 and 6.6.

6.1.4 Dissipated energy

When simplified collision analyses are performed, either by using simplified methods such as Amdahl's method or by forcing a bow into a structure in a NLFEA, the energy to be absorbed in the collision must be calculated using simplified methods. The complexity of the simplified methods vary greatly from the simplest with one degree of freedom [NORSOK N-004, 2004], to the method presented by Liu and Amdahl [2010] taking all six degrees of freedom into account. The two simplest methods presented in this thesis, with one and two degrees of freedom can give good estimates for head on collisions.

Energy ratio

Figure 6.11 shows the fraction of kinetic energy, E_k , to be dissipated as strain energy, E_s , as a function of the mass ratio for different impact angles for the ship

in ballast. The ship in full load will give similar results, and since a collision in ballast is the most probable, only the energy ratios for an impact in ballast condition are presented here. The energy dissipation is calculated using the three different methods presented in 1.2. The mass ratio is defined as the mass of the ship divided by the mass of the platform. Since the NLFEA are performed without added mass, the energy ratios are presented without added mass. The effect of including added mass is discussed in the discussion part of this chapter. For the 6 DOF method, it is assumed that the angle of the hull will not affect the collision since the top of the bow is higher than the top of the platform.

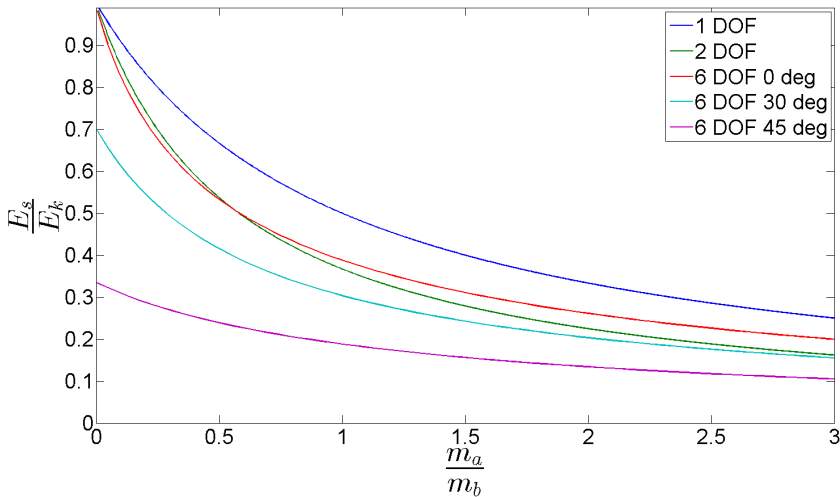


Figure 6.11: Energy dissipation ratio for head on collision without added mass.

It is observed from Figure 6.11 that almost all the kinetic energy must be absorbed if the mass ratio is small, i.e. the mass of the Octopus is much larger than the ship. For a collision between a shuttle tanker in ballast and the Octopus the mass ratio is 0.37. This gives an energy ratio of 0.72 if one degree of freedom is used in the calculations. However, if de Jonge and Laukeland [2013] or Liu and Amdahl [2010] methods are used, the factor is lower. In ballast condition the factor is approximately 0.6 if these methods are used.

It is important to keep in mind that the energy dissipation calculated using 2 DOF and 6 DOF is the energy dissipation in the initial part of the collision. For a head on impact, the center of mass for each of the structures must have a common velocity before the collision is finished.

Impact velocity

Shuttle tankers will have a reduced velocity in a close proximity to platforms. They do however need some speed in order to manuverate. An impact velocity of 2 m/s is therefore assumed.

A simple estimate of the energy dissipation

Using the energy ratios along with the impact speed and masses of the structures, estimates for the energy dissipation for the different collision scenarios can be estimated, Table 6.3. To see the effect of the vertical offset, the energy dissipation is also calculated using 3 DOF for the glancing impacts. The 3 DOF estimates are calculated using the 6 DOF method without a vertical offset. The estimates are presented below. Since none of the NLFEA include added mass, the energy dissipation is calculated without added mass.

Table 6.3: Estimates for the energy dissipation for selected collision scenarios.

Calculation method	Energy dissipation [MJ]	
	Full load	Ballast
1DOF	196	123
2DOF	169	104
6 DOF 0 deg	132	102
6 DOF 30 deg	88	79
6 DOF 45 deg	54	45
3 DOF 30 deg	152	96
3 DOF 45 deg	91	54

It is seen that the dissipated energy is larger for all cases when the ship is fully loaded. This is as expected. The ship in full load has almost twice the mass of the ship in ballast. It is seen that the difference in energy dissipation is less than the difference in mass. This is due to the change in mass ratio. When the mass ratio increases, the fraction of the kinetic energy that will be absorbed in the collision will be reduced, Figure 6.11.

6.1.5 Collision scenarios to be analyzed

Due to limited time, all collision scenarios cannot be analysed. Four different cases are chosen.

The first two are head on collisions. Both full load and ballast condition are analysed. The latter is more probable than the former since shuttle tankers are in ballast when they approach a platform. The head on collisions are chosen since

they will create the most damage to the platform. They have the largest energy dissipation estimates.

The two other scenarios analysed are glancing impacts with a 30 and 45 degree angel in ballast. A glancing impact is the most probable since normal operating procedures dictate that vessels should approach with an angle.

6.2 Finite element modeling

6.2.1 Software

The software used for the finite element modeling and numerical simulations are MSC Patran, LS-PrePost and LS-DYNA. MSC Patran is used for establishing a finite element model of the Octopus and LS-PrePost for setting up the collision analysis. The very efficient non-linear finite element solver LS-DYNA is used for solving the numerical simulations. Post processing of the results is done in LS-PrePost and MATLAB.

6.2.2 Reference ship

The bow of the tank ship used in the collision analyses is provided by NTNU, while the hull and the mass distribution is created for this thesis. The hull is modelled using only general ship parameters such as length, width and depth since detailed drawings were not available. Figures 6.12 and 6.13 show the finite element model of the bow and ship, respectively.



Figure 6.12: Bow model used in the collision analyses.

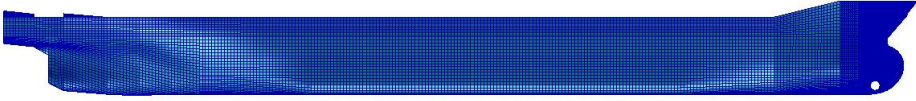


Figure 6.13: Tanker model used in collision analyses.

Mass properties

In addition to the shell of the ship, some internal structure was made to distribute the mass of the ship. Masses were distributed in the structure to achieve a typical mass distribution. Mass properties for the finite element model of the shuttle tanker are presented in Table 6.4 and 6.5. A mass distribution was created both for full load and ballast condition. To hopefully have the ship float at the correct draft, the mass of the ship is reduced by approximately 1 % compared to mass calculated in the Wadam analysis, according to findings in 4.2.3.

The mass distributions for the ship were created with the intention of performing the analyses in a water environment. Added mass is therefore not included in the mass models.

Table 6.4: Mass properties for the ship, full load.

Mass	[t]	1.69E+05
Longitudinal c.o.g.	[m]	135.2
Transverse c.o.g.	[m]	4.53E-07
Vertical c.o.g	[m]	14.7
Roll radius of gyration	[m]	15.82
Pitch radius of gyration	[m]	65.33
Yaw radius of gyration	[m]	66.20

Table 6.5: Mass properties for the ship, ballast.

Mass	[t]	8.56E+04
Longitudinal c.o.g. fwd AP	[m]	137.61
Transverse c.o.g.	[m]	6.35E-06
Vertical c.o.g	[m]	10.71
Roll radius of gyration	[m]	15.76
Pitch radius of gyration	[m]	65.63
Yaw radius of gyration	[m]	66.74

Mesh

The mesh for the bow of the structure was provided by NTNU. The front part of the bow is meshed with elements with a standard size of 100 mm. To keep the number of elements to a minimum, the element size is increased at the rear part of the bow. The standard element size used here is 400 mm.

Unfortunately the model provided by NTNU was modeled in mm while the Octopus is modeled in m. While converting the bow from mm to m, some of the nodes moved resulting in some poor elements. This gave the bow a small critical time step. Some of the worst elements were replaced manually to increase the critical time step. The critical time step for the bow is $2.77e-6$.

To avoid fluid structure interaction between the very small elements in the bow and the water, a mesh for the bow with 1 m elements was created on top of the fine mesh. The coarse mesh is fixed to the rigid part of the ships shell. The rest of the shell of the ship is also meshed with 1 m elements due to findings in 4.2.1. The internal structure is, for the rigid part of the ship, meshed with 2 m large elements to keep the number of elements to a minimum.

6.2.3 Moss Maritime's Octopus

The finite element model of the Octopus consists of a detailed part that is connected to a coarse model of the entire platform. The detailed part will deform during the collision, while the coarse part is created to get the correct external geometry and mass distribution of the Octopus. The coarse part of the model will be rigid in the analyses.

With the collision scenarios discussed in 6.1.2 in mind, an appropriate section of the Octopus is chosen to model in detail. With guidance from Storheim, it was found reasonable to model one flat side of the platform in a wedge shape, i.e. the shaded part in Figure 6.3 marked with a red square. Only the top 25 meters of the platform is modelled in detail. Bulb impacts are assumed to be unlikely due to the angle of Octopus' hull above the waterline.

Geometry

The level of detail varies greatly within the model. The deformable part of the platform is modelled with a high level of detail, while the surrounding structure has a low level of detail. The exception is the outer shell which is created accurately according to available drawings to give the platform a correct buoyancy. One small modification is however made for the outer shell. The sharp corners on the bilge keel are replaced with corners with a 1 m diameter. The internal structure in the rigid part of the model is not created accurately. Bulkheads and decks are created only to be able to give the platform a realistic mass distribution.

The deformable part of the model is also modelled with different levels of detail. The geometry near the outer skin is modeled with a high level of detail, i.e. the ballast tank is modelled accurately. Details in areas with large deformations are important to get a realistic structural response. Details such as cut outs for the stiffeners and girders are not included. It is instead assumed that the web of the girders/stiffeners and the flange of the girder is fixed to intersecting structures. The stiffener flanges are only fixed to the stiffener web. They are not connected with intersecting structures.

A simplification is made for the stiffeners and girders at the point where the hull angle changes. It is assumed that the girders and stiffeners will connect perfectly without an overlap. The height of the girder/stiffener is varied over a length of 2.4 meters until the correct height is achieved, Figure 6.14

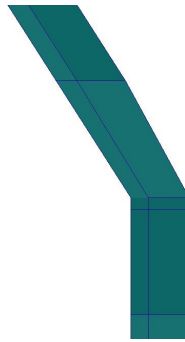


Figure 6.14: Simplification of girder/stiffener connection.

Drawings for the area above the waterline, i.e. where the hull angle changes, were absent. The structural arrangement in this area is therefore based on assumptions, with some guidance from Storheim. Due to the inclination of the outer skin, this section becomes wider making room for new girders/stiffeners. To ease modeling, it is assumed that new girders/stiffeners are vertical and will start when there is enough room. The assumed stiffening arrangement is shown in Figure 6.15.

Geometry behind the ballast tank, including the bulkhead between the ballast tank and the cargo tank, is modelled using simplifications. The stiffeners are smeared onto the plates. Girders are however modelled accurately with an exception of two vertical girders located more than 13 meters into the structure. These girders are assumed not to effect the strength of the structure with respect to a collision, and are therefore neglected. The final model of the Octopus is shown in Figure 6.16. Figure 6.16(a) shows the deformable part of the Octopus with a detailed geometry while Figure 6.16(b) shows the entire model.

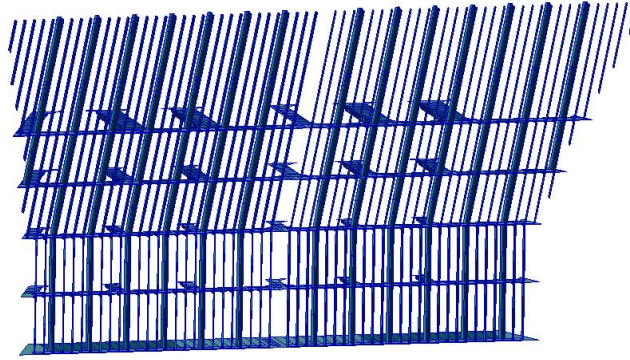


Figure 6.15: Stiffening arrangement of outer shell and stinger decks.

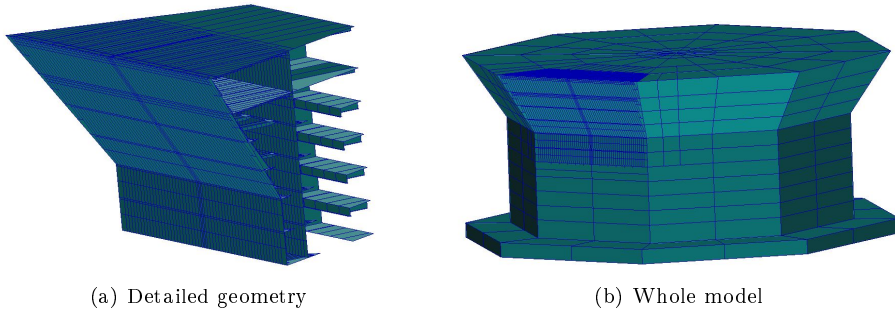


Figure 6.16: Structural model of the Octopus.

Mass Properties

In the integrated analyses, the Octopus must have a realistic mass distribution. The mass distribution is created by giving the rigid parts of the Octopus large plate thicknesses and a large material density. Using a spread sheet, the thicknesses of the plates in different parts were changed until a proper mass distribution was achieved.

The mass distribution was created for a collision analysis with external FSI. Due to the fact that there is leakage in LS-DYNA, the mass of the model is reduced by approximately 1 % to achieve equilibrium at the correct draft. Table 6.6 shows the Octopus' mass properties. Added mass values are not included since these should automatically be taken care of in an analysis with external FSI.

Table 6.6: Mass properties, Octopus.

Mass	[t]	2.30E+05
Longitudinal c.o.g.	[m]	1.12E-03
Transverse c.o.g.	[m]	0.02
Vertical c.o.g.	[m]	29.22
Roll radius of gyration	[m]	23.50
Pitch radius of gyration	[m]	23.48
Yaw radius of gyration	[m]	33.06

Mesh

Accurate results from the finite element analyses depend on having a good mesh. The element type will also have an effect on the results. The 4- node shell element is used as the main element category. 3- node elements were avoided since they are not as accurate as 4- node elements. However, a few 3- node elements appear in areas where the mesh size changes and in places with difficult geometry.

The mesh is especially important when there are large deformations. Results from Alsos [2008] states that the element lengths should preferably be 5 - 10 times the plate thickness. This is to give a good physical response during large deformations. An element size in the lower range was chosen to model Octopus' structure in the collision zone, 100 mm. Such a small element size is chosen due to the stiffeners height. To give the stiffeners a proper bending stiffness under large deformations, the stiffener must be modeled with at least three elements over the stiffeners height. The stiffeners on the outer shell and stringer decks have stiffener heights of 300 and 200 mm respectively. With a 100 mm element length both the elements on the stiffeners and shell will have reasonable aspect ratios. All areas where large deformations are expected are meshed with this element size. To save computation time, the element size is increased to 250 mm in areas where there will only be small deformations.

Since small elements will give a small critical time step, care was taken to avoid unnecessarily small elements in the model of the Octopus. To avoid an unnecessarily small time step, the mesh on the Octopus was improved until the critical time step was determined by the mesh in the bow of the ship.

The rigid shell of the Octopus is modeled using 1 m large elements. The size is chosen due to findings presented in 4.2.1. The internal rigid structures are modeled with 2 m large elements. A mesh with a one meter element size was created to cover the shell of the deformable part of the platform. The purpose of the mesh is to interact with the fluid. Coupling the small elements that are necessary for the deformable part with the water is very costly computationally.

Care has been taken to ensure that all of the element nodes are connected in the proper manner. Using Patrans built in function, verify free edges, the structure was systematically checked to verify that that the nodes are properly connected.

6.2.4 Material

The parameters used in the collision analyses are presented in Table 6.7 and 6.8. The material parameters used for the bow of the ship are the standard in house values for steel with a yield stress of 235 MPa. The parameters used for the deformable part of the Octopus are found in Alsos et al. [2009]. The critical strain is assumed to be equal to the ships critical strain. The yield stress in the analyses is larger than the yield stress presented on the ship and platform drawings. The yield stress is raised to take into account that the yield stress defined by classification societies is often a minimum requirement. Only the bow of the ship shown in figure 6.12 and the deformable part of the Octopus 6.16(a) are deformable. The rest of the models are rigid.

A rigid material is used for the rigid parts of the structures. The Young's modulus used is 2.1×10^{11} Pa, the Poisson ratio is 0.3 and the material density is 2×10^4 kg/m².

Table 6.7: Material parameters for the shuttle tanker.

Density [kg/m^3]	7850
Young's modulus [Pa]	2.07E+11
Poisson ratio	0.3
Shear modulus [Pa]	7.96E+10
Bulk modulus [Pa]	1.73E+11
Yield stress [Pa]	2.75E+08
Strength parameter, K [Pa]	7.40E+08
Powerlaw exponent, n	0.24
Equivalent plastic strain at plateau exit	1.00E-02
Critical strain	0.71

Table 6.8: Material parameters for the Octopus.

Density [kg/m^3]	7850
Young's modulus [Pa]	2.07E+11
Poisson ratio	0.3
Shear modulus [Pa]	7.96E+10
Bulk modulus [Pa]	1.73E+11
Yield stress [Pa]	3.90E+08
Strength coefficient, K [Pa]	8.30E+08
Powerlaw exponent, n	0.18
Equivalent plastic strain at plateau exit	1.00E-02
Critical strain	0.71

6.3 Attempt at a collision analysis with external FSI

This section presents an attempt to model a collision between a ship and a platform without introducing simplified coefficients or assuming a constant added mass.

It is seen from 4.2.1 that to achieve a reasonable equilibrium for the platform, a mesh with 1 m elements should be used to model the water. This was however not possible due to the amount of memory that the ALE solver requires. An analysis with only the environment would not start on vilje (NTNUs supercomputer) due to memory shortage. The environment was small, with just enough room for the ship and platform. Elements with a standard size of 2 meters were therefore used to model the environment for the ship-platform collision. The environment used is shown in Figure 6.17. The water environment is 450 meters long, 130 meters wide and 46 meters deep at the deepest. In the area under the ship, the water is 26 meters deep. There is a row of elements along all the sides of the environment allowing inflow and outflow while keeping the correct value for the hydrostatic pressure. This keeps pressure waves from being reflected by the edges of the environment. Important data is given in Table 6.9.

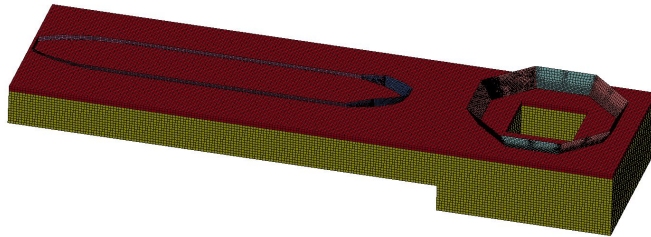


Figure 6.17: Environment used in the collision analyses.

Table 6.9: Air and water properties.

Density water	1025 kg/m ³
Bulk modulus water	1E8 Pa
Density air	1.185 kg/m ³

The complete models for both the ship and the platform were used in the analyses. To achieve a reasonable computation time, the analysis was to be split into two parts. The first part is the time up to the collision and the second part is the collision. It is necessary to have a very small time step when there is contact and deformations in the collision. This is however not necessary before the collision. Here, it is only important to give the ship and platform correct initial conditions such as velocity and draft.

How to technically do the switch from the first to second part was not solved, since there were some problems with the first part. The first problem was that the small deformable elements necessary to give a proper description of the deformation gave the analysis a very small time step. This gave the analysis a very large computation time. The time step was increased a lot by using the `*DEFORMABLE_TO_RIGID` card changing the deformable elements to rigid elements. The computation time for the initial part was however still unacceptably large. The interaction between all the small deformable elements and the water was very time consuming. A remedy for this was to create a "dummy" bow for the ship and a "dummy" shell for the platform which covered the deformable elements. The element size used for the dummy parts was 1 m. The idea was that the fluid was to interact with the dummy parts while contact between the structures was defined using the deformable parts.

Both the ship and the platform were able to find an "equilibrium" after tuning the stiffness for the FSI. They were of course not in complete equilibrium, but had motions with an amplitude of 30 cm over a period of 10 s. There was however a problem finding an equilibrium for the ship when it was given an initial velocity. The bow of the ship had a positive vertical displacement and the stern a negative vertical displacement. This represents the reality of suddenly accelerating a ship, but is not a desired motion for the analysis. Other have performed such analyses, so there must be a solution.

There were also some problems using the `*DEFORMABLE_TO_RIGID` card which make deformable elements rigid. The problem with the card was that the mass properties of the structures changed when this card was used. When this card is used the rigid parts must be merged, and it seemed like when the parts merged both of the parts got the same properties, i.e. both parts were given the properties of the master part. A solution for this problem was not found.

Due to limited time to fix these problems, the analysis with external FSI was postponed to further work. With more time it is likely that these problems can be solved.

Final attempt

A final attempt of performing a collision analyses with external FSI was made. To remove some of the problems, the FSI was removed from the ship. FSI was only included for the Octopus. To save computation time, a new smaller environment was created for the Octopus.

The analysis was successfully started, but do to the enormous computation time it was seen that it would not finish in time. The analysis was stopped after running on 720 cpus for 29 hours. Only 0.63 seconds of the collision was simulated. Using results from other analyses as a reference, it is seen that the analysis should be simulated for just over 4 seconds for the collision to be completed.

6.4 Analysis set- up

The purpose of the analyses is to see the effects of decoupling the collision problem into internal mechanics and external dynamics. Two different collision set-ups were used to analyse the ship- platform collision. One is a simplified analysis where the ship is pushed into the platform with a prescribed motion, while the second is more realistic. The two different analysis types are presented below.

6.4.1 Integrated analysis

Analyses are performed using models of the entire ship and platform. These analyses are referred to as integrated analyses.

In these analyses the ship is given an initial velocity. The Octopus has no motion before impact. Both the ship and the platform are free to move after impact. To give a better representation of reality, springs are included in most of the analyses to represent restoring forces in heave and pitch for both the ship and the platform.

Impact velocity

The tank ship will not have its normal cruising speed in a close proximity to the platform. Some speed is however necessary for maneuverability. An impact speed of 2 m/s assumed.

Restoring forces

Rigid body motions will be induced in both of the colliding structures due to the contact force. Restoring coefficients representing the water plane stiffness are therefore included in most of the analyses to better represent reality. The restoring forces are assumed to be linearly dependent of the structures rotation/translation.

The restoring forces are implemented in LS-DYNA using the following cards [Sætre, 2013].

- *DEFINE_CURVE_FUNCTION is used to track the vertical translation of chosen nodes.
- *LOAD_NODE_POINT is used to apply vertical forces in chosen nodes based on the translations found from *DEFINE_CURVE_FUNCTION.

The vertical restoring force is calculated in the following way

$$F_3 = C_{33}\eta_3 \tag{6.1}$$

Where C_{33} is the restoring coefficient in heave and η_3 is the heave motion.

There were problems using the rotation history of nodes and applying a restoring moment in a node. The restoring moment is therefore modeled using vertical forces with an eccentricity to the center of mass. The pitch angle is calculated by tracking the vertical motions of two nodes on either side of the center of gravity.

The size of the moment is determined using

$$F_5 = C_{55}\eta_5 \quad (6.2)$$

Where C_{55} is the restoring coefficient in heave and η_5 is the rotation in pitch.

The values for C_{33} and C_{55} used in the analyses are calculated in Wadam using the geometry of the hull for both the ship and the Octopus.

6.4.2 Decoupled analysis

Using only the deformable parts of the structures different collision analyses were performed. This analysis type is referred to as the decoupled analysis.

In this analysis, the bow of the ship is pushed into Octopus' side structure with different angles and impact positions. The rear end of the bow structure is given a constant velocity in the desired direction. The rear part of the bow is fixed against motions in the vertical and transverse directions. To prevent unrealistic stresses from a sudden acceleration, the bow is given an initial velocity equal to the prescribed velocity.

The free sides of the Octopus that should be connected to a surrounding structure are fixed against translation in all directions. These boundary conditions are reasonable since the connecting plates, girders and stiffeners will prevent motions in all these directions. Figure 6.18 shows the collision set- up.

Impact velocity

To avoid differences in dynamic effects in the collision, the velocity used in the decoupled analysis is equal to the velocity in the integrated analysis; 2 m/s. There may however still be differences in the impact velocity compared to the integrated analysis since the ships velocity will change in the integrated analysis. The differences are however minimized small when the same initial velocity is used.

6.4.3 Contact

For the ship- platform collisions, two types of contact are defined. The first specifies contact internally in each of the structures and is defined through the *CONTACT_ AUTOMATIC_ SINGLE_ SURFACE card. The second defines contact

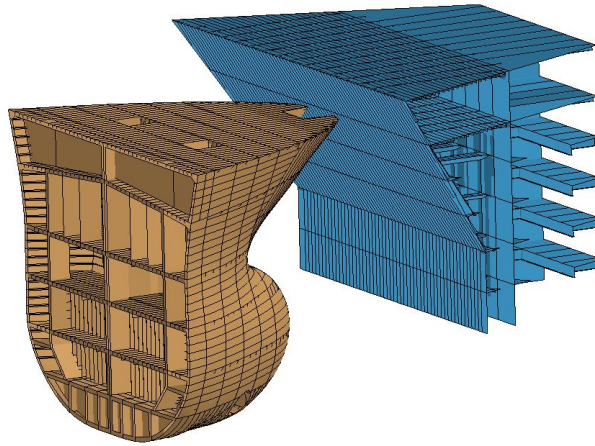


Figure 6.18: Set-up for the collision analyses with constant velocity.

between the ship and the platform. This card is defined using the `*CONTACT_AUTOMATIC_SURFACE_TO_SURFACE` card. The advantage of using a contact definition between the ship and platform is that the contact forces are easily available for post processing.

Since a detailed model of the Octopus does not exist in the area where the bulb will impact the platform, contact is only defined between the prow of the ship and the Octopus. Care is taken to only define contact for elements that are in contact with each other during the collision.

A static friction coefficient of 0.3 is used in the analyses. The static friction for clean and dry surfaces in steel-steel contact is between 0.5 and 0.8. For Lubricated and greasy surfaces the static friction coefficient is approximately 0.16, [Engineering ToolBox, 2014]. A factor between completely clean and dry and lubricated is chosen since the contact surfaces may be wet and/or dirty.

6.5 Results

Data from NLFEA can be used to analyze many different aspects in collision scenarios. Here, the most important output is presented such as force deformation curves and energy absorption curves.

The coordinate system used in the presentation of the results is fixed to the ship. The definition of the directions is as follows

- **x** Longitudinal.
- **y** Transverse.

- **z** Vertical.

The force displacement curves are created in the following matter. The force used is the contact force between the Octopus and the ship. The deformation of the bow is found by tracking the x coordinates at relevant places on the bow. The most forward x coordinate is used to describe the indentation of the bow. A representative deformation of the Octopus is found using two nodes. Since the hull of the Octopus has an angle, the point with the largest deformation may not move until some time after contact. The first node is chosen from the area where the initial contact takes place, and the second node is chosen where there is the most deformation. Nodes where fracture takes place are not chosen. For the decoupled analyses, the maxima of multiple points are used to describe the deformation of the Octopus.

6.5.1 Head on collision, ship in ballast

Two different collision analyses are performed for a head on collision between the Octopus and the shuttle tanker in ballast. The analyses are presented in Table 6.10.

Table 6.10: Overview for head on collision analyses in ballast.

Name	Motion ship	BC Ship	BC Ocoptus
Ballast0S	Prescribed	Prescribed	Fixed
Ballast0R	Initial velocity	Restoring springs	Restoring springs

Ballast0S is a decoupled analysis, and Ballast0R is an integrated analysis. The integrated analysis is run until the center of mass for the ship and platform have a common velocity.

External dynamics

The total energy dissipation has earlier been estimated using simple formulas. Figure 6.19 shows the estimates for the energy dissipation together with the energy dissipation from the integrated analysis.

It is seen that most of the absorbed energy is absorbed in the steel of the structures, i.e. internal energy. There is some sliding in the analysis, so it is reasonable to have some friction energy. The sliding energy consists of both friction energy and some numerical energy. The numerical energy is however small and will not affect the results much. In this case, the numerical energy in the sliding energy is only 0.03 % of the total sliding energy. The energy component referred to as external work, is the work done by the restoring forces. The energy from this component should go to zero when the time increases. The ship and platform will both lose their pitch angle when the effects from the collision die out.

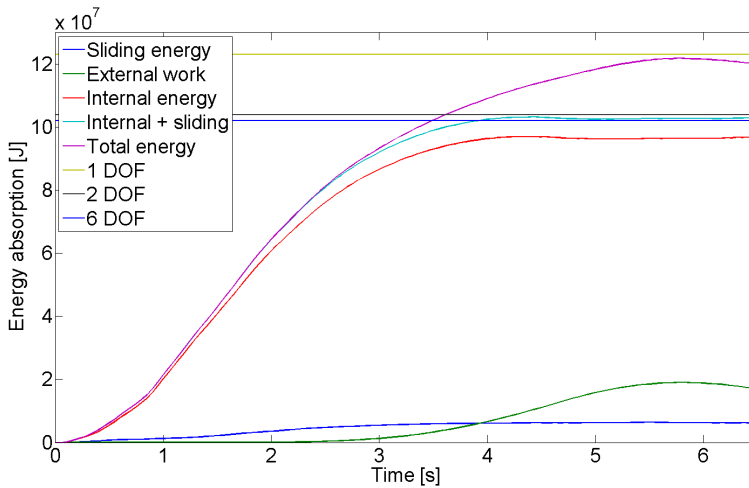


Figure 6.19: Energy absorption for a head on impact in ballast.

The two and six degree of freedom estimates fits perfectly to the actual energy absorption in the collision, i.e. sliding + internal energy. The 2 and 6 DOF methods do not take the restoring forces into account. So these are not included in the comparison. It is seen that not taking the hull angles of the Octopus and ship into account was a good assumption.

The maximum total energy that is absorbed in the collision is very close to the estimate for energy absorption using 1 DOF. The reason that the estimate is so close to the actual total energy absorption is that the ship and platform have a common velocity at 6.2 seconds. In addition, the inertia energy for the ship and platform in rotation are small at the time instant where the total energy absorption is the largest.

Internal mechanics

Figure 6.20 shows the force displacement curves for Ballast0S and Ballast0R. The force plotted against the deformation of the Octopus is the x component of the contact force. The z component of the contact force is plotted against the ships deformation in the x direction. This force is not plotted against the correct displacement and does not give an indication for the amount of energy absorbed in the collision.

It is seen that the force deformation curves are similar for the Octopus. The Octopus has a larger deformation in Ballast0S, but the deformations are generally small. Both of the force deformation curves for the ship are similar up to a displacement of 1.8 m. After this point, both the x component and the z component

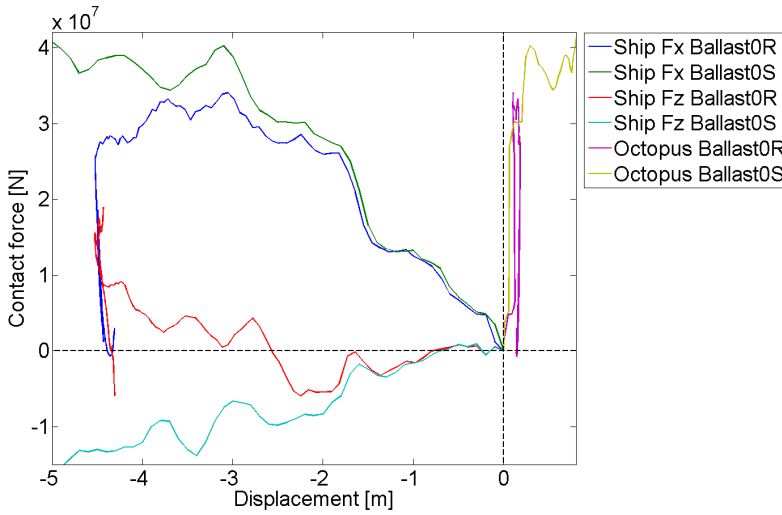


Figure 6.20: Force- displacement curves for a head on impact in ballast.

of the contact force are larger for Ballast0S. The difference is due to the motion of the platform in Ballast0R. The platform starts to get a visible roll motion when the displacement of the ship reaches 1.5 m.

The z component of the contact force is poorly estimated in Ballast0S for deformations larger than 1.8 m. Since the Octopus is fixed in Ballast0S, the only contribution to the z- component of the contact force is Octopus' hull angle. In Ballast0R, a rotational motion is induced. The rotational motion is prevented by the bow which is just above Octopus' deck, Figure 6.23. The bow is pushed upwards due to the rotational motion of the Octopus, giving a positive force in the z- direction. The vertical force acting on the top of the Octopus on the ship, is much larger than the figure indicates. This is because it is the total z- component that is presented. The angle of Octopus' hull will give a negative force in the z- direction which must be counteracted.

There is a much larger deformation in the Octopus for Ballast0S compared to Ballast0R. The increase in deformation is due to an increased contact force in Ballast0S compared to Ballast0R. The contact is larger in Ballast0S since the deck in contact with the platform fails in a different shape compared to Ballast0R, Figure 6.21. This is because the relative motions between the structures are different in the two analyses.

It is seen that only a small increase in contact force gives a much larger deformation for the Octopus. The deformations for the Octopus are small, but the increase in deformation is large, thus showing how small changes in relative strength can give different deformations in the structures.

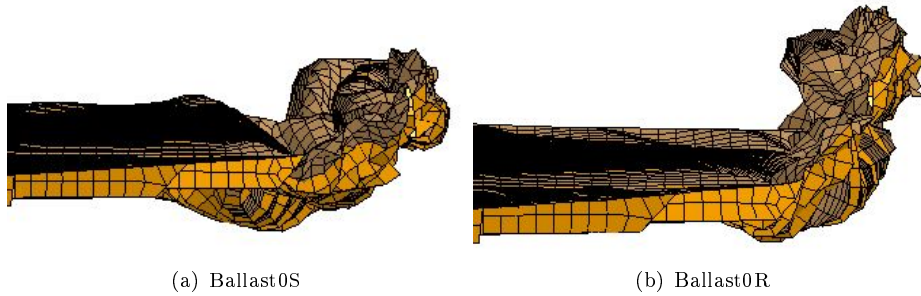


Figure 6.21: Failure shape for the deck for a head on collision in ballast.

Energy dissipation- displacement curves for Ballast0S and Ballast0R are presented in Figure 6.22. It is seen that both the internal energies and sliding energies are very similar for both cases for given displacements. There is some difference in the internal energies, but the difference is negligible in practical cases. The difference is however smaller than the difference between the x- forces in Figure 6.20 indicate. The reason that the internal energy dissipation curves are so similar must be that more work is done in the z direction for Ballast0R.

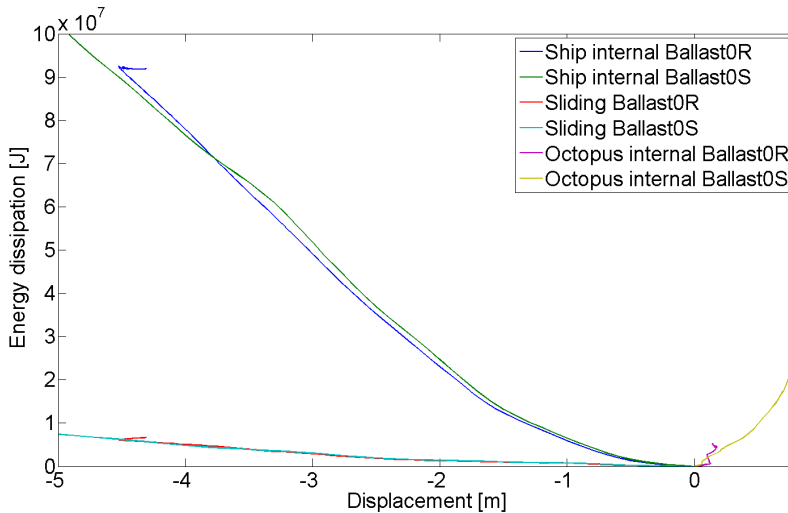


Figure 6.22: Energy absorption- displacement curves for a head on impact in ballast.

Using the 1, 2 and 6 DOF estimates to calculate the energy absorption, different estimates for the deformations of the ship and platform were calculated for the decoupled analysis and compared to the integrated analysis, Table 6.11. The deformation in the collision corresponding the energy absorptions and deformations

in Table 6.11, are shown in Figure 6.23.

Table 6.11: Ship and platform deformations. Ship in ballast.

Case	Energy absorption		Deformation [m]	
	Method	Magnitude [MJ]	Ship	Octopus
Full0R	Integrated	103	4.5	0.17
Full0S	2 & 6 DOF	103	4.6	0.73
Full0S	1 DOF	123	5.2	0.82

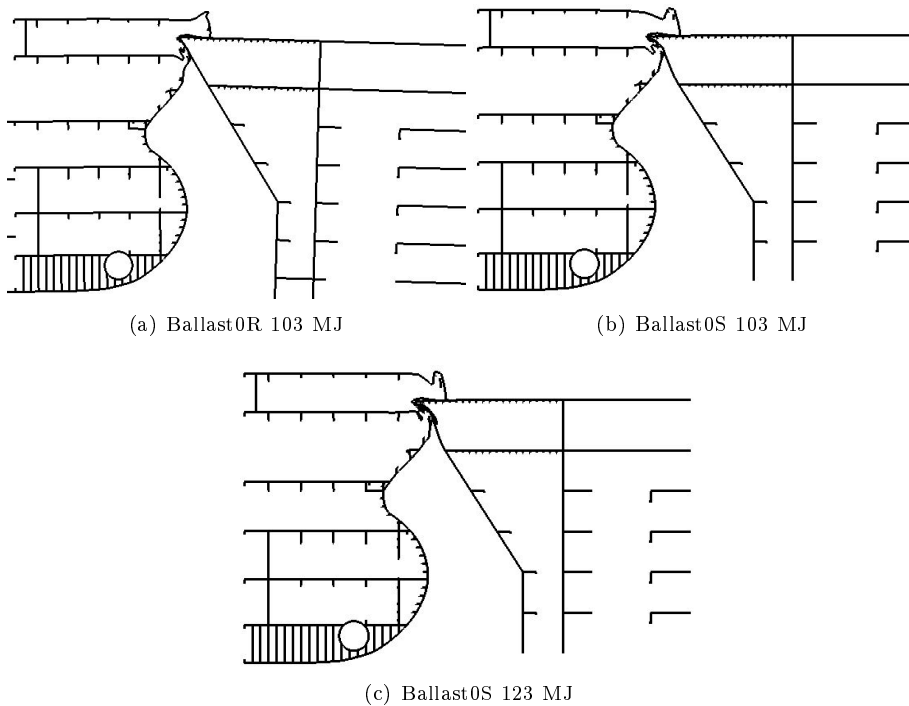


Figure 6.23: Deformations for a head on collision. Ship in ballast.

The deformations for the ship for the corresponding energy absorption is very similar. There is only 0.1 m difference. There is a much larger difference in the deformation of the Octopus for this energy absorption. The difference is 0.56 m. The reason for the increase in deformation in the Octopus is discussed earlier.

If only 1 DOF had been used to calculate the energy dissipation, it is seen that 20 MJ extra must be absorbed in the collision. The increased energy absorption will lead to a 13 % increase in deformation for the bow, and a 12 % increase in deformation for the Octopus if the results from Ballast0S are used.

6.5.2 Head on collision, ship in full load

Three different types of analyses were performed for a head on collision between the shuttle tanker and the Octopus when the tanker is fully loaded. In the simplest analysis, the bow of the tanker is forced into the side of the structure using a prescribed motion. Table 6.12 shows the analyses with names.

Table 6.12: Overview for head on collision in full load.

Name	Motion ship	BC Ship	BC Ocoptus
Full0S	Prescribed	Prescribed	Fixed
Full0	Initial velocity	Free	Free
Full0R	Initial velocity	Restoring springs	Restoring springs

External dynamics

Comparing the energy dissipations from the NLFEA to the estimates calculated in 6.1.4, it is seen that the 6 DOF method gives the best estimate. The 2 and 6 DOF estimates are plotted together with the actual energy dissipation for Full0 and Full0R in Figure 6.24. Keep in mind that these are energy levels for the initial collision. The velocity of the ship is still larger than the Octopus at the end of the simulation, and will impact the Octopus again. The external work shown in Figure 6.24 is the work performed by the restoring forces in the analysis.

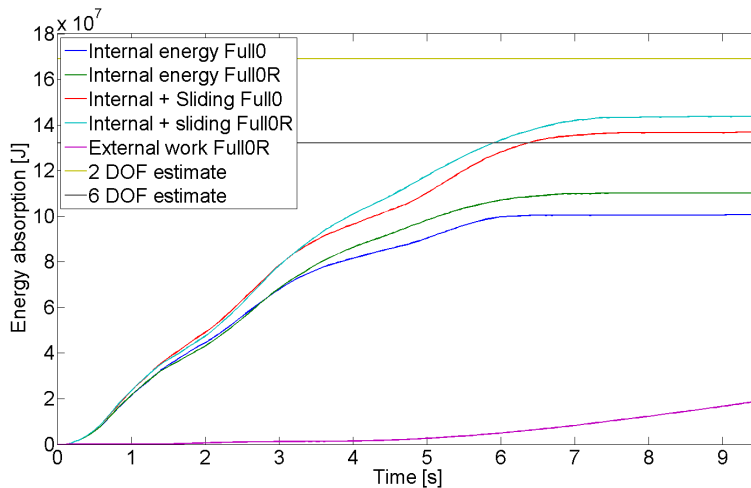


Figure 6.24: Energy absorption for a head on impact in full load.

The 6 DOF estimate for the energy dissipation is below the energy absorptions, internal + sliding, for Full0 and Full0R. The estimate is very close to Full0, which

is in fact the case that is assumed when the external dynamics are calculated. The restoring forces are not taken into account in the 6 DOF method. The 6DOF estimate is 8 % lower than Full0R and only 3 % lower than Full0.

The 2 DOF method overestimates the energy with 24 % and 18 %. This is mainly due to the fact that the 2 DOF method does not take the angle of the hull into account. The 1 DOF estimate is not valid for the initial collision since it is assumed that the collision is finished. This is not the case here.

Internal mechanics

Figure 6.25 compares the force deformation curves for Full0, Full0S and Full0R. The Octopus' deformation is plotted against the x component of the contact force. The z component of the contact force is plotted against the ships deformation in the x-direction, so the curve does not say anything about the energy absorption.

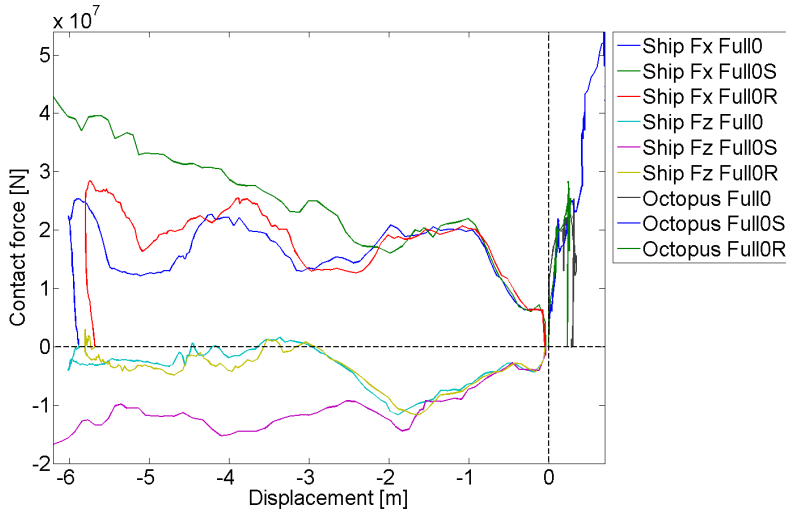


Figure 6.25: Comparison of force deformation curves for collision with fully loaded ship.

It is seen that the force deformation curves for the Octopus are quite similar. The deformations in the Octopus are very local, so the difference may be due to the nodes used to describe the deformation. Only two nodes are used to describe the deformation in Full0 and Full0R since the rigid body motion of the platform must be subtracted. The deformation in the side structure for the Octopus is small compared to the deformation of the ship for all three analyses.

Both of the force displacement curves for the ship differ for displacements after approximately 2 m. The reason for the initial difference is due to rigid body

motion of the ship in Full0 and Full0R. This allows the tip of the bow to deform upwards in a weaker shape, Figure 6.26.

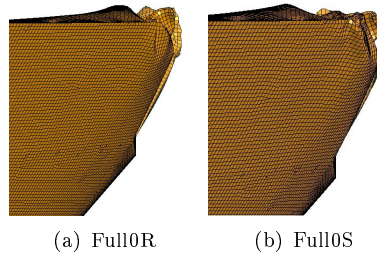


Figure 6.26: Effect of vertical motion on the deformation of the bow for Full0R and Full0S.

The rigid body motions change the angle of the ship compared to the platform, thereby changing the contact area. Figure 6.27 shows the contact area for the three different analyses for a displacement of 5 m. This will give large differences in the total contact force. It should also be mentioned that there is some difference in the deformations of the bow for Full0S compared to Full0 and Full0R. This makes the deformation plotted in the force deformation curves slightly smaller than it should be.

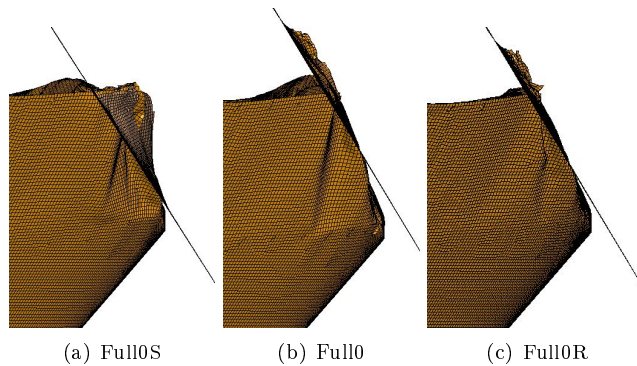


Figure 6.27: Contact area at a 5 m deformation for the ship.

It is seen that the z component of the contact force goes to approximately zero after a 2 m deformation of the bow for Full0 and Full0R. In Full0 and Full0R there is a considerable relative motion between the octopus which will lead to a vertical friction force. The friction force counteracts the part of the contact force that is due to the hull angle of the Octopus.

Figure 6.28 shows the energy displacement curves for the analyses. It is seen that the internal energy dissipation is very similar for the three analyses. There is more

sliding energy in Full0 and Full0R than in Full0S. This is due to the large amount of sliding that takes place in Full0 and Full0R.

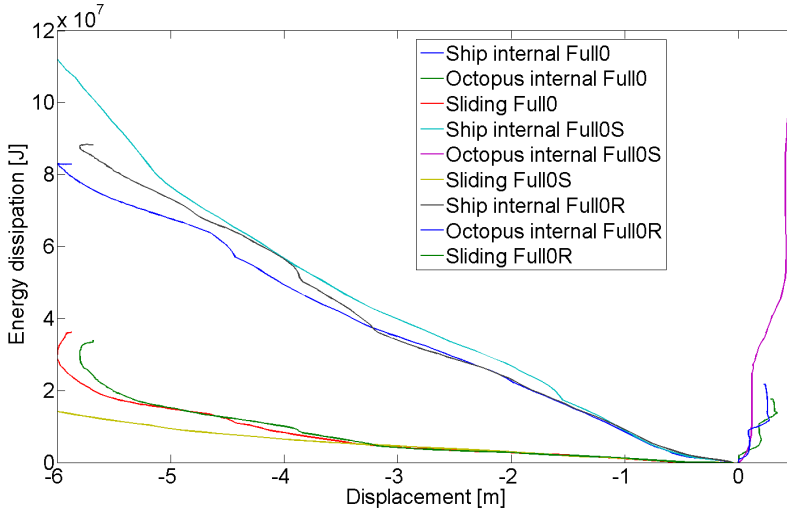


Figure 6.28: Comparison of energy absorption deformation curves for collision with fully loaded ship.

The deformation for Full0S is calculated using the 2 and 6 DOF estimates for the energy dissipation. The results are presented in Table 6.13.

Table 6.13: Ship and platform deformations. Ship in full load.

Case	Energy absorption		Deformation [m]	
	Method	Magnitude [MJ]	Ship	Octopus
Full0	Integrated	136	6.0	0.31
Full0R	Integrated	143	5.7	0.31
Full0S	2 DOF	169	6.3	0.45
Full0S	6 DOF	132	5.4	0.43

The deformations for the ship and platform are similar for all cases with an exception of the ships deformation when 2 DOF are used to calculate the energy dissipation. The platforms deformation is small for all cases compared to the ships deformation. It is a little larger for Full0S than for Full0R and Full0, since the defamation of the Octopus is more local in Full0S. The deformation at the end of the analyses is shown in Figure 6.29.

It is seen that the final contact point in the collision varies. Since the contact point is different in the analyses, the damage occurring during the collision will occur in different locations on the Octopus. Figure 6.30 shows the plastic strain on the

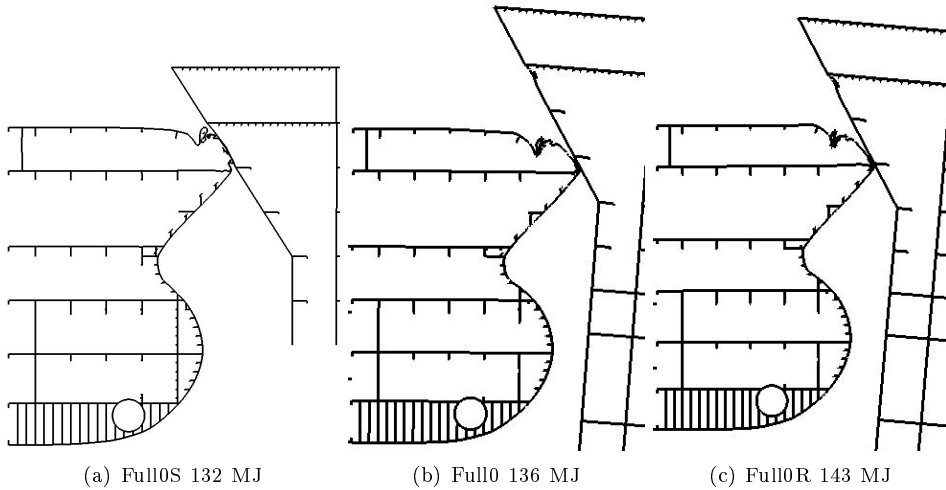


Figure 6.29: Deformations for a head on collision. Ship in full load.

deformable shell of the Octopus. Areas where the plastic strain is 0.02 or higher are marked with red. There are no plastic strains in the blue area.

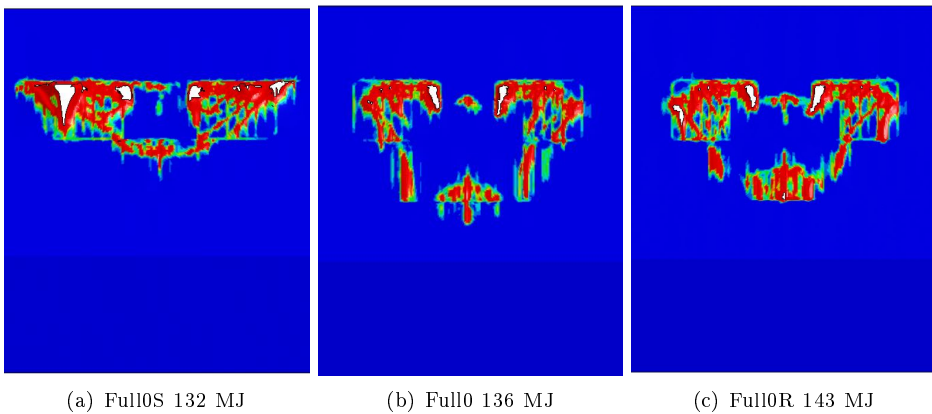


Figure 6.30: Plastic strains in outer shell. Ship in full load.

The majority of the plastic deformations in the shell of the Octopus are in the same area. This is the area where there is initial contact. It is seen that plastic deformations for Full0 and Full0R are similar in this area. The plastic deformations in this area are larger for Full0S since the contact point does not change during the analysis. Also since the contact point does not change, the simple analysis, Full0S, will not get plastic strains below the initial contact area.

The plastic deformations for Full0 and Full0R differ in the area below the contact point. There are larger plastic strains in Full0R. This is due to the water plane stiffness in Full0R. The vertical motion of the bow is prevented, and because of this, there is a larger contact force between the Octopus and the ship giving larger plastic strains.

6.5.3 Glancing impact, 30 degrees, ship in ballast

Two types of analyses are performed for a glancing impact with a 30 degree angel with the ship in ballast. The analyses with names are presented in Table 6.14.

Table 6.14: Overview for central impact with a 30 degree angle. Ship in ballast.

Name	Motion ship	BC Ship	BC Ocoptus
Ballast30S	Prescribed	Prescribed	Fixed
Ballast30R	Initial velocity	Restoring springs	Restoring springs

External dynamics

Unfortunately, the NLFEA did not impact the Octopus centrally. The energy estimates calculated in 6.1.4 are therefore modified to properly compare with the energy dissipation in Ballast30R. Giving an estimate for y-coordinate at the collision point, gave a 6 MJ increase in energy dissipation for the 6 DOF estimate and a 7 MJ increase for the 3 DOF estimate. It was not easy to estimate where the resultant force will act, so there is some uncertainty in the value. Although the estimate is uncertain, it is seen that increasing y coordinate for both the ship and the platform with one meter gave only an additional increase of 1 MJ. The energy dissipation estimates are plotted together with the energy absorption in the NLFEA in Figure 6.31.

Most of the energy is absorbed internally in the ship and platform. There is however much more sliding energy in this analysis than there is in the head on collision in ballast. The energy component referred to as external work is the work done by the restoring forces.

It is seen that the energy dissipation in the NLFEA is in between the 3 and 6 DOF estimates. The 6 DOF method underestimates the energy dissipation by 9.6% while the 3 DOF method gives a 9.6 % overestimate.

Internal mechanics

The force displacement curves for Ballast30S and Ballast30R are compared in Figure 6.32. The z and y component of the contact force are plotted against the x

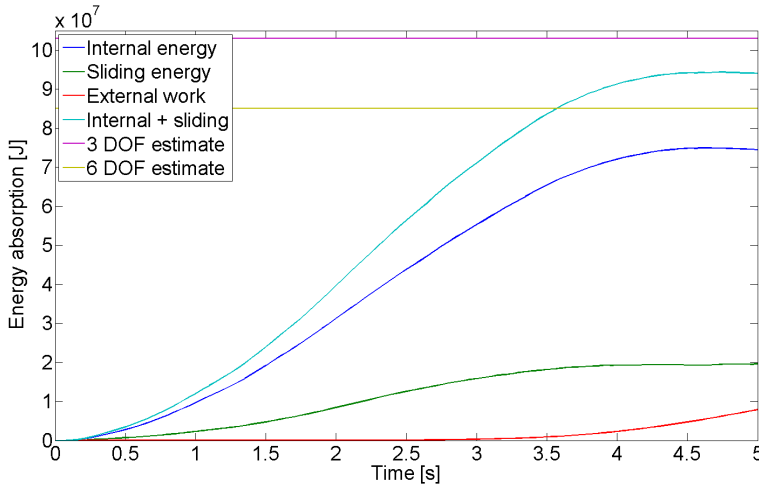


Figure 6.31: Energy absorption for a glancing on impact in ballast. Impact angle 30 deg.

deformation of the ship and do not give a representation of the energy dissipation. The deformation of the Octopus is plotted against the x component of the contact force.

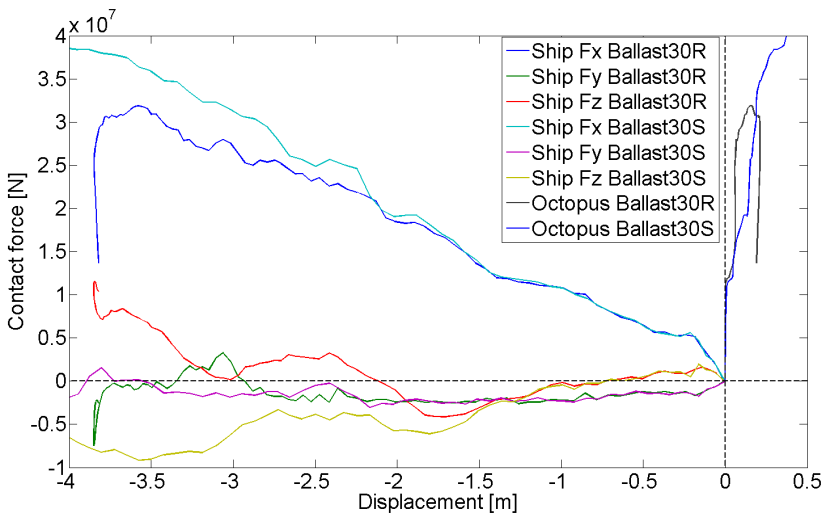


Figure 6.32: Comparison of force deformation curves for 30 deg impact. Ship in Ballast.

It is seen that all of the force deformation curves are quite similar. The largest

difference is in the z component of the contact force. The vertical contact force in Ballast30R increases due to the rotation of the Octopus which pushes the bow of the ship upwards as in Ballast0R. For displacements after 2 m, the x components of the contact force start to differ. The reason for the difference is the rigid body motions which allow the ship to deform in a weaker shape in Ballast30R.

A comparison of the energy dissipations is presented in Figure 6.33. The energy dissipation curves are quite similar for both cases. The internal energy is slightly higher for Ballast0S because of the larger contact force in this analysis. The sliding energies are also quite similar for both cases. The energy absorption curves for the Octopus differ, but end at approximately the same value. The reason for the difference is most likely due to the nodes used to describe the deformation.

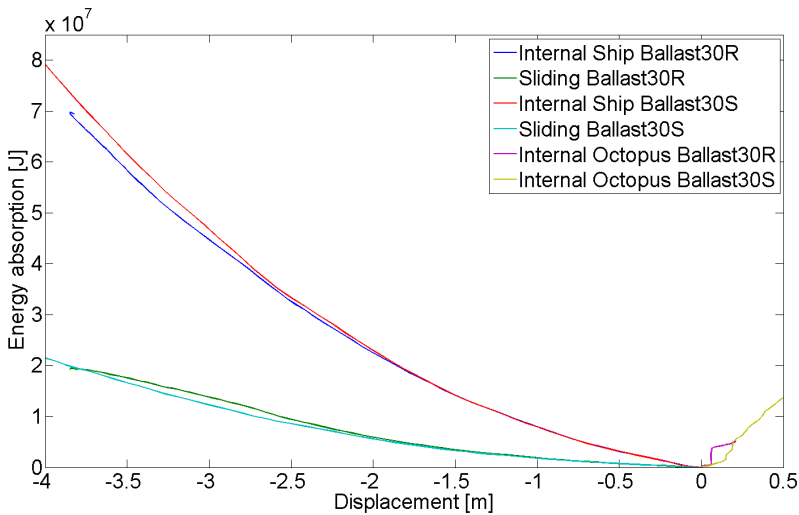


Figure 6.33: Comparison of energy absorption- deformation curves for 30 deg impact. Ship in Ballast.

The deformations in Ballast30S are calculated using the simplified energy dissipation estimates and are compared with the deformation in Ballast30R. The results are presented in Table 6.15.

Table 6.15: Ship and platform deformations. 30 deg, ship in ballast.

Case	Energy absorption		Deformation [m]	
	Method	Magnitude [MJ]	Ship	Octopus
Ballast30R	Integrated	94	3.8	0.2
Ballast30S	3 DOF	103	3.9	0.3
Ballast30S	6DOF	85	3.6	0.25

Although there is a quite large spread in the absorbed energy, it is seen that the

deformation of the ship is quite similar. There is only a 30 cm difference between the largest and smallest deformation. Figure 6.34 shows the plane with the largest deformation in both analyses. It is seen that the portion of the bow impacting the side of the Octopus deforms differently for the two analyses.

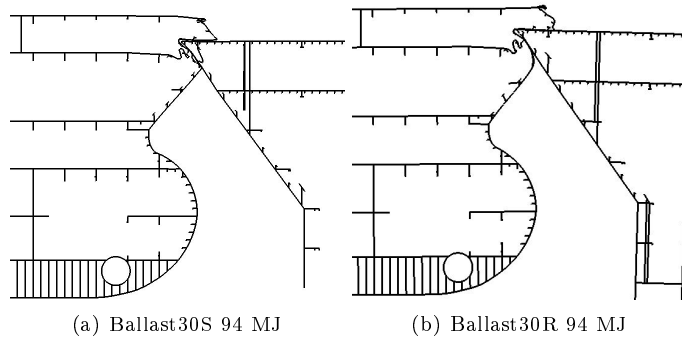


Figure 6.34: Deformations for glancing impact.30 deg, ship in Ballast.

The deformation of the Octopus is larger for Ballast30S. The reason is that the contact force is larger in Ballast30S. This results in more damage in the Octopus. Figure 6.35 shows the area where damage occurs for both analyses. The red areas in the figure are areas where the plastic strain is larger than 0.02. There is no plastic strain in the blue regions. It is seen that the region where the damage occurs is quite similar for both cases. There is however more plastic strain in Ballast30S.

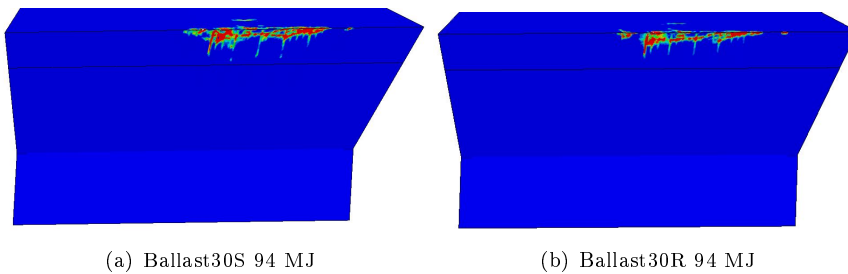


Figure 6.35: Plastic strains for glancing impact.30 deg, ship in Ballast.

6.5.4 Glancing impact, 45 degrees, ship in ballast

Two collision analyses are performed for a collision with a 45 degree impact angle. The ship is in ballast condition in the analyses. The analyses are presented with names in Table 6.16.

Table 6.16: Overview for central impact with a 45 degree angle. Ship in ballast

Name	Motion ship	BC Ship	BC Ocoptus
Ballast45S	Prescribed	Prescribed	Fixed
Ballast45R	Initial velocity	Restoring springs	Restoring springs

External dynamics

The impact position in the NLFEA did not impact the Octopus centrally as assumed in 6.1.4. However, updating both the ships and platforms impact point did not change the energy dissipation. It was also here difficult to give a good estimate for the impact position. The estimates for energy dissipation are plotted with the energy absorption in Ballast45R in Figure 6.36.

The NLFEA was not run until there was a common velocity in the contact point. There is however very little increase in internal energy after 4 s. The contact force drops to 5 MN after 4 s and start to drop further after 6 s. At the end of the analysis, the contact force is only 2 MN. Since further deformation does not occur, it is assumed that the first part of the collision is finished.

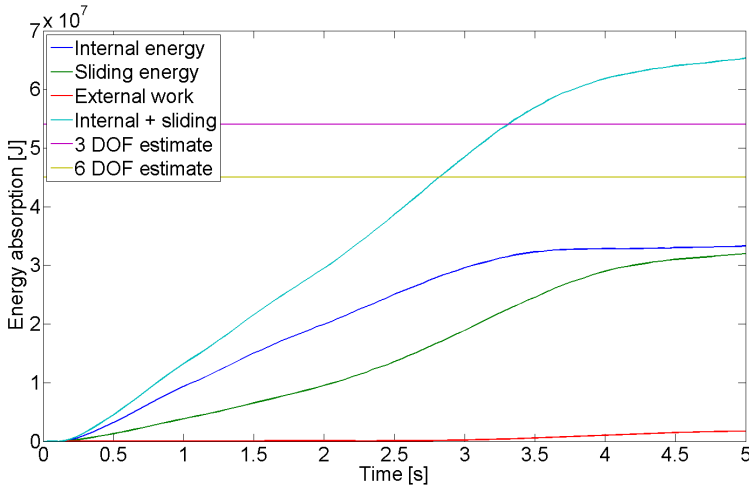


Figure 6.36: Energy absorption for a glancing on impact in ballast. Impact angle 45 deg.

There is a much larger sliding energy in this analysis than there has been in the previous analyses. At the end of the simulation time, the magnitude of the sliding energy is approximately the same as the internal energy. There is very little work performed by the restoring forces, meaning there are small motions in pitch for both structures.

The simple 2 and 6 DOF methods do not produce good estimates for the energy absorption in the collision. Comparing the energy dissipation at 3.75 s, where the internal energy stops increasing, it is seen that the 6 DOF method underestimates the energy absorption with 25 %. The 3 DOF underestimates the energy dissipation by 10 %. 10 % is not much, but the 3 DOF method should overestimate the energy dissipation since the vertical offset is not accounted for.

Internal mechanics

Force displacement curves for Ballast45S and Ballast45R are compared in Figure 6.37. The deformation of the Octopus is plotted against the x component of the contact force. The y and z component of the contact force is plotted against the x deformation of the ship and do not give a representation of the energy absorption.

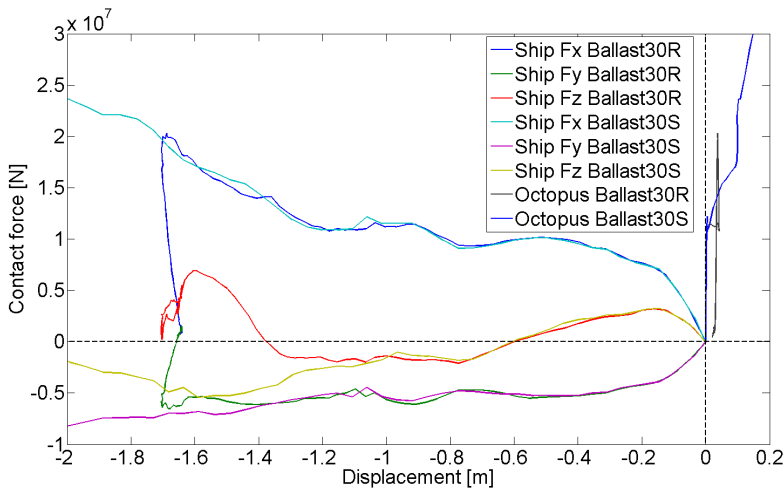


Figure 6.37: Comparison of force deformation curves for 45 deg impact. Ship in Ballast.

All of the force deformation curves are very similar. The force deformation curves for the ship with the x component of the contact force are identical until the ship stops deforming in Ballast45R. The contact forces in the y and z direction are also similar for most displacements. The z component differs for the same reason as Ballast0R and Ballast30R. The platform rotates and pushes the bow of the ship upwards giving a vertical contact force. The y component differs due to the rotation of the platform.

The energy absorption- displacement curves for the two analyses are compared in Figure 6.38. It is seen that the internal energy displacement curves for the ship are very similar for both cases. The energy dissipation curves for the Octopus differ however. The deformations in the side structure were small and very local

for Ballast45R. Picking relevant nodes to describe the displacement was therefore difficult.

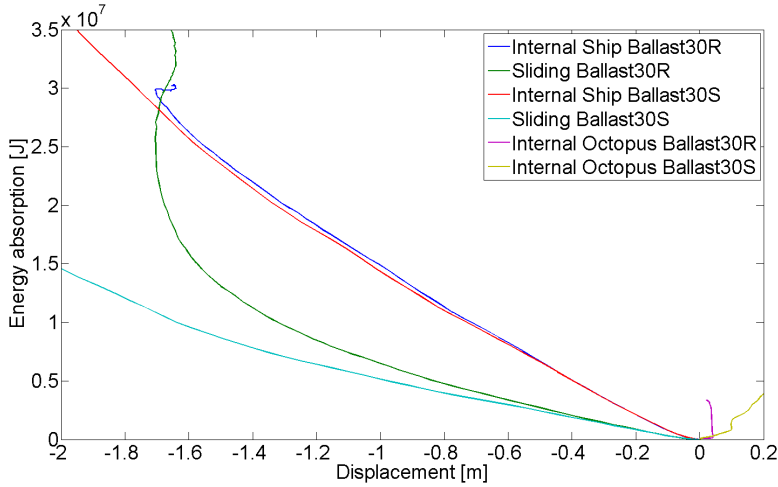


Figure 6.38: Comparison of energy absorption- deformation curves for 45 deg impact. Ship in Ballast.

Initially, the sliding energy curves for both analyses have the same slope. However, after a displacement of approximately 0.4 m, the curves start to differ. The ship is free to slide against the Octopus in Ballast45R, giving a large sliding energy in the analysis. The slope of the curve goes to infinity at the end of the simulation. The deformation stops, while the ship keeps sliding along the platform increasing the sliding energy.

The deformations in Ballast45S are calculated using energy dissipation calculated using the 3 and 6 DOF methods. The deformations are also calculated using the energy dissipation calculated in the integrated analysis Ballast45R. The results are presented in Table 6.17. Since the energy dissipation does not stop in the Ballast45R, the energy dissipation used is therefore taken at the time instant when the internal energy stops increasing.

Table 6.17: Ship and platform deformations. 30 deg, ship in ballast.

Case	Energy absorption		Deformation [m]	
	Method	Magnitude [MJ]	Ship	Octopus
Ballast45R	Integrated	60	1.7	0.04
Ballast45S	Integrated	60	2.1	0.14
Ballast45S	3 DOF	54	2.0	0.11
Ballast45S	6 DOF	45	1.8	0.10

The deformations for both the ship and the platform are overestimated in Ballast45S for a similar energy dissipation. They are overestimated since the sliding energy in Ballast45S is much smaller than the sliding energy in Ballast45R. The total energy dissipation for a given displacement is therefore much higher in Ballast45R towards the end of the analysis. It is seen that although the 3 and 6 DOF methods underestimate the energy dissipation, they overestimate the deformations in both the ship and platform. The deformations are in any matter not very large. There is hardly any deformation in the Octopus, and the ship deforms only approximately 2 m.

The deformations at the end of the collision for an energy absorption of 60 MJ are shown in Figure 6.39. Damage with equal energy dissipations are compared. It is seen that although the deformations are 0.4 m larger in Ballast45S, the deformation is quite similar. The deformations at the end of the simulation for 54 MJ and 47 MJ absorption are included in the appendix.

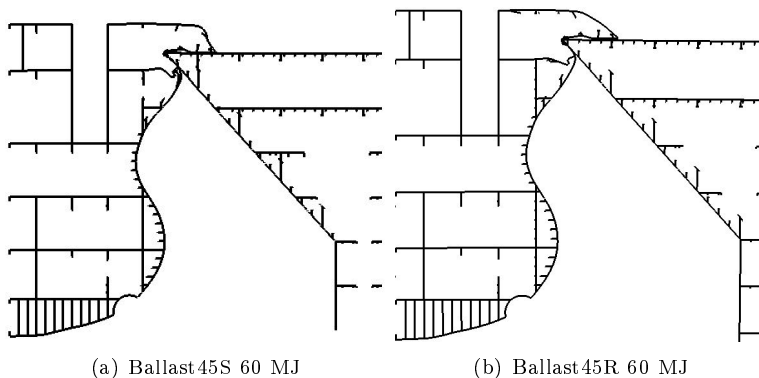


Figure 6.39: Deformations for glancing impact.45 deg, ship in Ballast.

Since there is a lot of sliding in Ballast45R, it is expected that the damage may occur in different locations on the ship and platform. This is however not the case. It is seen that the plastic deformations occur in the same area for both analyses, Figure 6.40. The area that is red has plastic strains exceeding 0.02. There are no plastic strains in the blue area. Plastic strains for a 60 MJ energy dissipation are compared in Figure 6.40. Plastic deformations for 47 and 54 MJ energy dissipation is included in the appendix.

There is very little plastic deformations on the Octopus. The strains are a little larger for Ballast45S. This is mainly because more of the energy must be dissipated as strain energy, since the sliding energy is smaller. The area where there are plastic strains is similar for the ship. The strains are also here larger for the same reason.

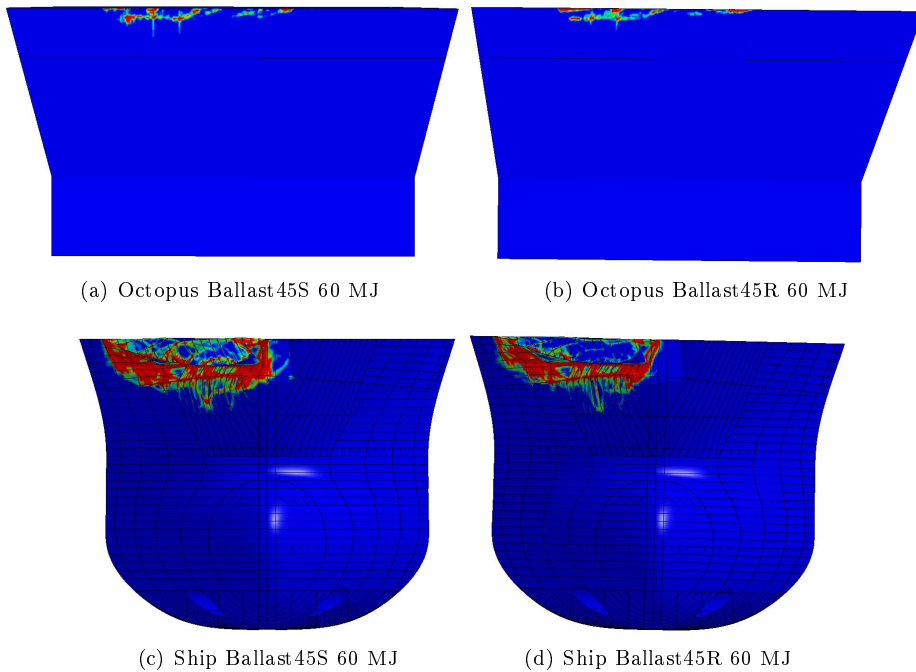


Figure 6.40: Plastic strains for glancing impact.45 deg, ship in Ballast.

6.5.5 Bulb impact

Bulbs are generally stronger than the prow, making a bulb impact more severe for a platform. The risk of fracture in the platforms outer skin is larger, and if fracture occurs, water will leak into the platforms ballast tanks.

The shape of Octopus' hull prevents the bulb from making contact. The bulb of the ship will however make contact with Octopus' hull in late stages for the head on impact in full load. In the case that the bulb makes contact, most of the energy will already have been absorbed in the initial collision between the Octopus and the prow. It is however of interest to see how much damage a bulb impact will create.

A simple analysis, where the bulb is pushed into the side of the platform with a predetermined motion is performed. The analysis set-up is shown in Figure 6.41. Since platform side is not modeled in detail below the waterline, the bulb is pushed into the Octopus above the waterline. Contact is only defined between the bulb and the Octopus.

The results from the analysis is presented in Figure 6.42. It is seen that the platform is stronger than the bulb, forcing the main deformation and energy absorption to take place in the bulb.

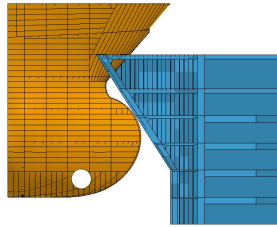


Figure 6.41: Analysis set-up for bulb impact

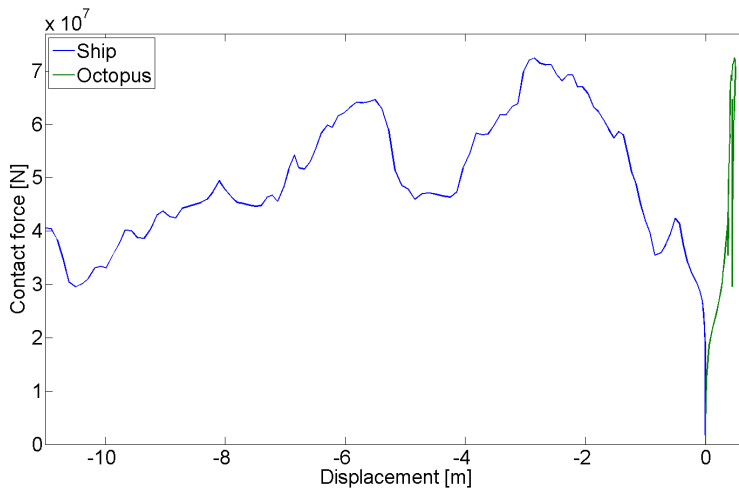


Figure 6.42: Force displacement curve for bulb impact.

Since the Octopus' side structure is stronger than the bulb, a bulb impact will not be a very severe incident for the Octopus. Fracture does however occur in the outer shell of the platform which may lead to a flooding of the impacted ballast tank.

6.5.6 Effect of hull angle

Octopus' hull has an angle above the water line. The effect of this angle on the crushing of the bow is investigated in this subsection. This does not have a direct connection with the other results, but it is however interesting to examine if the hull angle has an effect on the crushing of the bow.

The side structure of the Octopus is much stronger than the bow of the ship. There are only small deformations in the shell of the Octopus, and the deformations are local. The results from FullOS are therefore compared to a corresponding analysis where the ship's bow is pushed into a rigid wall. The results are presented in Figure

6.43. The deformation parameter used is the motion of the rear part of the bow after impact.

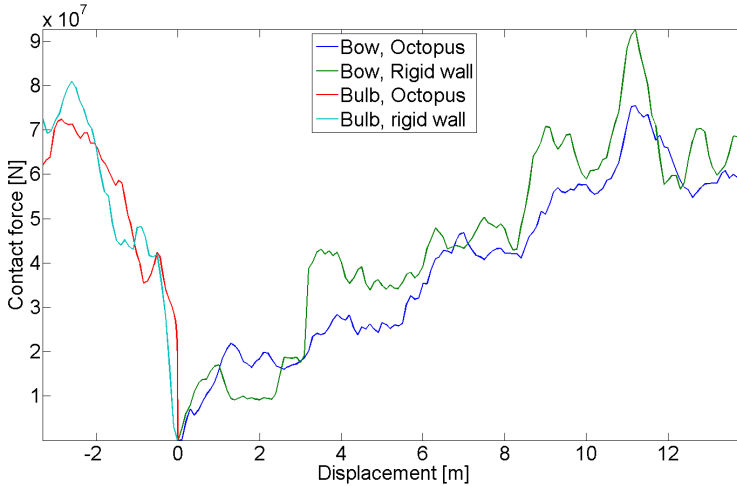


Figure 6.43: Force displacement curve with different hull angles.

Focusing on the bow, it is seen that the force is as expected larger for the impact against the rigid wall for most displacements. The difference is however smaller than expected. The contact area between the structures is larger for the impact against the rigid wall.

The contact force is however larger for the collision against the Octopus for displacements between 1 and 2.5 m. The reason for the difference is the same as the reason for the difference between the force displacement curves discussed in 6.5.2. The bow impacting the rigid wall is forced upward, therefore failing in a weaker shape. The shape of Octopus' hull prevents upward motion of the bow, forcing the bow to fail in a stronger shape. It is seen that the effect of the hull angle is small.

Comparing the strength of the bulb was more difficult than comparing the strength of the prow. After a displacement of only 3.3 m, the top of the bulb is fully crushed due to the angle of Octopus' hull. After this point the analyses are not comparable. In the small range the analyses can be compared, it is seen that the bulbs have similar strength for both analyses. There is no apparent difference in strength due to the hull angle.

6.6 Discussion

6.6.1 Added mass

The mass distributions for the models were created with the intention to be used in a water environment. Added mass was therefore not taken into account. Since the analyses with external FSI proved to be too difficult to perform, all the analyses are run without taking added mass into account. As seen in Table 6.2, the contribution from added mass is substantial in some of the directions. Not taking added mass into account will therefore not give a correct representation of reality.

One of the most important contributions the added mass has, is to give the ship more kinetic energy in to the collision. Assuming the mass distributions are the same (without added mass) the total energy dissipation should increase with approximately the size of the added mass coefficient for the ship in surge, 4 to 7 %, ref. Eq. 1.3.

The relative mass between the platform and the ship will change if added mass is included. The added mass factor in surge is 0.043 for the ship in ballast and 0.82 for the Octopus. The increase in mass will therefore be much larger for the Octopus. Since the Octopus' mass increases more than the ships, a larger percentage of the kinetic energy coming into the collision must be absorbed, ref. Figure 6.11. There is also a large added mass in pitch for both structures. This will also increase the energy dissipation.

An estimated energy dissipation is calculated for head on collisions including added mass using the methods presented in 1.2. The results are presented in Table 6.18.

Table 6.18: Energy dissipation for head on collision with added mass.

Calculation method	Energy dissipation [MJ]	
	Full load	Ballast
1DOF	252	146
2DOF	238	136
6 DOF 0 deg	205	136

When comparing Table 6.18 to Table 6.3, it is seen that there is a significant increase in energy dissipation when added mass is included. For a head on impact in full load, the energy dissipation increases with 29 % if one degree of freedom is used. The increase in the initial collision calculated using 6 DOF is 55 %. A lot more energy must be dissipated in a real case where there is added mass and the deformations will therefore be much larger.

Although more energy is dissipated when added mass is included, including added mass is not only negative. The platforms and ships moment of inertia will increase, giving the structures a smaller and slower pitch motion. For platforms with an inclined hull, the prow of the ship will contact the platform first. During the

collision both of the structures will start to rotate making it possible for the bulb of the ship to impact the platform. If the rotations are smaller, the chance of a bulb impact will be reduced if the increase in deformation is disregarded.

Most of the extra energy will most likely be absorbed by the ship's bow since the side structure of the Octopus is much stronger than the bow of the ship. The size of the extra deformation in the bow is difficult to determine since the contact force generally increases for increased displacements. Using the 6 DOF estimate and a head on collision in ballast, it is seen that the deformations for the ship and platform are 5.6 m and 0.86 m, respectively. The ships deformation is 15 % larger than when added mass is not included. It is seen that since the contact force increases, the increase in deformations is much smaller than the increase in energy.

Since added mass is not included in these analyses, the ship platform collisions cannot be directly used for design verification.

6.6.2 Energy dissipation estimates

None of the impact scenarios investigated had the collision force penetrate through the center of gravity. The most commonly used method, taking 1 DOF into account, overestimated therefore the energy dissipation for all cases. However, the 2 and 6 DOF methods were able to give good estimates for many of the investigated cases. The error in the estimated energy dissipation is less than 10 % for all cases if the 6 DOF method is used with an exception of the glancing impact with 45 degree angle. The estimates are however generally on the low side.

Three different aspects with regard to the estimates for the energy dissipation are discussed below; the duration of the collision, the sliding energy and the geometry at the point of the collision.

Collision duration

The length of the collisions vary from 3.75 seconds for Ballast45R to 7 seconds for Full0R. Comparing the collision duration to the Eigen periods for the ship and platform in pitch, it is seen that the assumption that the collision duration is short is valid for the Octopus, but not for the ship. The main motion with an Eigen period excited in the collision, is pitch for both the ship and the platform, and is therefore the relevant Eigen period to use in the comparison. Mooring for the Octopus is not included in the analyses, so there is no Eigen period in surge.

The Eigen period for the Octopus is 45 seconds which is large compared to the collision duration. The restoring forces will therefore only have a small effect on the response since the response will be inertia dominated. The ships Eigen period is however 6 seconds. Assuming that the collision is half of a loading period, it is seen that the ships Eigen period is below the loading period. The response of

the ship in pitch will therefore be dominated by the water plane stiffness, and not inertia effects as it is assumed in the simple methods.

The effect of not including the water plane stiffness is seen in the collision analyses where the ship is full loaded and impacts the platform head on. The 6 DOF estimate is closest to Full0, which is in fact the case assumed in the simple calculations. Comparing the 6 DOF estimate to Full0R, it is seen that the energy dissipation is underestimated. This is because the restoring forces are important for the response of the ship. Figure 6.44 shows the vertical motion for the bow for Full0 and Full0R. It is seen that including the stiffness has a large effect on the motion of the bow. Including the stiffness leads to an increased energy dissipation since the platform must rotate away from the ship in Full0R, while they can rotate away from each other in Full0. Including the water plane stiffness in the model of the Octopus, causes only a small change of Octopus' motions since the response is inertia dominated. The change is not of practical importance.

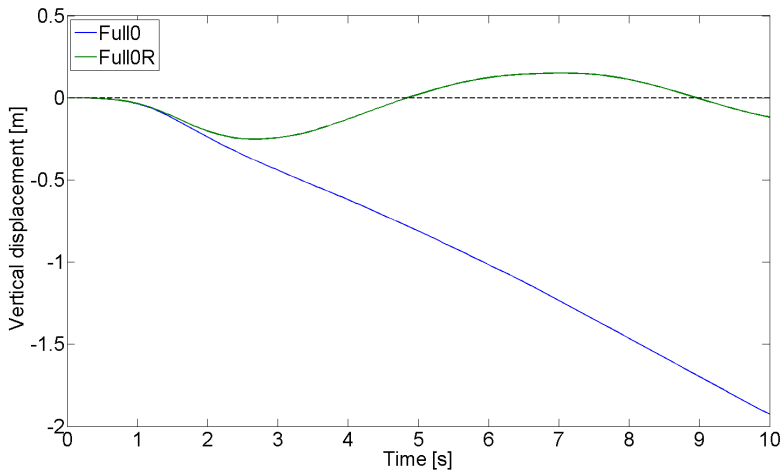


Figure 6.44: Vertical motions at the tip of the bow for Full0 and Full0R.

In the head on collision in ballast, the error of not including the restoring springs will be a lot smaller than for the fully loaded case. When the ship is in ballast it is assumed that the impacted geometry is vertical, and not inclined. For impacts on inclined surfaces, a vertical force will act on the impacting structure. For this case, the vertical force has a very large arm to the center of gravity, 130 m. Pitch motions can easily be induced in the ship even for rather small forces. If the impacted geometry is vertical, there will only be a horizontal force. The arm of the force is only 14 m in the analyses, so a much larger force must act to induce the same motions. Thus, the ship for the ballast condition will not rotate as much, and the error of not including the water plane stiffness in the simplified methods will therefore be smaller.

Sliding energy

In the NLFEA a static friction coefficient of 0.3 is used in the analyses. After conferring with Zhenhui Liu it was found reasonable to use the same friction coefficient in the 6 DOF method. It is however not certain that the same friction coefficient will in fact give the same physical representation of the friction.

For glancing impacts, it is seen that the energy is under estimated using the 6 DOF method. In these NLFEA, the sliding energy gives a large contribution to the total energy dissipation. If the friction is handled differently in the codes, it may be part of the reason for the simple methods under estimations. However, the 6 DOF method estimated the energy dissipation quite accurately for the fully loaded case. This shows that the problem may be something else.

One of the assumptions in Stronge's impact theory, which is the basis for the 6 DOF method used here, is that the deformations are limited to a small area within the contact surface. For the glancing impacts, a rather large area of the bow is in contact with the Octopus compared to the deformations. This will lead to a rather large sliding energy compared to the strain energy.

Another factor that may affect the friction energy is the impacted geometry. In the simplified method it is assumed that the ship impacts a flat structure. In the NLFEA, the upper deck of the Octopus penetrates into the bow. It is uncertain how this effects the friction energy.

Impacted geometry

For a head on collision in full load, the 2 and 6 DOF methods give different estimates for the energy dissipation. The main reason for the difference is that the impacted geometry is assumed to be vertical and flat in the 2 DOF method, while it is assumed to be inclined in the 6 DOF method. Another factor is that the ship cannot absorb energy by rotating in the 2 DOF method.

The 6 DOF method gives a quite accurate estimate for the energy dissipation for the head on collision in full load. The assumptions in the 6 DOF method seem therefore to be correct. The 2 DOF method, assuming a non-inclined geometry, overestimates the energy dissipation with 18 % when comparing to FullOR.

For the all of the ballast collisions, some engineering judgment was used to determine angle of the impacted geometry. The top of the bow is above the upper deck of the Octopus, and the upper deck of the Octopus will therefore penetrate into the bow of the ship. Due to the inclined angle of Octopus' hull, a negative vertical force will act on the ship. However, since the upper deck of the Octopus is below top of the bow, a downward motion of the ship will be prevented by Octopus' deck. A flat vertical impact geometry is therefore assumed for the collisions where the ship is in ballast.

It is seen that assuming that the impacted geometry was flat and vertical was good. Both the 2 and 6 DOF method gave the same estimate for the head on collision in ballast, where a flat vertical impact geometry is assumed for both methods. The estimates were close to the actual energy dissipation. The 6 DOF estimate was also close to the energy dissipation for the 30 degree impact.

6.6.3 Damage

The damage estimated decoupling the internal and external mechanics has been compared in 6.5. Three different aspects regarding damage in the collision are discussed below: the contact force, the area where the damage occurs, and the size of the deformation.

Contact force

Force deformation curves for the analyses where the collision problem is decoupled into internal and external mechanics, are compared with results from integrated analyses, in 6.5. It is seen that the force deformation curves are identical for the first phase of the collision, but start to differ after a deformation of 2 m. The largest difference in force deformation curves is for the head on collision in full load. Common for all cases is that the curves start to differ when the platform visibly starts to rotate. This happens just under a second after the initial impact.

The reason that the force deformation curves vary the most for the head on collision in full load, is that this is the case where the largest pitch motion is induced in the Octopus. The bow will therefore be freer to deform in a weaker shape for this case, compared to the analysis with a prescribed motion. The contact area may also change due to the relative motions. For the collisions when the ship is in ballast, the ship and platform lock to one another and large motions are prevented. The impact geometry will therefore be very similar in the integrated and simplified analyses.

Deformation length

The deformation of the ship and platform for the simplified analyses were estimated using simplified methods for calculating the external dynamics. The deformations were compared to the deformations calculated in the integrated analyses. In the comparison below, the 6 DOF method is used to calculate the energy dissipation.

Comparing the deformation of the ship calculated decoupling the problem with the results from the integrated analyses, it is seen that the estimate found by decoupling the problem is quite accurate. The largest difference in the deformation is only 5.9 % and occurs for the impact with a 45 degree angle in ballast. The energy dissipation estimate using the 6 DOF method is for this case 25 % lower than

the energy dissipated in the integrated analysis. However, since the sliding energy is much smaller in the simplified analyses than in the integrated analyses, the deformation is actually over estimated.

Although the deformations for decoupled analysis with a 45 degree impact angle are accurate, the energy dissipation was inaccurate. The small differences in deformations may therefore just be a coincidence. The sliding energy is greatly underestimated in the decoupled analysis, and the results are therefore only similar since the estimated energy dissipation was too low. If the estimated energy dissipation had been correct, the deformation would have been much larger. Since the energy dissipation is not correctly estimated, the results from the decoupled analysis with a 45 degree impact angle are not trusted.

The difference in the deformations for the Octopus are however larger. The largest difference is an overestimation of the deformation by 430 %. The reason for the large difference is that the contact force in the simplified analyses is generally larger than in the integrated analyses for large deformations. For the case with a 430 % overestimate, two girders fail due to the increased contact force giving much larger deformations.

It is seen that the force deformation curves for the Octopus are similar up to the maximum contact force that occurs in the integrated analyses. Since the maximum contact force is larger in the simplified analyses, the deformation of the Octopus becomes larger. This applies for all cases except for Ballast45. The deformation of the Octopus is however small compared to the deformation of the ship for all cases.

Deformed area

The area where the deformation occurs is very similar for the ship in all cases. The largest difference is seen in the impact with a 45 degree angle, Figure 6.40. The damaged areas on the Octopus however, vary for one of the cases when the simple analyses are compared to the integrated analyses. The largest difference here is seen for the head on impact in full load, Figure 6.30. Here, the platform rotates and damage occurs below the initial contact point. This effect is important to take into account if there are large differences in the structural strength of the platforms side at different vertical positions.

For the other analyses, the area where the deformation takes place is very similar. There are however generally larger plastic strains on the Octopus in the simplified analyses, but this is discussed earlier.

6.6.4 Numerical errors

Numerical errors were a problem in all of the collision analyses for the ship- platform collision in full load, Full0, Full0R and Full0S. The total energy was fairly constant, changing with less than 5 %, but spurious stresses were discovered for

large simulation times. It was also seen that the internal energy increased even after the collision was completed. All of the other analyses seemed to be fine.

The time step was reduced to see if that was the problem. Reducing the time step gave good results for Full0S and Full0R. Nothing indicated that there were numerical errors of practical interest in these two analyses. For Full0 however, there were still problems. The spurious stresses disappeared and the internal energy did not increase after contact, but a lot of energy disappeared in the analysis. The total energy at the end of the simulation was 10 % less than in the beginning.

A final attempt was made to reduce the numerical error in Full0. The analysis was run with double precision, and the contact definition was removed from elements that do not need contact in the analyses. With these improvements, the total energy remained constant throughout the analysis. The total energy increase was only 0.3 %, which is very little. The results presented in this thesis are the results without any apparent numerical error.

The force displacement curves and energy absorption curves for two analyses are shown in Figures 6.45 and 6.46. The analysis is two versions of Full0; one with apparent numerical errors, and one without. Full01 refers to the analysis with a loss of total energy and no spurious stresses, and Full02 refers to the analysis that was run with double precision.

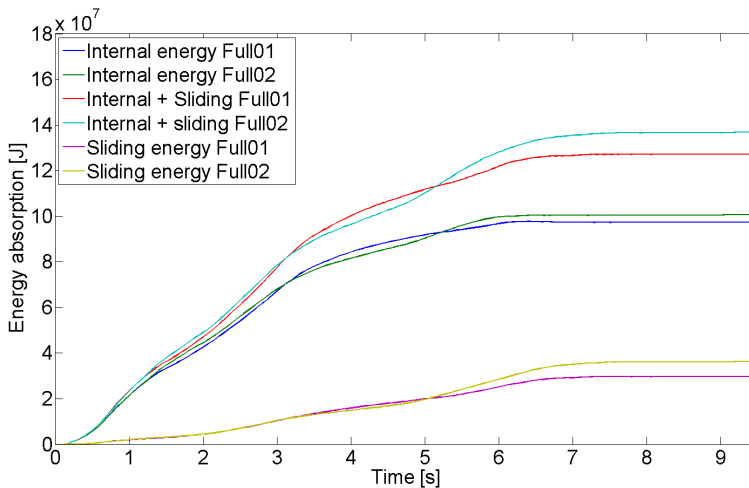


Figure 6.45: Comparison of energy dissipation with single and double precision.

The results are similar, but there is a clear difference. The main difference is that the energy absorption is higher for Full02. Both the sliding and internal energy is larger here. The force deformation curves are however very similar. This comparison shows that it is important to check the results to see if there are any apparent errors.

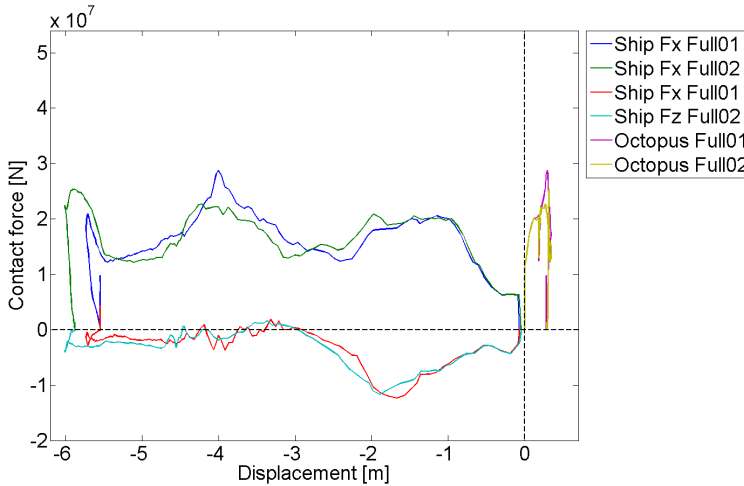


Figure 6.46: Comparison force displacement with single and double precision.

If using double precision will affect the results for the other analyses, is unknown. A good practice could be to run the problem at hand with both double and single precision to see if it affects the results, as the first analysis. There are however some drawbacks using double precision. The computation time increases with 30 % and the size of the result files double. Double precision is therefore only used when the results clearly change as they did here.

6.6.5 Octopus' boundary conditions

The model of the Octopus used for the integrated analysis consists of a deformable part connected to a rigid part. In reality the whole structure of the Octopus will deform, making the connection between the deformable part of the Octopus and the rigid part unrealistic. To see the effect of using these boundary conditions, two analyses using only the deformable part of the Octopus and ship are performed.

In the first analysis, Boundary 1, all the free sides that should be connected to internal structure in the Octopus are fully constrained. In the second analysis, Boundary 2, the vertical sides of the Octopus are completely free while the back and bottom of the model are fully constrained. Figure 6.47 shows the sides of the model that are constrained. The nodes that are constrained are marked in black.

The force deformation curves from both analyses are presented in Figure 6.48. It is seen that the curves are quite similar. The force deformation curves for the Octopus are nearly identical and the force deformation curve for the ship is similar for both cases. After a deformation of approximately 6 meters, the force displacement curves of the bow starts to differ. The difference is however small, indicating that

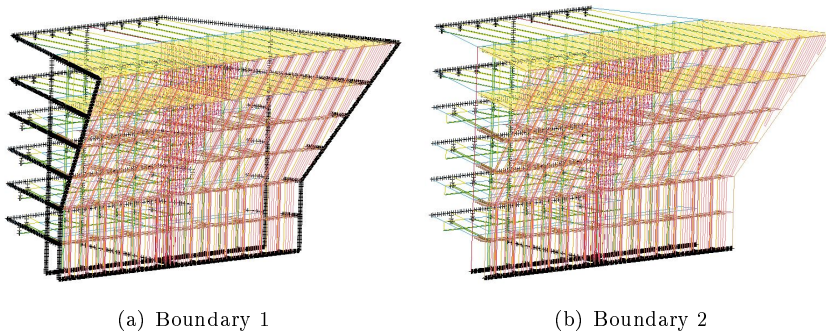


Figure 6.47: Fixed edges for Boundary 1 and Boundary 2.

using fixed boundary conditions for the free edges of the deformable model is a good assumption. In reality, the boundary conditions will be somewhere between Boundary 1 and Boundary 2. The reason that there is such a small difference between the two cases is that the platform deforms very little during the collision, giving a very similar impact geometry for both cases.

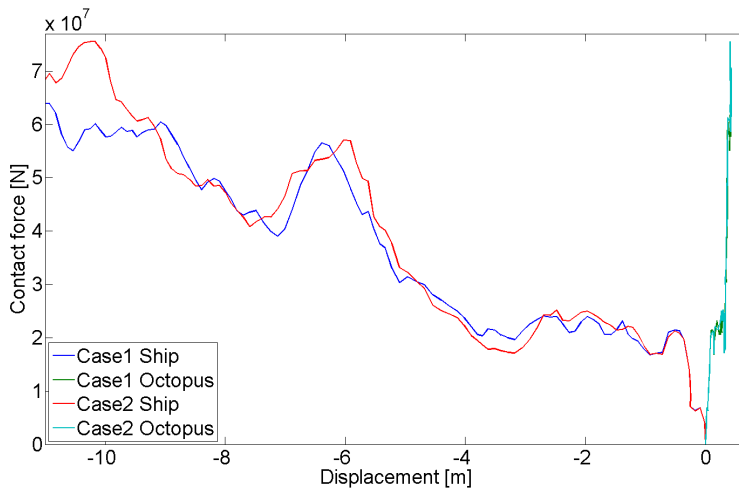


Figure 6.48: Comparison of force displacement curves for Boundary 1 and Boundary 2.

6.7 Conclusion

Different collision scenarios are analyzed in this chapter. All of the chosen scenarios are analyzed with an integrated analysis, and an analysis where the problem is decoupled into external dynamics and internal mechanics. The results from the two analysis are compared.

When the collision problem is decoupled, the energy dissipation must be calculated using simplified methods. Comparing the energy dissipation estimated by the 6 DOF method to the energy dissipation in the analyses, it is seen that the energy dissipation is estimated within 10 % for all cases with an exception of one. For the collision in ballast with a 45 degree impact angle, the 6 DOF method underestimated the energy dissipation with 25 %.

The force deformation curves for the bow of the ship are generally steeper for large deformations in the simplified analyses where the problem is decoupled, than it is in the integrated analysis. This results in a generally larger deformation of the Octopus if the problem is decoupled. The deformation of the ship estimated decoupling the problem is very close to the deformation of the ship in the integrated analysis. If the 6 DOF estimate is used, the largest difference in deformation is an overestimation of 5.9 %.

The damaged area is similar for all cases analyzed with an exception of the head on collision in full load. Here the damage occurs over a larger vertical area in the integrated analysis, than it does in the simplified analysis. The damage is however smaller, so as long as the strength of the platforms side does not change vertically, the results should be conservative. The damaged area for the ship is similar for all cases.

Based on the analyses, it is seen that the decoupling of the problem into internal mechanics and external dynamics gives reasonable results for impact angles that are 30 degrees and less. The energy dissipation is estimated fairly accurately for all cases except for the impact with a 45 degree impact angle. The deformation of the ship is also accurately estimated for all cases but tends to be smaller than the deformation in the integrated analyses. The deformation of the Octopus is however overestimated in the decoupled analyses since the force deformation curve is steeper for the ship for large deformations. The results from the decoupled analyses are therefore slightly conservative if the platform is of interest, and slightly non-conservative if the ship is of interest.

Chapter 7

Conclusion

In this thesis literature review of collisions with FSI is performed. Both cases with internal and external FSI interaction are included.

Modeling fluids and fluid structure interaction in LS-DYNA has been learned. Analyses where the a floating structure floats with an almost constant draft is successfully performed.

Using parameters that gave the most correct buoyance, analyses were performed to investigate the how large the added mass is in LS-DYNA. Added mass coefficients were calculated for a number of periods, and compared to added mass coefficients calculated in Wadam. The comparison showed that the added mass is not included properly using the modeling parameters used in this thesis. For small periods the added mass coefficients were reasonable, but they were completely wrong for periods over 10 seconds. More work should therefore be performed to find more adequate parameters for ALE modeling.

Collision analyses on a simple case including internal fluid structure interaction is performed. The results show that including ballast water in the impacted ballast tank has a clear effect on both the contact force and energy dissipation. The effect is small for the smallest velocity before the water reaches the ceiling of the tank. For the two larger velocities the presence of water inside the tank strengthens the tank throughout the analysis. Since the water strengthens the ballast tank, it is concluded that it is non-conservative for the empty structure and conservative for the water filled structure to neglect the effect of ballast water in the analyses.

Realistic collisions between a shuttle tanker and Moss Maritimes Octopus were analyzed using NLFEA. Both an integrated analysis and an analysis where the problem is decoupled, were performed for each case. The results were compared. Attempts were made to perform collision analyses with external FSI, but this proved to be too difficult and was not performed.

Decoupling the problem into external dynamics and internal mechanics gave results

similar to the integrated analyses for most of the scenarios. The energy dissipation estimated was accurate for all cases with an exception of a 45 degree impact. The damage of the platform was typically too large, and the damage in the ship too small in the decoupled analyses. The difference in damage was however not very large. There was however a difference in where the damage occurred on the platform for one of the cases.

The results show that the energy dissipation can be estimated for impact angles up to 30 degrees. The results from the decoupled analyses are typically non-conservative for the ship and conservative for the platform.

Chapter 8

Further work

Validate simple model tests with internal FSI simulations

A small model of a tank can be created in rammed with an indenter with different filling levels. The results can be used to see how accurate the simulations run in LS-DYNA with internal FSI are.

Realistic collision with internal FSI

Perform realistic collisions between a ship and a real ballast tank including internal FSI.

Check energy dissipation estimates

Compare the energy dissipation from more integrated analyses with the 6 DOF energy dissipation estimate to determine its validity range. Compare also the velocities of the colliding structures after the collision with the estimates from the 6 DOF method.

Collision analysis with external FSI

Continue working on collision analyses with external FSI. Investigate the added mass contribution in LS-DYNA for large periods.

Referances

- Hagbart S. Alsos, Jørgen Amdahl, and Odd S. Hopperstad. On the resistance of penetration of stiffened plates, Part II: Numerical analysis. *International Journal of Impact Engineering*, 36:875–887, 2009.
- Hagbart Skage Alsos. *Ship groground - Analysis of ductile fracture, bottom damage and hull girder response*. PhD thesis, NTNU, 2008.
- Marco Anghileri, luigi M.L. Castelletti, and Maurizio Tirelli. Fluid-structure interaction of water filled ttank during the impact with ground. *International Journal of Impact Engineering*, 31:235–254, 2005.
- N. Aquelet, M. Souki, and L. Olovsson. Euler-lagrange coupling with damping effects: Application to slamming problems. *Computer methods in applied mechanics and engineering*, 195:110.132, 2006.
- Jim Day. Guidelines for ale modeling in ls-dyna. Draft, October 2010.
- T. de Jonge and L. Laukeland. Collision between a spar platform and a tanker. *Collisino and Grounding of Ships and Offshore Structures*, pages 267–272, 2013.
- Ian Do and Jim Day. Overview of ale method in ls-dyna. Presentation, March 2014. URL http://awg.lstc.com/tiki/tiki-download_file.php?fileId=23%E2%80%8E.
- DYNA Examples. ALE FSI, February 2014. URL <http://www.dynaexamples.com/ale/fsi>.
- The Engineering ToolBox, 2014. URL http://www.engineeringtoolbox.com/friction-coefficients-d_778.html02.05.14.
- O. M. Faltinsen. *Sea Loads on Ships and Offshore Structures*. Camebridge, 1998.
- R. E. Gagnon and A. Derradji-Aouat. First results of numerical ssimulation of bergy bit ccollision with the ccgs terry fox icebreaker. In *Proceeding ih the 18th IAHR International Syposium in ice*, 2006.
- R.E Gagnon and J. Wang. Numerical simulations of a tanker collision with a bergy bit incorporating hydrodynamics, a validated ice model and damage to the vessel. *Cold Regions Science and Technology*, 81:26–25, 2012.

- Marilena Greco. *A Two-dimensional Study of Green- Water Loading*. PhD thesis, NTNU, 2001.
- LS-DYNA Keyword Manual. Volume I. Livermore software technology corporation, May 2007.
- Sang-Gab Lee and Hong-Anh Nguyen. Lngc collision response analysis with iceberg considering surrounding seawater. In *Proceedings of the Twenty-first International Offshore and Polar Engineering Conference*, 2011.
- S.G. Lee, T. Zhao, and J.H. Nam. Structural safety assessment of ship collision and ground using fsi analysis technique. In *Collision and Grounding of Ships and Offshore Structures*, 2013.
- Zhenhui Liu and Jorgen Amdahl. A new formulation of the impact mechanics of ship collisions and its application to a ship-iceberg collision. *Marine Structures*, 23:360–384, 2010.
- LS-DYNA Theory manual, March 2006.
- NORSOK N-004. Design of steel structures, 2004.
- Bjørnar Pettersen. *Marin Teknikk 3 Hydrodynamikk*. 2007.
- Jan Børge Sætre. Collision between platform deck and service vessel wheelhouse. Master's thesis, NTNU, 2013.
- Time step size, May 2014. URL <http://www.dynasupport.com/tutorial/ls-dyna-users-guide/time-step-size/?searchterm=time%20step>.
- Ainian Zhang and Katsuyuki Suzuki. Numerical simulation of fluid-structure interaction of liquid cargo filled tank during ship collision using ale finite element method. *International Journal of Crashworthiness*, 11:291–298, 2006.

Appendix A

Deformations for glancing impact. 45 deg, ship in ballast

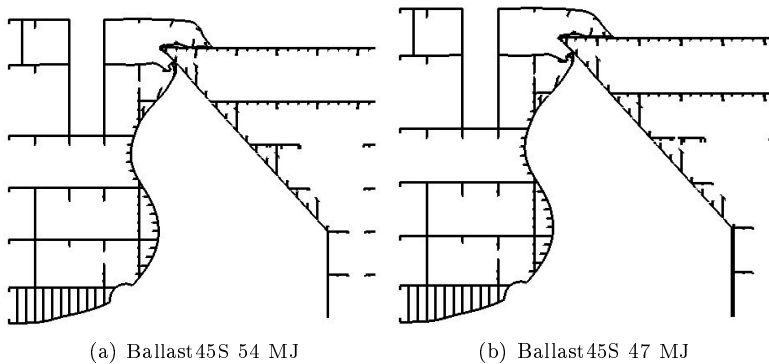


Figure A.1: Deformations for glancing impact.45 deg, ship in Ballast.

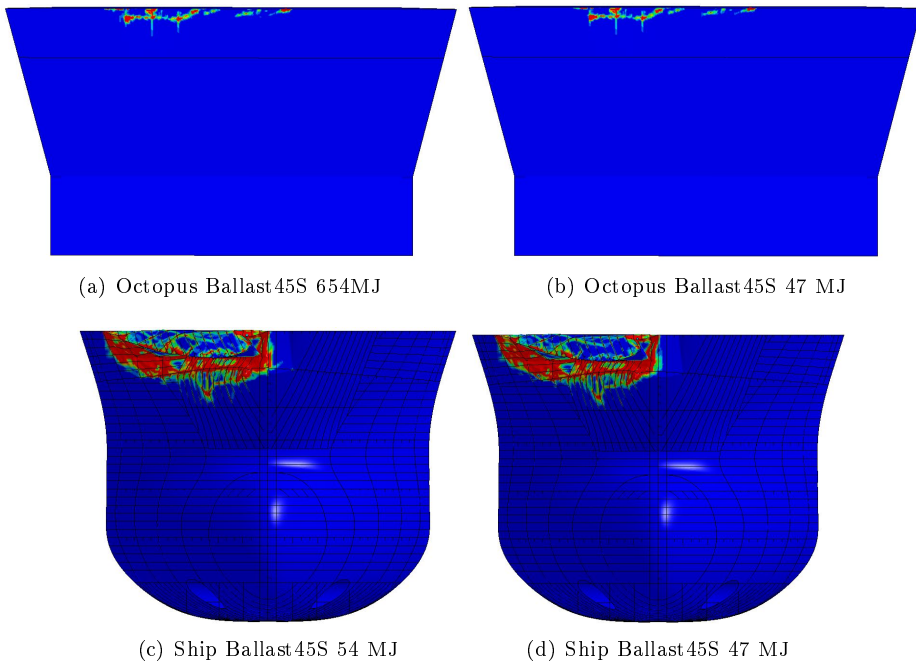


Figure A.2: Plastic strains for glancing impact.45 deg, ship in Ballast.

Appendix B

Deformation area for head on impact, ship in full load

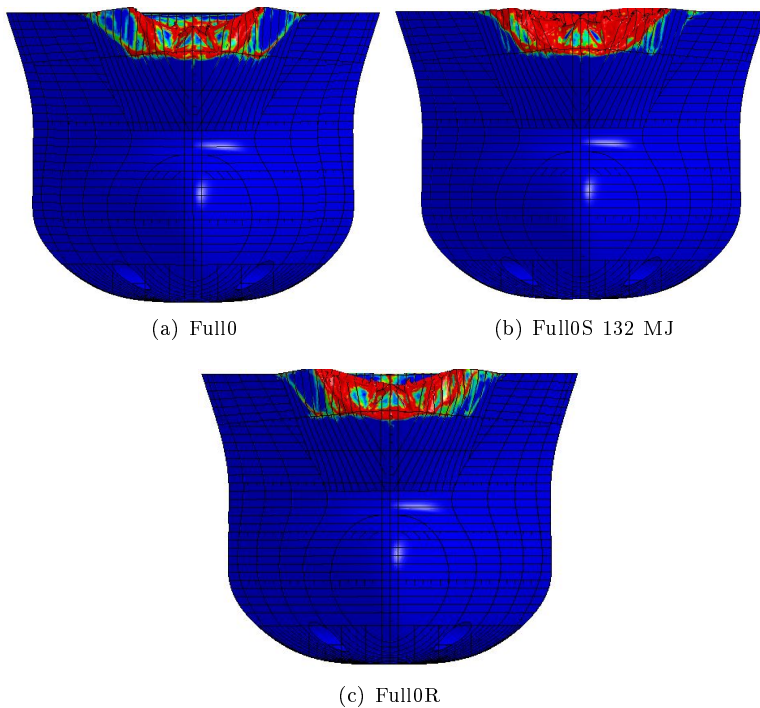


Figure B.1: Plastic strains in bow for head on collision in full load.

Appendix C

Dissipated Energy, Matlab code

```
1  %-----  
2  %-----Subroutine for 3D external mechanics -----  
3  %----- by Dr. Z.Liu, March,2013 -----  
4  %-----  
5  function [tt,ttm,dvv,ve_af,ve_bf,flag,miu,mass1,mass2]= ...  
6      stronge3d(Mass1,Mass2,Am,Bm,Amr,Bmr,Ra,Rb,alpha,gama,betap, ...  
7      cp_a,cp_b,res,miu0,ve_a,ve_b)  
8  %  
9  % INPUT PARAMETERS  
10 % Mass1 : mass of object a, no added mass included [kg]  
11 % Mass2 : mass of object b, no added mass included [kg]  
12 % Am    : translational added mass of object a under body frame of ...  
13         object a  
14 % Bm    : translational added mass of object b under body frame of ...  
15         object b  
16 % Amr   : rotational added mass of object a under body frame of ...  
17         object a  
18 % Bmr   : rotational added mass of object b under body frame of ...  
19         object b  
20 % Ra    : inertia radius square of object a under body frame of ...  
21         [m2]  
22 % Rb    : inertia radius square of object a under body frame of ...  
23         object b  
24 %      [m2]  
25 % alpha : waterline angle [deg]  
26 % gama  : angle between body frame of object a and b [deg]  
27 % betap : normal frame angle [deg]  
28 % cp_a  : collision point under body frame of object a, array (3x1)  
29 % cp_b  : collision point under body frame of object b,array (3x1)  
30 % ve_a  : velocity of object a under body frame of object a,array (3x1)  
31 % ve_b  : velocity of object b under body frame of object b,array (3x1)
```

```

27 % res    : restitution factor, res=0 (fully plastic), res=1 (fully ...
           elastic)
28 % miu0   : the static friction
29 %-----
30 % OUTPUT PARAMETERS
31 % tt     : total dissipated energy [J]
32 % ttm    : an array for dissipated energy in each direction [J]
33 % dvv    : relative velocity increase under the local frame nln2n3
34 % ve_af  : velocity after impact of object a under body frame of ...
           object a
35 % ve_bf  : velocity after impact of object b under body frame of ...
           object b
36 % flag   : stick (1) or slide (2)
37 % miu    : static friction factor between object a and b
38 % mass1  : mass matrix for object a
39 % mass2  : mass matrix for object b
40 %
41 %-----
42 mass1=[1+Am(1) 0 0; 0 1+Am(2) 0; 0 0 1+Am(3)]*Mass1; % mass matrix ...
           for object a
43 mass2=[1+Bm(1) 0 0; 0 1+Bm(2) 0; 0 0 1+Bm(3)]*Mass2; % mass matrix ...
           for object b
44 rxa=Ra(1); % gyration radius square for a
45 rya=Ra(2); % gyration radius square for a
46 rza=Ra(3); % gyration radius square for a
47 rxb=Rb(1); % gyration radius square for b
48 ryb=Rb(2); % gyration radius square for b
49 rzb=Rb(3); % gyration radius square for b
50 Itrx1=[(1+Amr(1))*rxa 0 0; 0 (1+Amr(2))*rya 0; 0 0 ...
           (1+Amr(3))*rza]*Mass1; % Inertia matrix for a
51 Itrx2=[(1+Bmr(1))*rxb 0 0; 0 (1+Bmr(2))*ryb 0; 0 0 ...
           (1+Bmr(3))*rzb]*Mass2; % Inertia matrix for b
52 oba_g=[0 0 0]'; % gravity center of a under body frame of object a
53 obb_g=[0 0 0]'; % gravity center of b under body frame of object b
54 alpha=alpha/180*pi; %wanterline angle
55 gama =gama/180*pi; % angle between body frame a and b
56 betap=betap/180*pi;
57 % calculate the relative impact vector under body frame a and b
58 radla=cp_a-oba_g;
59 rad2b=cp_b-obb_g;
60 % trasnformation matrix between body frame a and b
61 Mab=[cos(gama) sin(gama) 0;
        -sin(gama) cos(gama) 0;
        0 0 1];
62
63
64 % transformation matrix between local and global system for a
65 l=sin(alpha)*cos(betap);
66 m=cos(alpha)*cos(betap);
67 n=-sin(betap);
68 Mlg=[cos(alpha) -sin(alpha) 0;
        -sin(alpha)*sin(betap) -cos(alpha)*sin(betap) -cos(betap);
        l m n];
69
70
71 % transformation matrix between local and global system for b
72 Mtr2=Mlg*Mab;
73 % calculate the transformed inertia matrix
74 Rtrx1=inv(Mlg*Itrx1*inv(Mlg));
75 Rtrx2=inv(Mtr2*Itrx2*inv(Mtr2));
76 mass1f=inv(Mlg*mass1*inv(Mlg));

```

```

77 mass2f=inv(Mtr2*mass2*inv(Mtr2));
78 % calculate the impact vector under local frame
79 rad1=Mlg*rad1a;
80 rad2=Mtr2*rad2b;
81 % calculate the relative velocity under local system
82 rvl=Mlg*ve_a-Mtr2*ve_b;
83 % Input the reversed mass matrix
84 m11=(mass1f(1,1)+rad1(2)^2*Rtrxl(3,3)-2*rad1(2)*rad1(3) ...
85     *Rtrxl(2,3)+rad1(3)^2*Rtrxl(2,2))+(mass2f(1,1)+rad2(2)^2 ...
86     *Rtrx2(3,3)-2*rad2(2)*rad2(3)*Rtrx2(2,3)+rad2(3)^2*Rtrx2(2,2));
87 m12=(mass1f(1,2)+mass2f(1,2))+(rad1(1)*rad1(3)*Rtrxl(2,3)- ...
88     rad1(3)^2*Rtrxl(2,1)-rad1(1)*rad1(2)*Rtrxl(3,3)+rad1(2) ...
89     *rad1(3)*Rtrxl(3,1))+(rad2(1)*rad2(3)*Rtrx2(2,3)-rad2(3)^2 ...
90     *Rtrx2(2,1)-rad2(1)*rad2(2)*Rtrx2(3,3)+rad2(2)*rad2(3)*Rtrx2(3,1));
91 m13=(mass1f(1,3)+mass2f(1,3))+(rad1(1)*rad1(2)*Rtrxl(3,2)- ...
92     rad1(2)^2*Rtrxl(3,1)-rad1(1)*rad1(3)*Rtrxl(2,2)+rad1(2)* ...
93     rad1(3)*Rtrxl(2,1))+(rad2(1)*rad2(2)*Rtrx2(3,2)-rad2(2)^2* ...
94     Rtrx2(3,1)-rad2(1)*rad2(3)*Rtrx2(2,2)+rad2(2)*rad2(3)*Rtrx2(2,1));
95 m22=(mass1f(2,2)+rad1(1)^2*Rtrxl(3,3)-2*rad1(1)*rad1(3)*Rtrxl(1,3) ...
96     +rad1(3)^2*Rtrxl(1,1))+(mass2f(2,2)+rad2(1)^2*Rtrx2(3,3)-2* ...
97     rad2(1)*rad2(3)*Rtrx2(1,3)+rad2(3)^2*Rtrx2(1,1));
98 m23=(mass1f(2,3)+mass2f(2,3))+(rad1(3)*rad1(1)*Rtrxl(1,2)-rad1(3) ...
99     *rad1(2)*Rtrxl(1,1)-rad1(1)^2*Rtrxl(3,2)+rad1(1)*rad1(2)* ...
100     Rtrxl(3,1))+(rad2(3)*rad2(1)*Rtrx2(1,2)-rad2(3)*rad2(2)* ...
101     Rtrx2(1,1)-rad2(1)^2*Rtrx2(3,2)+rad2(1)*rad2(2)*Rtrx2(3,1));
102 m33=(mass1f(3,3)+rad1(1)^2*Rtrxl(2,2)-2*rad1(1)*rad1(2)*Rtrxl(1,2) ...
103     +rad1(2)^2*Rtrxl(1,1))+(mass2f(3,3)+rad2(1)^2*Rtrx2(2,2)-2* ...
104     rad2(1)*rad2(2)*Rtrx2(1,2)+rad2(2)^2*Rtrx2(1,1));
105 m21=m12;
106 m31=m13;
107 m32=m23;
108 m=[m11,m12,m13;m12,m22,m23;m13,m23,m33];
109 %syms dv1 dv2 dv3 dp1 dp2 dp3
110 rm=inv(m);
111 % calculate the extreme case for stick together get the critical ...
112     value miu
112 dv1=-rvl(1);
113 dv2=-rvl(2);
114 dv3=-rvl(3)*(1-res);
115 dp1=subs(rm(1,1)*dv1+rm(1,2)*dv2+rm(1,3)*dv3,{dv1,dv2,dv3}, ...
116     {-rvl(1),-rvl(2),-rvl(3)*(1-res)});
117 dp2=subs(rm(2,1)*dv1+rm(2,2)*dv2+rm(2,3)*dv3,{dv1,dv2,dv3}, ...
118     {-rvl(1),-rvl(2),-rvl(3)*(1-res)});
119 dp3=subs(rm(3,1)*dv1+rm(3,2)*dv2+rm(3,3)*dv3,{dv1,dv2,dv3}, ...
120     {-rvl(1),-rvl(2),-rvl(3)*(1-res)});
121 miu=sign(dp1)*sqrt(dp1^2+dp2^2)/dp3;
122 miu2=dp2/dp1;
123 % friction matrix
124 flag='Stick';
125 if miu==0
126     sm1=Inf;
127 else
128     sm1=m11+m12*miu2+m13*sqrt(1+miu2*miu2)/miu;
129     if miu2==0
130         sm2=Inf;
131     else
132         sm2=m21/miu2+m22+m23*sqrt(1+miu2*miu2)/miu/miu2;

```

```

133     end
134 end
135 sm3=m31*miu/sqrt(1+miu2*miu2)+m32*miu*miu2/sqrt(1+miu2*miu2)+m33;
136 if abs(miou)>miu0 % sliding case
137     flag='Slide';
138     dv3=-rvl(3)*(1-res);
139     fai=atan(miou2);
140     if dp2==0
141         fai=0/180*pi;
142     end
143     if miu0==0
144         sm1=Inf;
145     else
146         sm1=m11+m12*miu2+m13*sqrt(1+miu2*miu2)/miu0;
147         if miu2==0
148             sm2=Inf;
149         else
150             sm2=m21/miu2+m22+m23*sqrt(1+miu2*miu2)/miu0/miu2;
151         end
152     end
153     sm3=m31*miu0/sqrt(1+miu2*miu2)+m32*miu0*miu2/sqrt(1+miu2*miu2)+m33;
154     AA=[miu0*cos(fai)*1e06 -rm(1,1) -rm(1,2);
155         miu0*sin(fai)*1e06 -rm(2,1) -rm(2,2);
156         1e06 -rm(3,1) -rm(3,2)];
157     BB=[rm(1,3)*dv3 rm(2,3)*dv3 rm(3,3)*dv3]';
158     CC=AA\BB;
159     dp3=CC(1,1)*1e06;
160     dv1=CC(2,1);
161     dv2=CC(3,1);
162     dp1=miu0*cos(fai)*dp3;
163     dp2=miu0*sin(fai)*dp3;
164 end
165 %dpp=sqrt(dp1^2+dp2^2+dp3^2);
166 % energy on direction 1
167 %E1=abs(dp1/2.*(dv1+2*rvl(1)));
168 E1=abs(1/sm1/2*dv1*(dv1+2*rvl(1)));
169 % energy on direction 2
170 if miu2==0
171     E2=0;
172 else
173     %E2=abs(dp2/2.*(dv2+2*rvl(2)));
174     E2=abs(1/sm2/2*dv2*(dv2+2*rvl(2)));
175 end
176 %E3=abs(dp3/2.*(dv3+2*rvl(3)));
177 E3=abs(1/sm3/2*dv3*(dv3+2*rvl(3)));
178 % velocity change vector
179 dvv=[dv1;dv2;dv3]; % this is in local frame
180 % total energy
181 % do control to output if NaN, usually a result of Inf*0
182 if isnan(E1)==1
183     E1=0;
184 elseif isnan(E2)==1
185     E2=0;
186 elseif isnan(E3)==1
187     E3=0;
188 end
189 tt=E1+E3+E2;

```

```
190 ttm=[E1,E2,E3];
191 %% compute the velocity after impact at body frame a and b
192 FF=mass1+mass2*inv(Mtr2)*Mlg;
193 SS=mass1*ve_a+mass2*ve_b;
194 QQ=mass2*inv(Mtr2)*(rvl+dvv);
195 ve_af=inv(FF)*(SS+QQ); % velocity of body a after ...
    impact under body frame a
196 ve_bf=inv(Mtr2)*(Mlg*ve_af-(rvl+dvv)); % velocity of body b after ...
    impact under body frame b
197 end
```